Max-Planck-Institut
für Meteorologie

MAX-PLANCK-GESELLSCHAFT

International Max Planck Research School
on Earth System Modelling

Simulation of atmospheric krypton-85 transport to assess the detectability of clandestine nuclear reprocessing

Jens Ole Roß

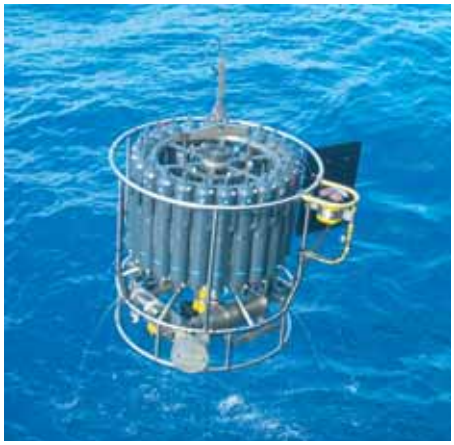

Berichte zur Erdsystemforschung 82/2010

Reports on Earth System Science

Hinweis

Die Berichte zur Erdsystemforschung werden vom Max-Planck-Institut für Meteorologie in Hamburg in unregelmäßiger Abfolge herausgegeben.

Sie enthalten wissenschaftliche und technische Beiträge, inklusive Dissertationen.

Die Beiträge geben nicht notwendigerweise die Auffassung des Instituts wieder.

Die "Berichte zur Erdsystemforschung" führen die vorherigen Reihen "Reports" und "Examensarbeiten" weiter.

Notice

The Reports on Earth System Science are published by the Max Planck Institute for Meteorology in Hamburg. They appear in irregular intervals.

They contain scientific and technical contributions, including Ph. D. theses.

The Reports do not necessarily reflect the opinion of the Institute.

The "Reports on Earth System Science" continue the former "Reports" and "Examensarbeiten" of the Max Planck Institute.

Anschrift / Address

Max-Planck-Institut für Meteorologie
Bundesstrasse 53
20146 Hamburg
Deutschland

Tel.: +49-(0)40-4 11 73-0
Fax: +49-(0)40-4 11 73-298
Web: www.mpimet.mpg.de

Layout:

Bettina Diallo, PR & Grafik

Titelfotos:
vorne:
Christian Klepp - Jochem Marotzke - Christian Klepp
hinten:
Clotilde Dubois - Christian Klepp - Katsumasa Tanaka

Berichte zur Erdsystemforschung 82/2010

Simulation of atmospheric krypton-85 transport to assess the detectability of clandestine nuclear reprocessing

Jens Ole Roß

aus Freiburg im Breisgau

Hamburg 2010

Reports on Earth System Science 82/2010

ISSN 1614-1199

Jens Ole Roß

Carl Friedrich von Weizsäcker-Zentrum
für Naturwissenschaft und Friedensforschung

Universität Hamburg
Beim Schlump 83
20144 Hamburg

Als Dissertation angenommen
vom Department Geowissenschaften der Universität Hamburg

auf Grund der Gutachten von
Prof. Dr. K. Heinke Schlünzen
und
Prof. Dr. Martin B. Kalinowski

Hamburg, den 2. Februar 2010
Prof. Dr. Jürgen Oßenbrügge
Leiter des Departments für Geowissenschaften

ISSN 1614-1199

Simulation of atmospheric krypton-85 transport to assess the detectability of clandestine nuclear reprocessing

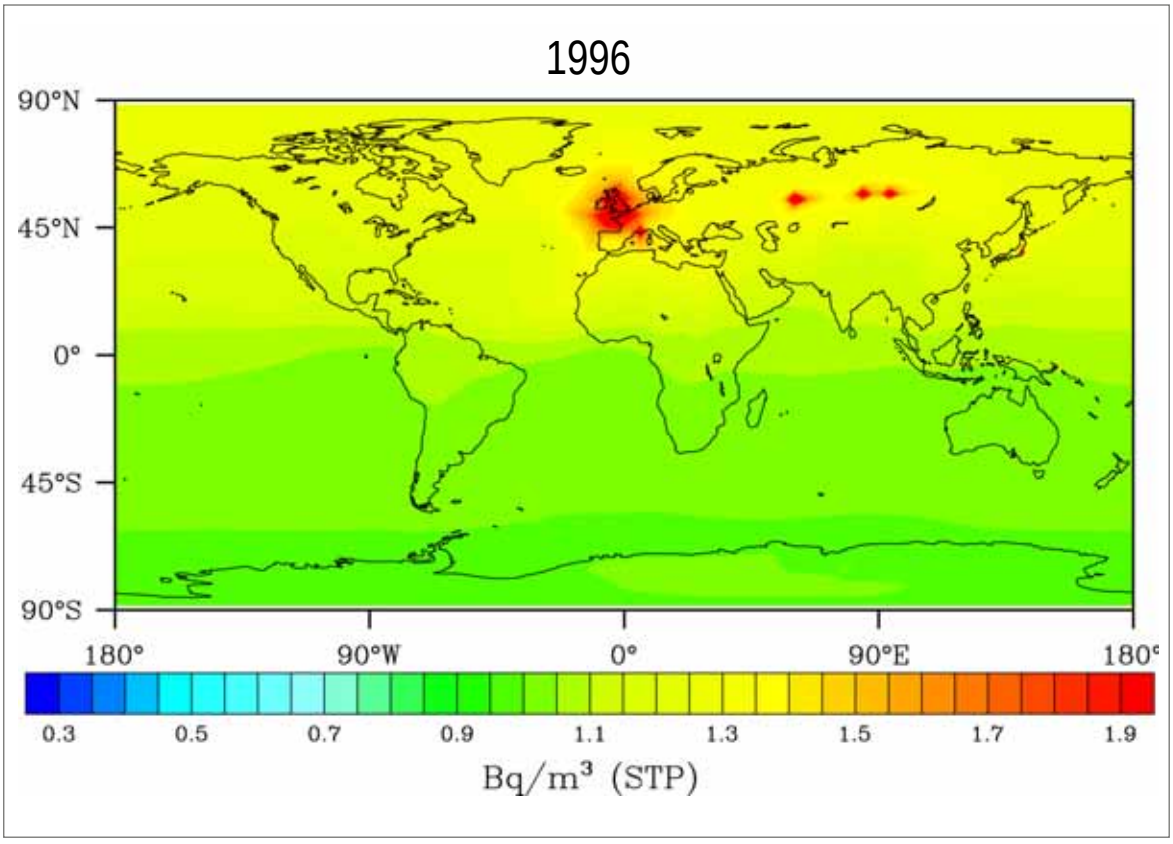

Jens Ole Roß

Hamburg 2010

Everything comes to him who knows how to wait.

(Wolfgang Pauli, 1956)

Abstract

The radioactive noble gas krypton-85 is released into the atmosphere during reprocessing of spent nuclear fuel or irradiated breeding targets. This is a necessary step for plutonium separation. Therefore the ^{85}Kr signature of reprocessing could possibly be used for the detection of undeclared nuclear facilities producing nuclear weapon-usable material. The ^{85}Kr content of the atmosphere has grown over the last decades as the emissions from military and civilian nuclear industry could not be compensated by the decay with a half-life of 10.76 years.

In this study, the global ^{85}Kr background distribution due to emissions of known reprocessing facilities for the period from 1971 until 2006 was simulated using the atmospheric general circulation model ECHAM5 applying the newest available annual emission data. The convective tracer transport scheme and the operator splitting for the physical calculations in the model were modified in order to guarantee physically correct results for tracer point sources, in particular non negative concentrations. An on-line routine controlling the ^{85}Kr –budget in the model enforced exact mass conservation. The results of the simulation were evaluated by extensive comparison with measurements performed by the German Federal Office for Radiation Protection with very good agreement at most observation sites except those in the direct vicinity of ^{85}Kr sources. Of particular interest for the ^{85}Kr detection potential was the variability of ^{85}Kr background concentrations which was evaluated for the first time in a global model. In addition, the interhemispheric transport as simulated by ECHAM5 was analyzed using a two-box model providing a mean exchange time of $\tau_{\mathrm{ex}} = 10.5\,\mathrm{months}$. The analysis of τ_{ex} over simulated 35 years indicates that in years with strong South Asian or African Monsoon the interhemispheric transport is faster during the monsoon season. A correlation analysis of interhemispheric transport time with the Southern Oscillation Index and other climate indices over the 35 year period does not show statistically significant correlations.

The potential detectability of emissions from a set of specified source locations was investigated for a hypothetical inspection scenario which allows to take samples close to the concentration maximum of the plumes. For this part of the study, the Lagrangian particle dispersion model HYSPLIT was used. In combination with the location specific background variability derived from ECHAM5, minimum detectable ^{85}Kr releases are calculated depending on the time after release and the distance of the plume center from the hypothetical source location. The results show that the smallest of the ^{85}Kr reference releases, 3.2 TBq, is potentially detectable within 24 hours after stop of release in most cases. The detection probability decreases significantly during the following days. In presence of favorable background conditions as predicted on the Southern Hemisphere, ^{85}Kr plumes stay detectable even about several thousand kilometers from the source location in some cases. These results serve as first benchmark on the capability of using ^{85}Kr for IAEA Safeguards on the Non-Proliferation Treaty and its possible contribution to the verification of a future Fissile Material Cut-off Treaty.

Zusammenfassung

Das radioaktive Edelgas Krypton-85 wird während der Wiederaufbereitung abgebrannter nuklearer Brennstäbe in die Atmosphäre freigesetzt. Dieser Prozess ist auch für die Abtrennung von Plutonium notwendig. Daher kann die ^{85}Kr Signatur von nuklearer Wiederaufbereitung möglicherweise zur Entdeckung ungemeldeter Anlagen verwendet werden, die kernwaffenfähiges Material herstellen. Der weltweite ^{85}Kr Gehalt der Atmosphäre wuchs über die letzten Jahrzehnte an, da militärische und zivile Nuklearanlagen mehr ^{85}Kr emittierten als der radioaktive Zerfall mit einer Halbwertszeit von 10,76 kompensiert.
Für diese Arbeit wurde die globale ^{85}Kr Hintergrundverteilung, wie sie von bekannten Wiederaufbereitungsanlagen von 1971 bis 2006 verursacht worden war, unter der Verwendung der aktuell verfügbaren jährlichen Emissionsdaten mit dem allgemeinen Atmosphärenzirkulationsmodel ECHAM5 simuliert. Die Konvektionsparameterisierung des Modells und das Operatorsplitting der physikalischen Prozesse wurde modifiziert, um nicht-negative Konzentrationen zu garantieren. Außerdem wurde über eine permanente ^{85}Kr Budgetüberwachung exakte Massenerhaltung im Modell erzwungen. Die Ergebnisse der Simulation wurden durch den Vergleich mit umfangreichen Messdaten des Bundesamtes für Strahlenschutz evaluiert und erzielten außer in direkter Quellumgebung sehr gute Übereinstimmung. Von besonderem Interesse für die ^{85}Kr Entdeckbarkeit ist die Variabilität der ^{85}Kr Hintergrundkonzentration, die hier erstmals in einem globalen Modell untersucht wird. Zusätzlich wurde der interhemisphärische Transport in einem Zwei-Boxen-Modell untersucht. Dabei wurde eine mittlere Austauschzeit von 10,5 Monaten ermittelt. Die Analyse über den simulierten 35-Jahres-Zeitraum zeigte, dass der interhemiphärische Transport in Jahren mit starkem Südasiatischem und Afrikanischem Monsun beschleunigt abläuft. Eine Korrelationsanalyse mit dem Southern Oscillation Index und anderen Klimaindizes ergab keine statistisch signifikanten Zusammenhänge.
Die potentielle Entdeckbarkeit hypothetischer Emissionen von einem Muster festgelegter Quellorte wurde für den Fall untersucht, dass es ein Inspektionsszenario geben wird, das Messungen nah am Maximum einer Abluftfahne ermöglicht. Dafür wurden Simulationen mit sechsstündigen Emissionen im Lagrangschen Partikeldispersionsmodell HYSPLIT verwendet. In Kombination mit der von ECHAM5 berechneten ortsspezifischen Hintergrundvariabilität wurden kleinste noch entdeckbare Freisetzungen in Abhängigkeit von der Zeit nach der Emission und Entfernung von der Quelle berechnet. Die Ergebnisse zeigen, dass die kleinste der drei Referenzemissionen 3.2, 10 and 100 TBq in den meisten Fällen innerhalb von 24 Stunden nach Ende der Emission entdeckbar bleibt. Die Entdeckungswahrscheinlichkeit sinkt deutlich während der folgenden Tage. Aus den Ergebnissen folgen erste Bewertungsmaßstäbe für die Eignung von ^{85}Kr für IAEO Sicherungsmaßnahmen des Nichtverbreitungsvertrages und den möglichen Beitrag für die Verifikation eines zukünftigen Vertrages über das Ende der Produktion spaltbaren Materials für Kernwaffen (FMCT).

Contents

1 Introduction

The effectiveness of nuclear non-proliferation and arms control treaties as well as future fissile material control and a ban of nuclear weapons depends fundamentally on the implementation of reliable verification systems for assuring treaty compliance. Alleged insufficient provableness has been used as an argument by opponents to the Comprehensive Nuclear Test Ban Treaty. In the current debate about starting negotiations of a Fissile Material Cut-Off Treaty the possibilities of verification play a crucial role. The biggest challenge and weakness of non-proliferation surveillance results from clandestine activities. Therefore, an improvement of scientific and technological methods for the detection of unreported nuclear activities can stabilize the non-proliferation regime and encourage the willingness of state actors for nuclear disarmament. Radioactive tracers in the atmosphere are potential indicators for the detection of nuclear activities. In this thesis, the suitability of the radioactive noble gas isotope krypton-85 as indicator for clandestine plutonium separation is investigated. The noble gas ^{85}Kr is produced along with plutonium in nuclear reactors. It is released into the air during reprocessing of spent nuclear fuel rods or plutonium breeding targets. With a radioactive half-life of 10.76 years, the ^{85}Kr content of the atmosphere increased continuously since 1945. In order to assess the feasibility of detection of unreported reprocessing, the global ^{85}Kr distribution, its variability, and the sensitivity to specific source locations are investigated.

1.1 Introduction to atmospheric transport modeling

When using measurements of trace gases for detection of emissions from nuclear activities, the measurements are usually conducted far apart from the source location, and some time has passed since the emission. The connection between emission and immission is determined by atmospheric dynamics and possibly further influenced by chemical or radioactive transformation processes of the trace species.

The lack of accurate knowledge of atmospheric conditions can partly be compensated by using numerical models describing an approximative reproduction of the meteorological parameters. With the raised interest in climate science and the enormous increase in computing performance in the last decades, atmospheric models became more capable in describing the meteorology with high resolution in time and space. A particular motivation for studying atmospheric transport originated from the danger of accidental releases of toxic species from industrial facilities (Schlünzen, 2002).

As the trace gas concentration in mass or particle per volume depends on temperature and pressure, mass mixing ratios c_m or volume mixing ratios c_v are usually considered in the models:

$$c_m = \frac{m_{\text{tracer}}}{m_{\text{air}}} \qquad c_v = \frac{V_{\text{tracer}}}{V_{\text{air}}}. \tag{1.1}$$

The concentration of radioactive tracers is often given in activity per volume ($\mathrm{Bq\,m^{-3}}$) which is proportional to the particle or mass concentrations. When giving concentrations in $\mathrm{Bq\,m^{-3}}$ in this study the reference volume is normalized to standard temperature and pressure (STP), which is 0°C and 1000 hPa.

For the tracer transport calculation two approaches exist: The Lagrangian method considers an air parcel following trajectories conserving the local concentration in the traveling air parcel. The result are discrete particle pathways according to the present wind vectors. A further development of the Lagrangian trajectories are plume dispersion models, which consider the turbulent diffusion of the plume stochastically. Purely Lagrangian plume dispersion models could better represent the point character of the sources, but there are difficulties in applying Lagrangian models over long

integration times as the number of transported particles and therefore the computational effort is increasing with simulated time.

The other approach is the fixed grid box based Eulerian method. In this method tracer balances for each grid cell are calculated.

$$\frac{\partial X}{\partial t} + u\frac{\partial X}{\partial x} + v\frac{\partial X}{\partial y} + w\frac{\partial X}{\partial z} = \frac{\partial X}{\partial t} + \vec{u} \cdot \nabla X = s \tag{1.2}$$

with a mass mixing ratio like quantity X, the wind vector components u, v, w and sources or sinks s in the grid cell.

All Eulerian models have the problem of distributing emissions from a point source over the whole volume of a grid cell. This effect does not harm the influence on the global tracer background concentrations far from the source if the numerical diffusivity of transport is in the right order. For the Eulerian models, there are so called semi-Lagrangian flux form schemes implemented for advection, which calculate the transport of the air content of the grid boxes along trajectories and then reassign the boxes to the fixed grid after each transport step.

For performing the transport the knowledge of the atmospheric dynamics and its development in time is necessary. There are two ways to obtain the meteorological data for transport calculations: The model can calculate the meteorology itself by solving prognostic equations derived from physical principles like energy and momentum conservation for the variables describing the state of the atmosphere. The other possibility is to receive externally generated meteorological data sets, e.g. reanalysis data (Feichter et al., 2002). General Circulation Models (GCM) produce their own meteorology solving the fundamental prognostic equations in a dynamical core and applying several parameterizations for further physical influences, in particular sub-grid scale processes. In contrast, Chemical Transport Models (CTM) are driven by reanalysis or prediction data. While meteorological variables like pressure, temperature, humidity and wind data are forced from the data, physical process calculations on sub-grid scale are parameterized in a similar way as in a GCM.

The reanalysis data used as input for a CTM are produced by data assimilation methods to a global forecast model. This is necessary to assign the data to the grid and to raise the physical consistency of the data according to the numerical

model. The fields produced and used by a GCM are therefore self-consistent. They also provide a higher temporal resolution, as reanalysis data usually exist for every six or three hours and have to be interpolated in between. Furthermore, depending on the model resolution, the reanalysis data have to be assigned to the grid of the transport model. For the CTM only a certain selection of meteorological variables in low temporal resolution is available from reanalysis data, while the GCM has a full set of consistent variables produced by itself for any time step. ECHAM5 in T63L31 e.g. has a calculation time step length of 12 minutes. To adapt historic meteorological conditions from the past, there is the possibility to run GCMs like ECHAM5 in a "nudged" mode. This means the dynamical core of the model is constrained towards the values of corresponding reanalysis data and leads to better agreement of the model results with historic observations. The additional fact that climate models are tuned and tested to run stable over long integration times was also a reason to chose ECHAM5 as the evolution of the ^{85}Kr background over several decades is of interest.

Thus, in this study the Eulerian GCM ECHAM5 is used for the long term ^{85}Kr background calculation. For the assessment of detection scenarios with tracers emitted from hypothetical emission sites, the Lagrangian particle dispersion model HYSPLIT is applied.

1.2 Structure of the thesis

The structure of this dissertation is as follows: Chapter 2 introduces the framework and previous studies on using radioactive noble gas isotopes for verification of arms control treaties with a particular focus on the detection of clandestine nuclear reprocessing through its ^{85}Kr signature. Then the properties, emission sources and observations of ^{85}Kr are discussed as used for the following atmospheric ^{85}Kr transport model studies. In Chapter 3 the transport processes implemented in the global atmospheric general circulation model ECHAM5 are described and necessary modifications and performance tests are presented. The results of the ^{85}Kr background simulation experiment are presented and evaluated in Chapter 4. In the following Chapter 5 an analysis of the air mass exchange between the hemispheres is performed

and correlations between the interhemispheric transport time and several climatological indices are investigated. Chapter 6 shows the project results of the sensitivity study on the detectability of additional ^{85}Kr sources above the simulated variability of the global background using the Lagrangian particle dispersion model HYSPLIT. Finally, the findings are summarized and future research questions and prospects of using ^{85}Kr as indicator for clandestine reprocessing are discussed in the conclusions.

2 Radioactive noble gases for verification purposes

Radioactive noble gas isotopes in the environment can be used for many purposes. The short lived radon-222 evading from the ground is often used to evaluate vertical transport in atmospheric models (Feichter and Crutzen, 1990; Gupta et al., 2004). Various noble gas isotopes with appropriate half-life and known initial concentration are applied in dating methods investigating the age of groundwater (Lehmann et al., 2003), deep water or ice core samples (Collon et al., 2004).

This chapter deals with the use of radioactive noble gas isotopes as indicator for human nuclear technology activities, in particular in the framework of nuclear arms and non-proliferation control treaty verification. First the application of radioactive xenon isotopes for the detection of nuclear explosions is introduced in Section 2.1. After that Section 2.2 describes the possibility of using krypton-85 for the detection of nuclear reprocessing. Finally from Section 2.3 on an overview of properties, emissions and measurements of ^{85}Kr explains the basis for the following chapters dealing with numerical models for atmospheric transport simulation.

2.1 Detection of nuclear test explosions

As an example for a successfully implemented technical verification system the International Monitoring System of the Comprehensive Nuclear Test-Ban Treaty (CTBT) is introduced briefly. The CTBT prohibits to conduct any kind of nuclear explosion. It is "comprehensive" in this full coverage of the ban and because of its universality treating all member states equally. The technical verification system is being set up

at the Provisional Technical Secretariat (PTS) of the Preparatory Commission for the CTBT-Organization in Vienna, and is designed to detect any nuclear explosion on earth which has a yield of at least 1 kiloton TNT equivalent. The International Data Centre collects data from 321 stations of the International Monitoring System. The wave-form based technologies seismology, hydroacoustics, and infrasound are used for the detection of explosion events and for analyzing their time, location and strength. A network of 80 radionuclide stations is in place to detect radioactive fission products of nuclear explosions. Among the fission products gaseous radioactive xenon isotopes are particularly important. Although ^{85}Kr is produced in nuclear explosions as well, it is not considered as indicator for the CTBT verification because of its relatively low yield and the inconvenient background situation due to the large civilian emissions.

2.1.1 Radioactive xenon isotopes

To establish the meteorological connection between the monitoring station(s) and possible source regions of the emission, Atmospheric Transport Modelling is applied (Wotawa et al., 2003; Becker et al., 2007). The meteorologists at PTS use the Lagrangian Models FEXPART and HYSPLIT driven by analysis data. For the investigation of the source area of regard, source receptor relationships are evaluated. For the detection of nuclear tests, radioactive xenon isotopes are very important, as they have a high fission yield and are likely to be released even from underground explosions. Through the combination of specific isotopic ratios it is possible to distinguish reactor and explosion sources (Kalinowski and Pistner, 2006). The signal of radioactive xenon isotopes produced by a nuclear explosion is much stronger than the regular civilian emissions (Kalinowski and Tuma, 2009). As the radioactive half-lives of the four xenon isotopes of interest range from 9 hours to 12 days, the background from civilian isotope production facilities and nuclear reactors is not persistent, but due to the long distances between the noble gas monitoring stations the discrimination often remains difficult.

2.1.2 North Korean nuclear tests

The announced nuclear test of the Democratic Peoples Republic of Korea (DPRK) on October 9, 2006, produced a seismic signal with a body wave magnitude of $m_b = 4.1$. It was detected by observatories around the globe. The relationship between magnitude and explosive yield indicated a strength below one kiloton TNT equivalent (Kalinowski and Ross, 2006). After the event three independent measurements of increased radioxenon were reported: First, on Oct 11, US Air Force took air samples with an aircraft over the Sea of Japan (Office of the Director of National Intelligence, 2006). Second, from October 12–16, Swedish scientists took air samples in South Korea close to the border with a mobile SAUNA (*Swedish Automatic Noble Gas Analyser*) (Ringbom et al., 2007). Finally, two weeks after the event, the Canadian IMS station Yellowknife detected elevated ^{133}Xe concentrations which could not be explained with emissions of the medical isotope production facility in Chalk River, Canada (Saey et al., 2007). The measurements were meteorologically consistent with the DPRK test site as source location. With an analysis of specific isotopic ratios of the Swedish measurements it is possible to prove that the elevated concentrations originate from a nuclear explosion and not from a reactor source (Kalinowski et al., 2010, accepted for publication). Therefore, it is finally clear that the DPRK 2006 event was actually a nuclear test.

On May 25, 2009 another explosion was detected at the same location as the first nuclear test. Although in this case the seismological signals were stronger than those of the first event, no elevated concentrations of radioxenon have been found in spite of intensive observation efforts and meteorological conditions favorable to carry sufficient traces to various sampling sites. Probably there was a better containment of the fission gases of the second underground explosion. Because of the tremendous effort it is not likely, but nevertheless possible, that a huge chemical explosion was conducted instead to feign a second nuclear test. But as the first test explosion was only partially successful in terms of the achieved yield, a second test by the DPRK seems plausible. The absence of radioxenon observations after the second test is not due to weakness of the system - the full containment of fission gases underground is possible under certain circumstances. In any case, the seismic signal detected would have been clear enough to justify an on site inspection - an instrument which becomes

available to the CTBTO when the treaty enters into force.

2.1.3 Outcome of CTBT experience

The success of the International Monitoring System was to show that it is indeed possible to develop a functioning technical verification system in cooperation with scientists. After many experiments in the testing phase, the proof of the first North Korean nuclear test as well as the seismological detection of both explosions, showed the functionality of the system, although the closest IMS noble gas stations were not yet in place and other actors supported the measurements. The performance of the Atmospheric Transport Modelling system is now on high level and operational since several years for source attribution of relevant radionuclide detections.

Other treaties for the control of fissile material and its production can benefit from this experience if similar technical surveillance measures become implemented. In this study, the possibility of environmental sampling of ^{85}Kr in the context of treaties controlling fissile material and their production is assessed. Using ^{85}Kr to detect reprocessing activities is more challenging: As the radioactive half-live of ^{85}Kr is 10.76 years, it remains in the atmosphere for decades. As a result, there is a high ^{85}Kr background, and the signals of interest are small.

2.2 Using ^{85}Kr as an indicator for plutonium separation

The radioactive noble gas isotope ^{85}Kr is produced along with the plutonium in nuclear reactors. It remains enclosed in the nuclear fuel rods or breeding targets until reprocessing. When the fuel rods become chemically dissolved in acid during reprocessing, the ^{85}Kr gets released into the air. There exist only small other sources of ^{85}Kr. Natural generation by cosmic rays is by five orders of magnitude weaker than the anthropogenic reprocessing sources. The operational releases of nuclear power plants and isotope production are small in comparison to the reprocessing emissions (Section 2.3 and following).

2.2.1 Historic examples and previous studies

The general suitability of ^{85}Kr as an indicator for the detection of nuclear reprocessing has been known for decades. Already in the 1950s US national military services used ^{85}Kr in a project which is referred to as "Operation Bluenose" (Goodman, 2007) to estimate the Soviet plutonium production. In the 1980s scientists around Frank von Hippel and David Albright assessed the Soviet plutonium stockpile (von Hippel et al., 1986) by deriving the missing ^{85}Kr emissions for explaining the evident atmospheric content.

A first study calculating ^{85}Kr transport spatially in a three dimensional atmospheric model was published by Zimmermann et al. (1989). A more detailed investigation applying the general circulation model ECHAM4 to ^{85}Kr concentrations was performed by Winger et al. (2005). One achievement of this work was the update and enhancement of the existing emission inventory. The evaluation of the climate model ECHAM4 also achieved qualitatively good results. However, the atmospheric simulation had shortcomings in mass conservation (60% loss over the simulated period) and the resolution (T31) was too coarse for the representation of the correct spatial concentration patterns on the Northern Hemisphere, especially in Central Europe. A simulation of the global ^{85}Kr background is also a part of this thesis. For this, the successor model version ECHAM5 is chosen with improved tracer transport properties and a higher resolution. The tracer transport and the modifications are described in Chapter 3, the results with special focus on the variability of the background concentrations are presented in Chapter 4.

Concerning the detectability of reprocessing activities several case studies have been performed: For two and a half years from 1985 to 1988 weekly air samples were taken in four distances from the German pilot reprocessing plant in Karlsruhe (Kalinowski et al., 2004). The observational data were statistically evaluated for increased concentrations above background. The resulting detection probability on 2 sigma level was 72% at 5 km distance and 42% at 40 km distance with false alarm rates of 2.1% and 9.9%. Assuming a source term of 16 TBq ^{85}Kr per kg separated plutonium, the study assessed a minimum detectable production of 40g Pu per week at 5 km distance and 200g Pu at 40 km distance.

Statistical analysis of weekly samples taken from 1991 to 2005 at Tsukuba, 60 km from the Tokai reprocessing facility in Japan, have shown a clear coincidence between weeks with elevated ^{85}Kr concentrations and operation times of the plant. A more recent assessment of detection potential based on the Tsukuba dataset is published by Kemp and Schlosser (2008). These studies derived the background variation from statistical data analysis but did not apply atmospheric transport modeling.

With the experience from the developed atmospheric transport model system at the CTBTO and the progress of models in the last decades, the goal of the present study is to determine detection probabilities by applying state of the art atmospheric models on ^{85}Kr . If successful, a useful tool for the IAEA Safeguards described in the next section and a verification system for a future Fissile Material Cut-Off Treaty could be developed.

2.2.2 Non-Proliferation Treaty and its verification by IAEA Safeguards

The nuclear Non-Proliferation Treaty (NPT) entered into force 1970 and has 189 member states (IAEA, 1970). The treaty defines five nuclear weapon states (USA, USSR, UK, China and France) and prohibits the spread of nuclear weapons to non-nuclear weapon states (Article 1). The states without nuclear weapons are obliged not to attempt to manufacture or acquire nuclear weapons (Article 2) whilst the nuclear weapon states must aim for disarmament (Article 6). To counteract the imbalance of the treaty, all states have the right to use nuclear energy peacefully and can expect support in doing so (Article 4). The non-nuclear weapon state parties conclude safeguards agreements with the International Atomic Energy Agency (IAEA) to verify compliance and control of all nuclear material used in all facilities (Article 3). The IAEA applies a broad range of methods for safeguarding nuclear facilities and fissile materials in the framework of the safeguard agreements with member states. Still the original safeguard Agreements turned out to be insufficient for the detection of undeclared activities. After the nuclear program of Iraq was discovered during the 1991 war without being detected by safeguard inspections beforehand, the IAEA developed a Model Additional Protocol with more comprehensive and technically advanced methods against non-compliance (IAEA, 1997). Additional Protocols

are in force in about 90 member states. Inspections on short notice (24 hours) are possible and rigorous declarations are obligatory. Furthermore the possibility of environmental sampling is introduced. Location specific samples are taken directly at the facilities, in particular so called swipe samples collecting dust from surfaces for analysis in the laboratory. The possibility of wide area environmental sampling – i.e. sampling not in the direct vicinity of known facilities – is foreseen in principle but its application would require a further decision by the IAEA-Board of Governors. In the report STR-321 the IAEA (1999) assumes that permanent Wide Area Environmental Sampling of ^{85}Kr with a fixed global grid of observation stations is too expensive.

2.2.3 IAEA Novel Technologies Program

In September 2004 the IAEA General Conference approved the "Resolution on Strengthening the Effectiveness and Improving the Efficiency of the safeguards System including Implementation of Additional Protocol" (IAEA, 2004). This resolution requires the Secretariat "to examine, subject to the availability of resources, innovative technological solutions to strengthen the effectiveness and to improve the efficiency of safeguards". Subsequently, in 2005, the IAEA Department of safeguards started the so called Novel Technologies Program under the full project title "Novel Techniques and Instruments for Detection of Undeclared Nuclear Facilities, Material and Activities". In this framework the IAEA conducted a technical experts meeting on "Noble Gas Monitoring Sampling and Analysis for Safeguards Applications" in September 2005. Although considering the suitability of ^{85}Kr , the conclusive statement in the written report is as follows: "Because of the high costs to implement a capability and the low probability of definitive detection, the Technical Meeting recommends that the IAEA not pursue long range detection of noble gases" (IAEA, 2005).

Large parts of the Novel Technologies Program are performed and funded by national support programs of the member states. In late 2005 a proposal for a ^{85}Kr model study was submitted to the Joint Programme of IAEA and the Federal Government of Germany which is organized by the Ministry for Economy and Technology and administered by a program committee with delegates from research institutions and companies of the nuclear industry. The first phase of the project "Simulation of atmospheric noble gas concentrations to assess sampling procedures for the detection

of clandestine reprocessing" was designed as feasibility assessment to prepare further IAEA decisions on that issue. In the first phase of the project global background of ^{85}Kr and detectability of additional sources was investigated (Ross et al., 2009). The report was accepted by the German program committee and the IAEA so that a second project year investigating the localizability of ^{85}Kr sources and a cost estimate for the various inspection scenarios will be performed in 2010.

2.2.4 Sampling procedures for the detection of illicit nuclear reprocessing

According to the procedural framework of IAEA safeguards there are legal restrictions on the possibilities for inspectors to take environmental samples. Disregarding possible legal obstacles in detail the following three scenarios are considered for ^{85}Kr measurements in order to detect undeclared plutonium separation.

a) Spot samples at nuclear facilities

There is a large number of nuclear facilities under safeguards which are routinely visited by IAEA inspectors. The inspectors could collect air samples at the occasion of their visit and evaluate the ^{85}Kr concentration. The detection of elevated ^{85}Kr concentration levels could indicate either undeclared reprocessing at the facility under inspection or reprocessing activities upwind from the facility. The advantage of this sampling method is that the inspections take place routinely and thus minimize additional efforts for air sampling. The disadvantage is that the frequency of these inspections is quite low and the locations are fixed. Thus the degree of surveillance efficiency will be limited.

b) Temporal regional monitoring

If a certain country is suspicted to separate plutonium at an unknown location the IAEA could install a small regional observation network monitoring ^{85}Kr concentration for a limited period of time. This network could consist of two to ten strategically chosen sampling sites. With an assessment of the location specific background and

an analysis of the time series of measurements such a network could allow to draw conclusions about close ^{85}Kr emission sources.

c) The "Catch the plume"-Scenario

If there is a suspicious source region one can forecast the dispersion of a hypothetical release. Inspectors could then travel to the predicted position of the assumed plume and take air samples. This method depends on the knowledge of the source region and the quality of the plume prediction. As the samples in this scenarios are grab samples taken at various locations the background analysis has to rely on model results. If the location of the source is known exactly, it would be more effective to inspect the facility itself directly in most cases. Outside the legal restrictions of the IAEA safeguards framework the method could be important if the country under suspicion is not cooperating and does not permit taking air samples on its territory but the borders are reached by ^{85}Kr plumes from a suspicious site.

2.3 Properties of ^{85}Kr

Krypton is a chemically inert noble gas with the atomic number 36. The atomic mass ranges from 71 to 95 while the stable isotopes are ^{78}Kr, ^{80}Kr, ^{82}Kr, ^{83}Kr, ^{84}Kr, and ^{86}Kr (Firestone et al., 1999). The isotope ^{84}Kr has the highest abundance as listed in Table 2.1. Besides that, there are also the short lived metastable states ^{79m}Kr, ^{81m}Kr, ^{83m}Kr and ^{85m}Kr. An analysis of isotopic ratios of stable noble gases in the gaseous effluents of a reprocessing facility was also discussed for safeguards applications (Aregbe et al., 1997). The krypton background part can be determined according to the measured purely natural ^{82}Kr and the isotopic ratios can get analyzed by mass spectrometry. The advantage of using ^{85}Kr for safeguards applications is that it occurs as fission product exclusively. The solubility of ^{85}Kr in water in the equilibrium is given by Izrael et al. (1982) as $1.85 \cdot 10^{-10}$, thus dissolution in oceans and wet deposition as concentration sink can be neglected but ^{85}Kr is soluble in resins and fats.

Kr	Spin	Half-Life	Natural abundance	^{8x}Kr/Kr fission gas
78	0+	stable	0.35 %	
79	1/2-	35.04 h		
80	0+	stable	2.25 %	
81	7/2+	$2.29 \cdot 10^5$ y	$5.2 \cdot 10^{-13}$	
82	0+	stable	11.6 %	
83	9/2+	stable	11.5 %	11%
84	0+	stable	57.0 %	31%
85	**9/2+**	**10.756 y**	$< 10^{-14}$	**6%**
86	0+	stable	17.3 %	52 %
87	5/2+	76.3 m		

Table 2.1: Isotopic composition of krypton - natural abundance according to Firestone et al. (1999) and Collon et al. (2004), measured fission product proportions according to Hudson (1993) for 3.5% ^{235}U fuel with $\approx$ 31 GWd/tU burn up after one year cooling time.

The effective radiation dose on humans caused by ^{85}Kr is about $8 \cdot 10^{-9}$ Sv per year and $\mathrm{Bq\,m^{-3}}$ (Eckermann and Ryman, 1993). Therefore, it can be considered as irrelevant under radiation protection aspects. As shown by Grassl (1989) ^{85}Kr ionizes the air through its β-decay. Nevertheless an effect on air-electricity relevant to weather or climate is highly unlikely as the absolute concentrations are negligible in comparison to ionization by cosmic rays and environmental radioactivity.

2.4 Emissions of ^{85}Kr

The natural background of ^{85}Kr produced by cosmic neutrons is estimated in Styra and Butkus (1991) to 0.15 TBq per day globally – so the natural production rate is smaller by 5 orders of magnitude than the current anthropogenic emissions, and the natural part of the ^{85}Kr background concentration is in the order of $10^{-4}\,\mathrm{Bq\,m^{-3}}$. Thus, any relevant appearance of ^{85}Kr in the atmosphere is of anthropogenic origin. Furthermore, the very small cosmogenic background is homogeneously distributed over the globe. In this section the various anthropogenic sources and their influence are discussed.

Figure 2.1: Sites of nuclear fuel reprocessing included in the emission inventory.

2.4.1 Database for emissions from reprocessing facilities

As long as the nuclear fuel rods stay assembled, less than 1% of the krypton produced by fission escapes. During opening and mechanical chopping in the reprocessing plant 2%–6% gets released. The remaining 94%–98% are emitted during the chemical dissolution of the fuel in acid (Hudson, 1993). Winger (2002) compiled a comprehensive inventory of the ^{85}Kr emissions of reprocessing facilities from 1945 to 2000 on the basis of previous publications and information provided by Martin Kalinowski. For the current project this inventory was extended to 2007 and updated by Ahlswede et al. (2009). For some facilities new information sources are available for a reviewed estimation of emissions. For the current study, facilities at 28 locations were taken into account as shown on the map in Figure 2.1 and listed in Table 2.2. The emission inventory used for the global background simulation is attached in Appendix A. For the European and Japanese sites declarations published by the plant operators are available. The emission strength for other sites is estimated according to the heavy metal throughput, the amount of plutonium separated, or the burn-up of treated spent nuclear fuel. In some cases only guesses depending on capacity and operation time as far as known could be made. The accuracy of the declarations is supposed to be better than 3%. The uncertainty of the estimated emissions is in the 10%–20%

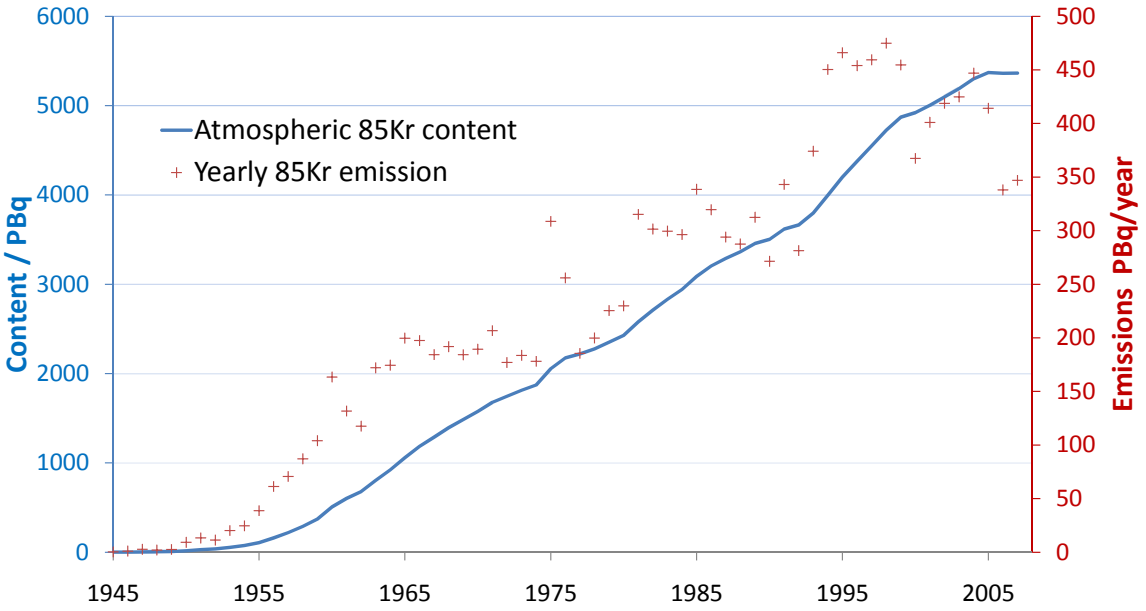

Figure 2.2: Global atmospheric ^{85}Kr content (radioactive decay included) and yearly emissions from reprocessing according to Ahlswede et al. (2009).

range und even higher for some small facilities without any reliable information. The emission data are available on annual basis. For the long term global ^{85}Kr distribution in coarse resolution this is sufficient. On the regional scale for advanced background prediction, temporally higher resolved emission data would be desirable. Figure 2.2 shows the temporal evolution of the global amount of ^{85}Kr in the atmosphere and the yearly global emissions. The total initial emissions add up to 14458 PBq. The contemporary ^{85}Kr content of the atmosphere reached a plateau of about 5360 PBq in 2005. When the new Japanese reprocessing plant Rokkasho becomes operational on full scale, the global ^{85}Kr content is expected to increase again.

2.4.2 Unconsidered sources of ^{85}Kr

The simulation study of this thesis focuses on reprocessing plants as main emitters of ^{85}Kr. In the following sections other types of ^{85}Kr sources are presented and the strength of their influence is estimated.

Site	Country	Operation	max PBq p.a	
Ezeiza	Argentina	1989-1990	< 1	
Mol	Belgium	1966-1994	8	(1973)
Guangyan	China	1975-1990	3	
Jiuquan	China	1968-1991	1	
La Hague	France	1965-	320	(1998)
Marcoule	France	1959-1997	23	(1983)
Karlsruhe	Germany	1971-1990	4.3	(1977)
Kalpakkam	India	1996-	6	
Tarapur	India	1979-	1.2	
Trombay	India	1964-	1.2	(1974)
Dimona	Israel	1965-	< 1	
Rotondella	Italy	1975-1980	< 1	
Saluggia	Italy	1971-1983	< 1	
Rokkasho	Japan	2006-	46	(2007)
Tokai	Japan	1977-	14.5	(1991)
Yongbyon	North Korea	1989-2006	< 1	
Nilore	Pakistan	2000-	< 1	
Mayak RT-1	Russia	1950-	114	(1975)
Seversk	Russia	1955-	63	(1975)
Zheleznogorsk	Russia	1958-	50	(1975)
Pelindaba	South Africa	1986-1992	< 0.1	
Dounray	UK	1976-1995	< 1	
Sellafield	UK	1952-	120	(2004)
Hanford	USA	1945-1988	67.6	(1964)
Idaho	USA	1953-1983	5.5	(1970)
Oak Ridge	USA	1980-1981	< 1	
Savannah	USA	1955-1988	70.3	(1960)
West Valley	USA	1966-1971	10.5	(1969)

Table 2.2: Reprocessing facility sites with operation time and maximum annual emissions (and year of the maximum emission) in the emission database for the background simulation (Ahlswede et al., 2009).

a) Operational releases of nuclear power plants

As discussed above, more than 99% of the ^{85}Kr content of a nuclear reactor remains in the fuel rods. Therefore there are only minor ^{85}Kr releases from nuclear reactors during normal operation. As far as emission data are available, they were evaluated by Kalinowski and Tuma (2009) with respect to radioxenon. Where ^{85}Kr emissions were reported, the analogous evaluation gives a global estimate of in total 0.17 PBq ^{85}Kr activity of reactor emissions per year which would correspond to 0.46 GBq ^{85}Kr per MW electric power per year (Ahlswede et al., 2009). This is not required to be taken into account for the background simulation study as it contributes well below one percent of the global emissions from reprocessing. La Hague for example has the capacity to emit more than 1 PBq of ^{85}Kr per day.

b) Isotope production facilities

Additional emissions of ^{85}Kr are caused by isotope production for medical purposes. There are only five large isotope production facilities active in the world. The reactors in Canada and the Netherlands account for 70 % of the world's molybdenium-99 production, the facilities in Belgium, South Africa and France contribute another 25%. According to Reistad and Hustveit (2008) 5% are produced in smaller facilities. Grosch (2008) estimated the world technetium-99m demand for medical use to be 25.2 PBq. The concurrent ^{85}Kr production is dependent on the assumed irradiation scenario and ranges according to calculations by Hebel (2008) from 0.8 TBq to 4 TBq per year. Thus the emissions can be neglected for the global background.

c) Reactor accidents

If a nuclear reactor becomes damaged and nuclear fuel elements are ruptured, connected with very high temperatures and loss of the reactor shielding, large amounts of the trapped ^{85}Kr can be released into the atmosphere.

The fire at the British reactor Windscale in 1957 lead to an emission of 45 TBq ^{85}Kr as estimated by Garland and Wakeford (2007). The Three Mile Island accident in 1979 released approximately 1.7 PBq ^{85}Kr into the environment (Kunz et al., 1985).

The catastrophe of the Chernobyl reactor in 1986 caused a release of 33 PBq ^{85}Kr according to IAEA (1986). Sich et al. (1994) gave 28 PBq as total ^{85}Kr source term of the Chernobyl accident. This led to a ^{85}Kr concentration peak observed at many European stations. The Chernobyl emissions are not included in the annual emission data for the global background simulation and thus have to be considered for the interpretation when comparing with measurements. This effect is most evident in the observation data from Krakow (Appendix B, Figure B.1).

d) Nuclear explosions

From 1945 to 1996, 2398 nuclear explosion were conducted by the five NPT acknowledged nuclear weapon states. The nuclear tests had a cumulative explosive yield of 520 Mt TNT equivalent (Andryushin et al., 1999). 522 of these test explosions took place in the atmosphere which account for 440 Mt TNT eq. as they had stronger yields than the following underground tests (1519 tests, about 79 Mt TNT equivalent). The nuclear explosions conducted by India, Pakistan, –if so– South Africa, and North Korea are not included in these numbers. The total initial production of ^{85}Kr in atmospheric tests up to 1980 is estimated in the UNSCEAR (1982) report to equal 160 PBq. As most of the tests in the atmosphere took place until 1962, a large fraction of ^{85}Kr has already decayed in 1980. Rózanski (1979) calculated that 74 PBq ^{85}Kr from nuclear weapon testing were still present in the atmosphere at the end of 1977 – which accounted for about 3% of the total ^{85}Kr content at that time. The emission quantity of ^{85}Kr from underground testing is harder to determine as the noble gases are not necessarily completely released into the atmosphere. Nevertheless various pathways for the noble gases to evade from underground test explosions are known, as for instance direct venting, later operational releases, barometric pumping. Due to the radioactive decay and the strong increase of ^{85}Kr released by reprocessing activities, ^{85}Kr originating from former nuclear explosions can be estimated to count nowadays less than 1% of the ^{85}Kr in the atmosphere. The 74 PBq ^{85}Kr from 1977 decayed to remaining 10.7 PBq until 2007 which was 0.2% of the global ^{85}Kr content at that time. Hence, for the assessment of present ^{85}Kr concentrations, the contribution of historical nuclear explosions is negligible.

e) Industrial applications of ^{85}Kr

The isotope ^{85}Kr has some technical applications as calibration beta source in measurement technologies. For example automatic thickness gauge is performed in the paper-, textile- and plastic-industry by measurement of beta transmission (Shimizu, 1981). The activity of the encapsulated sources used in this kind of procedure is usually only in the range of 100 MBq to 50 GBq (Bergman and Pettersson, 1994). If they are accidentally released, radiation protection measures in the factory –e.g. ventilation– have to be taken. Nevertheless, the possible emissions in case of an accident are by three orders of magnitude smaller than daily emissions of a medium scale reprocessing facility and thus irrelevant for the scope of this study.

2.4.3 Countermeasures to a possible ^{85}Kr detection

When assessing the potential detectability of nuclear reprocessing, possible countermeasures have to be considered. The grade of difficulty of hiding ^{85}Kr emissions is an important criterion for the IAEA for the assessment of the feasibility of the method. In principle the operator has several basic possibilities in order to hide ^{85}Kr emissions:

- Keeping ^{85}Kr production in the fuel as low as possible
- Configuring the initial dilution of emissions and use large stack heights
- Selecting weather conditions unfavorable for assumed sampling scheme
- Retaining ^{85}Kr from the off-gas stream and store it or delay and dilute the emission pulse

The potential of success for these countermeasures is briefy discussed in the following sections.

a) Specific source term

The amount of ^{85}Kr produced during plutonium breeding depends on the irradiated material and the fuel burn-up. Earlier estimates were provided in the study of von

Hippel et al. (1986). The most recent calculations of the specific ^{85}Kr source term were performed by Stanoszek (2008). For different grades of enrichment and burn-ups the values of the specific source term ranges from 10 to 50 TBq ^{85}Kr per kilogram separated plutonium. Depleted uranium as target material provides the lowest ^{85}Kr production. For the distinct weapon grade plutonium production low burn-up is used to avoid too large fractions of ^{240}Pu and consequently the ^{85}Kr release is smaller. Nevertheless, if fuel rods from commercial power plants are reprocessed, the specific source term is in the higher range (Stanoszek and Kalinowski, 2009). For the emission scenarios applied in Chapter 6 a specific source term of 20 TBq ^{85}Kr per kg separated plutonium was agreed with the IAEA.

b) Source configuration

In the direct vicinity of a ^{85}Kr source the ^{85}Kr concentrations can depend on stack height, emission gas temperature, local orography, and actual atmospheric stability conditions. These factors are to be considered when measuring or simulating concentrations within 30 kilometers from the site. To avoid detection, the operator of a facility could try to chose parameters and times of emission, that minimize the induced ^{85}Kr concentrations in the surrounding area. For the large scale background distribution shown in Chapter 4 the local source configuration is not relevant as the emissions are considered to be well mixed over the planetary boundary layer.

c) Retention technologies

One possibility to avoid detection is to separate the ^{85}Kr from the gas effluents. Storage of the radioactive gas is a further challenge for the operator of a reprocessing facility with retention. As ^{85}Kr is chemically inactive, separation technologies have to be based on physical properties of krypton. The following techniques are considered, a detailed description is given by Nichols and Binford (1971), the technologies are also briefly described by Schoetter in the project report (Ross et al., 2009)

- cryogenic distillation
- selective absorption in fluorocarbons

- charcoal adsorption
- selective membrans

The cryogenic distillation was successfully tested at Tokai reprocessing plant, the selective absorption was only successfully tested with non radioactive krypton. For the storage of ^{85}Kr different approaches such as the ion implantation method or the zeolith encapsulation method exist (Ross et al., 2009). To develop and implement such a technology imposes a immense effort to the operator – the risk of an accidental ^{85}Kr release remains. Especially for a large scale plant the complete ^{85}Kr confinement is very difficult because of the large volume of radiative gas effluents and the storage demand. If only very small amounts of spent fuel are reprocessed, adsorption of ^{85}Kr in charcoal at liquid nitrogen temperature may be possible.

2.5 Measurement technologies

Common ^{85}Kr measurement methods rely on the measurement of the radioactivity. This is why ^{85}Kr concentrations are usually given in $\mathrm{Bq\,m^{-3}}$ instead of mass or particle concentrations and mixing ratios. The classical measurement using beta decay is described briefly, then alternative measurement technologies are introduced.

2.5.1 β-counting

First, the noble gases are separated from the air sample by filtering through a charcoal adsorption canister. After that, they are extracted from the charcoal by heating. Then the noble gas fractions are separated using gas-chromatography. Finally the concentrated krypton sample is analyzed in a β-counting chamber. In order to obtain the concentration of ^{85}Kr in the original air sample, the amount of ^{85}Kr in relation to the total krypton in the sample is determined and the ^{85}Kr per air volume at standard temperature and pressure (STP) is calculated which is 0 degree Centigrade and 1000 hPa.

2.5.2 Observation network

The German Federal Office for Radiation Protection (BfS) operates a network of ^{85}Kr monitoring stations (Figure 2.3) in Europe and a few stations on other continents. Since 2008 there is an additional sampling station operating at the Centre for Science and Peace Research, University of Hamburg. Due to the comparatively low activity level, the air samples have to have a certain minimum size; at least 30 liters but more commonly around 200 liters have to be collected for a determination of the ^{85}Kr-concentration level. The main dataset of weekly sampling with air accumulated in the sample during the week (except Antarctica with one day sample per week) is summarized in Table 2.3. It was provided by BfS in the framework of a cooperation agreement with the University of Hamburg. In addition, supplementary measurement data from various publications are used for evaluation of the simulated concentrations in Chapter 4. For a comprehensive evaluation of the coarse global model the distribution of the observation sites with several stations in Europe and only a few on other continents, especially on the Southern Hemisphere is unsatisfactory, but corresponds at least partially to the distribution of the big reprocessing sites.

2.5.3 Novel Technologies

For an application of new ^{85}Kr sampling procedures which will be discussed in Section 2.2.4 more flexible measurement technologies for operation in the field are desirable. The two methods introduced here are also laboratory based for the final ^{85}Kr evaluation but reductions in sample size are possible. The goal for the atom trap trace analysis is to collect bottled air samples with the size of only one liter. The separation of the krypton part of the sample beforehand is also necessary for these methods.

a) Mass spectrometry

The ratios of krypton isotopes in the off–gas of reprocessing facilities are sometimes analyzed in a mass spectrometer (Hudson, 1993). The challenge in environmental air samples is the extremely small fraction of ^{85}Kr. To get this ultra fine traces isolated

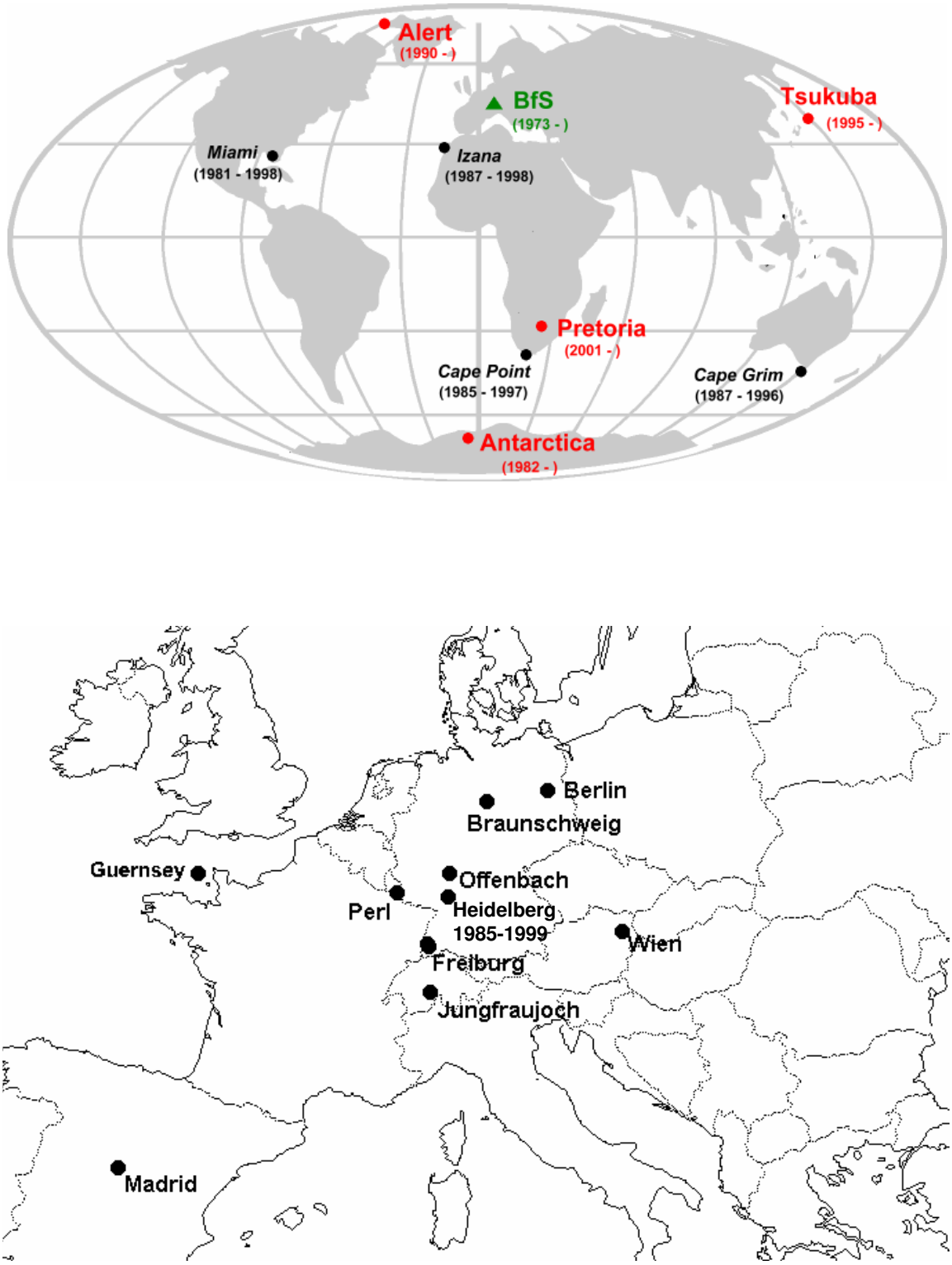

Figure 2.3: Locations of BfS measurement sites as of 2003 (source: BfS).

Location	LAT	LON	Alt. a.s.l./m	Available period
Freiburg	48.0°N	7.9°E	276	1973 – 2006
Schauinsland	47.9°N	7.9°E	1205	1975 – 2006
Miami	25.7°N	80.3°W	10	1981 – 1998
Antarctica	70.6°S	8.4°W	42	1982 – 2000
Krakow	**50.1°N**	19.9°O	261	1981 – 1988
Heidelberg	49.4°N	8.7°E	116	1985 – 1996
Madrid	40.4°N	3.7°W	650	1981 – 2006
Tsukuba	36.1°N	140.1°E	40	1995 – 2006
Jungfraujoch	46.6°N	8.0°E	3454	1990 – 2006
Perl	49.5°N	6.4°E	353	1989 – 2006
Alert	85.5°N	62.0°W	187	1990 – 2001
Vienna	48.2°N	16.4°E	172	1988 – 2006
Cape Point	34.4°S	18.5°E	210	1985 – 1997
Cape Grim	40.6°S	144.6°E	94	1987 – 1996

Table 2.3: Observation sites and sampling periods provided by BfS according to the cooperation agreement with the University of Hamburg for evaluation of model results in Chapter 4.

from isobars in a mass spectrometer, a huge effort, for example with accelerator techniques, is necessary. An advantage of mass spectroscopy is the availability of the full isotopic fingerprint of the sample.

b) Atom trap trace analysis

A new measurement technology is currently under development at the Centre for Science and Peace Research in Hamburg for future flexible measurement procedures: Using the spectroscopic Atom Trap Trace Analysis (ATTA) method the krypton atoms are cooled (i.e. slowed down) by lasers of a specific wave length and caught in a magneto–optical trap (Chen et al., 1999). The fluorescent emissions of ^{85}Kr as well as of ^{81}Kr can be identified by switching between the specific frequencies. So the ratio between those two isotopes can be determined and the ^{85}Kr concentration in air can be calculated because the ^{81}Kr background concentration can be considered as globally constant due to its half–life of 229000 years and constant production rate in nature (Table 2.1).

3 Modelling tracer transport with ECHAM5

For the calculation of the global long term ^{85}Kr background and its variability caused by known nuclear reprocessing facilities the general circulation model ECHAM5 is used. ECHAM5 was proofed to simulate the global atmospheric dynamics well in long term climate predictions (Gleckler et al., 2008). The model supports the transport of passive trace species. These additional tracers are transported like water vapor, which is of special importance for cloud-climate feedbacks. But the knowledge of the exact global budget of water vapor is not such important for climate prediction and the gradients of water vapor are rather smooth. However, for the calculation of ^{85}Kr background concentrations and their application in IAEA Safeguards, the accuracy of the mass budget and the stability under occurrence of strong concentration gradients is of special importance. Hence, the model first had to be tested on its transport properties with respect to the requirements of simulating ^{85}Kr point sources. After a general introduction to the model more details on the tracer transport processes are given. In particular, the tests and modifications which were applied to the model for this specific project are described.

3.1 Model description

ECHAM5 is based on the global weather forecast model of the **EC**MWF (Simmons et al., 1989) and was partly developed at the Max Planck Institute for Meteorology in **HAM**burg. ECHAM5 is the fifth generation of the European Centre-Hamburg general circulation model. It is a hydrostatic model. The prognostic equations of the dynamical core are solved in a spectral representation. The vertical levels are

terrain following hybrid sigma pressure coordinates. An energy and angular momentum conserving finite differences scheme is implemented for the vertical integration. The tracers are transported on an Arakawa C-grid (Mesinger and Arakawa, 1976). A more detailed model description is given in (Roeckner et al., 2003). ECHAM5 contributed to the scenario experiments used in the Fourth Assessment Report of the Intergovernmental Panel on Climate Change (IPCC) (Solomon et al., 2007).

3.2 Tracer transport in ECHAM5

The tracer transport in the model consists of large scale advective transport, vertical turbulent diffusion, and cumulus convection. The following basic requirements are imposed to a tracer transport scheme:

- the tracer mass mixing ratio has to be positive semi-definite
- in absence of sources or sinks, a spatially constant tracer mass mixing ratio must remain constant in time
- tracer mass has to be conserved in the column during convection

For this study, a new sub-model called `mo_transport` for implementation of ^{85}Kr emissions and initializing of transport and radioactive decay was implemented into ECHAM5. A brief technical description of the sub-model is given in Appendix D.1. First, the transport properties of ECHAM5 have been tested with a single tracer point source in an atmosphere initially free of tracer. These tests have shown that negative tracer concentrations occur using the original version of the transport scheme in ECHAM5. Additionally, the spatial distribution of the tracer calculated by the model has shown unreasonable patterns. It was found, that the convection and advection scheme cause these erroneous results. The convection scheme allows large upward fluxes which may lead to negative concentrations, if there is more tracer transported out of a grid box in one time step than its tracer content. These negative concentrations force the zonal mass fixer applied in the advection scheme to produce artificial concentration extrema at 0°longitude as shown in Figure 3.1. In the following, each transport process which changes the tracer concentrations is shortly analyzed and the modifications implemented for the ^{85}Kr background simulation are described.

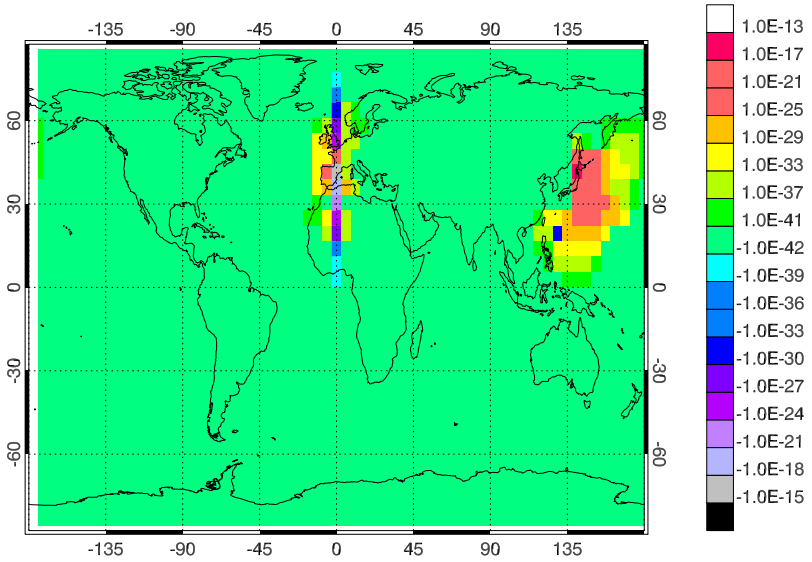

Figure 3.1: Negative mass-mixing ration at 0°longitude 6 hours after start of emissions positioned in north-east Japan.

3.2.1 Advective tracer transport

The equation for passive tracer (mixing ratio X) advection in an incompressible fluid with velocity $\vec{v}$ is

$$\frac{\partial X}{\partial t} + \nabla \cdot \vec{v} X = 0. \tag{3.1}$$

The advective tracer transport in ECHAM5 is calculated according to the Semi-Lagrange flux form scheme developed by Lin and Rood (1996). This transport scheme is intrinsically mass conserving if surface pressure (respectively air mass) and tracer mass mixing ratios are processed in the same way. However, in ECHAM5 the logarithmic surface pressure is integrated in spectral space over time while the tracer concentrations are transported in grid point space. As the tracer mass mixing ratios depend on the total air mass, the tracer mass is not conserved exactly.

After implementation of the correction routine on the original Tiedtke (1989) scheme described in 3.3.1, test runs with a single point source over a longer time period were performed (starting on a spatially constant initial tracer field). They have shown that the global tracer mass was not exactly conserved but increasing by about 4% per year. In a test series to investigate the mass error with the different transport processes active and inactive, respectively, it has been shown that the advective transport

alone is responsible for the poor conservation of mass. A further mass inconsistency between the transported tracer and the dry air is caused by the calculation of the sigma hybrid levels from the surface pressure, which implies a vertical redistribution of air mass at each time step (Jöckel et al., 2001). There is an iterative routine implemented in the advection module which adjusts the wind fields to avoid the latter mass wind field inconsistency. The number of cycles of this mass wind field iterator was set to 8 instead of the default value 0. The mass error of advection was decreased by nearly one order of magnitude in this way. The remaining mass error was in the order of 10^{-7} per 12 minutes time step.

It is not possible to apply an exact global mass fixer to the advection routine due to the specific time integration scheme and influence of the time filter (described in Section 3.2.5). As the dry air mass after advection is not available within the current time step the tracer mass related to the new surface pressure is not known and therefore not correctable. It has to be noted, that the total mass of dry air represented in the average surface pressure – spectral coefficient 0 – is fixed in ECHAM5.

3.2.2 Vertical diffusion and emissions

The vertical mixing of air by diffusive turbulent exchange is one of the basic vertical transport mechanisms. The vertical propagation of quantities in the model depends on the exchange coefficients K. In ECHAM5, it is parameterized over a turbulent kinetic energy closure with the mixing length approach according to Blackadar (1962). The mixing length is 150 m in the boundary layer and exponentially decreasing above. The emissions are injected as lower boundary conditions i.e. surface fluxes into the vertical diffusion equation. Due to the coarse resolution of the global model it seems to be realistic to distribute the tracer immediately over the boundary layer in comparison to an injection only into the lowest box of the column in the model. In the resolution applied the time step length was 12 minutes. Thus, depending on the meteorological conditions, a vertical distribution of the tracer over the boundary layer within the time step of emission is plausible.

3.2.3 Cumulus convection

As cumulus convection is a subscale process in ECHAM5 even in the high resolutions, only empirically parameterized equations can be used. In ECHAM5 the parameterization of Tiedtke (1989) is used with modifications introduced by Nordeng (1994). In this convection scheme the grid box is divided into a fraction of upward mass flux M_u, a downward mass flux M_d, and the environment mass flux M_e without convection where differences between updraft and downdraft are balanced so that $M_u + M_d + M_e = 0$. The equation for the convective part of tracer transport in ECHAM5 is

$$\frac{\partial \overline{X}}{\partial t} = -\frac{1}{\overline{\rho}} \frac{\partial}{\partial z} \left[M_u X_u + M_d X_d - (M_u + M_d)\overline{X} \right]$$

where X is the tracer mass mixing ratio. The overbar indicates box averages. The change of convective mass flux with height is governed by entrainment and detrainment. Tiedtke distinguishes between turbulent mass exchange at the cloud edges and organized in- and outflow at cloud base and top. Details about the exact definition of parameters for up- and downdrafts and mass-fluxes are given in the original publication (Tiedtke, 1989). The deficit of this convection scheme is the possibility of negative concentrations in presence of strong gradients. In Section 3.3 the modifications in order to correct this misbehavior are described.

3.2.4 Numerical diffusion

As discussed in Section 1.1 the calculation of tracer transport on an Eulerian grid implies numerical diffusion. The emissions are immediately distributed over the whole grid cell in which the source is located. This intrinsic start dilution is an obvious property of modeling tracer concentrations in the Eulerian domain. Another effect, which is briefly described in this section is the resolution dependence of the horizontal transport on numerical diffusion. There is no physical parameterization of horizontal turbulence in ECHAM5 as the numerical effects represent the phenomenological characteristics by chance. For testing the resolution dependence of the horizontal diffusive transport a test series with the following setup was conducted:
An emission pulse of 40 minutes length with the same total mass of tracer was injected starting at 6 a.m. in three different model configurations:

1. Emission in one grid cell in T63 resolution
2. Emission distributed over 9 (3×3) grid cells in T63 resolution covering approximately the same area as one T21 cell
3. Emission in one grid cell in T21 resolution

The vertical resolution was the same for every setup (19 levels). The temporal development of the maximum concentration was observed for an integration time of two days. The comparison of the first two cases with T63 resolution shows that the initial dilution becomes less important with time: After 35 hours integration time, the maximum concentrations in T63, which differed initially by a factor of nine, converged again to a difference of 23 %. However, the maximum plume concentration simulated in the T21 resolution with the same starting concentrations as case 2. at 6:40 a.m. is by a factor of 3.6 smaller than the respective concentration in the run in higher resolution after 35 hours. This indicates that the tracer transport in the model is much more diffusive in T21 resolution. As the atmospheric dynamics were similar but not exactly the same in the two different resolutions, the numbers given are only an estimate to give a qualitative description of the issue. For an exact assessment of the numerical diffusion in different resolutions, simulation experiments with forced identical conditions have to be constructed. The resolution dependence of concentrations caused by pulse emissions is not as important for the simulation of the long term global ^{85}Kr distribution with constant emissions, as fresh plumes close to sources are not considered for the evaluation of the background concentrations in the global model.

3.2.5 Time integration scheme

The time integration method used in ECHAM5 is a semi implicit leap frog scheme. At each time (t) the prognostic variables for the next time step (t^+) are calculated based on the one before (t^-) with a small contribution from the actual one by the time filter explained below. The actual prognostic calculation time step covers a difference of (t^+)-(t^-) = 2 Δt. To prevent oscillations and runaway effects, a time filter is implemented in the semi implicit time integration scheme. According to the

equation

$$X_f = X + \epsilon_f(X_f^- - 2X + X^+)$$

it mixes a fraction of terms of the current time step X to the value for the prognostic time step. In the code, the time filter has to be split into two steps since X^+ is not available yet within the current time step. The coefficient ϵ_f is chosen empirically, there is no theoretical foundation for the strength of the time filter. A special problem caused by the time filter is that it slows down fast changes of concentrations. This is in particular relevant for chemistry processes, where some short-lived species should vanish completely within one time step. So the life-time of the tracer is artificially modified. This raises the question, whether it is necessary to process tracer mass mixing ratios through the time filter or if it is sufficient to filter the prognostic variables. If doing so, it has to be guaranteed, that the concentrations on the two parallel time lines do not diverge.

3.3 Modifications applied to the transport scheme

The occurrence of strongly negative concentrations above a single point source and the worldwide spread of the negative values caused by the advection scheme cannot be accepted for the simulation of ^{85}Kr background. Consequently, the model was changed in a way that non-negative tracer concentrations are guaranteed. The first issue was to prevent the convection scheme from generating negative tracer mixing ratios. In the following, the operator splitting was changed so that negative concentrations are impossible.

There exists a modified version of the Tiedtke mass flux scheme developed by Brinkop and Sausen (1997a) in order to maintain positive tracer concentrations. An implementation of this scheme into ECHAM5 was tested, but two difficulties appeared: If the levels above the emission source did not contain any tracer, the convection was suppressed by the last step of the Brinkop-Scheme, the so called security check (Brinkop and Sausen, 1997b). Furthermore, the Brinkop scheme changed vertically uniform tracer fields in regions of strong convection (Figure 3.2). Cross checking tests with another implementation of Brinkop's changes in the regional model version REMO showed similar effects (Teichmann, 2009). The constancy of tracer mass

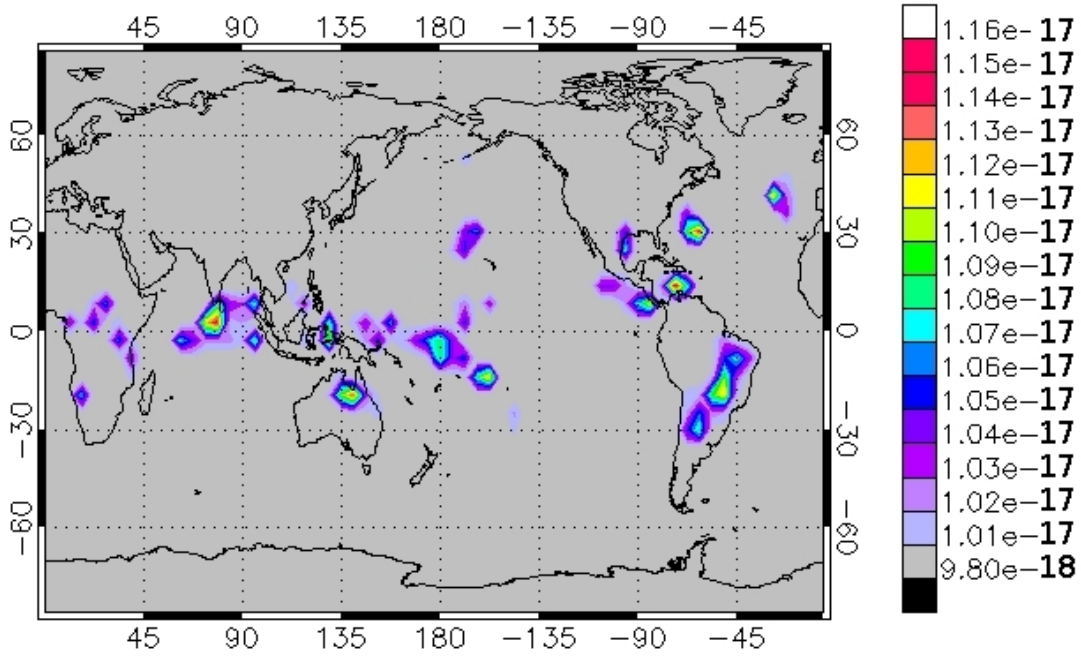

Figure 3.2: An originally uniform tracer field of mass mixing ratio 10^{-17} is modified by the Brinkop convection after 24 hours.

mixing ratios in absence of sources is a basic property of any transport process and very important for ^{85}Kr with only small concentration gradients far from the sources. Consequently, the Brinkop scheme is not suitable for the purpose as more than 10% variation was observed after 24 hours in the concentration profiles of an initially uniformly distributed tracer. Thus an alternative correction routine was developed to be applied on the concentrations after convection which guarantees non-negative tracer concentrations and mass conservation.

3.3.1 New correction routine for the convection

As stated before, there are the basic requirements on tracer transport schemes to maintain positive concentrations, conserve mass and not to arbitrarily modify tracer concentrations. In order to achieve these aims for the parameterization of cumulus

convection, a simple but computational efficient correction was developed which is described below. Quantities entering the convection scheme are denoted by an index $t-$, those after the convection scheme by an index $t+$. Thus from the knowledge of the tracer tendencies ΔX_{t-} and ΔX_{t+} before and after the call of convection in ECHAM5, the tracer tendency due to convection alone can be calculated by

$$\Delta X_{\text{conv.original}} = \Delta X_{\text{t+}} - \Delta X_{\text{t-}} \tag{3.2}$$

With this tendency of the convection an intermediate concentration X'_{t+} as it would result without correction is calculated based on the mass mixing ratio which entered the convection:

$$X'_{t+} = X_{t-} + \Delta X_{\text{conv.original}} \Delta t \tag{3.3}$$

This is the tracer concentration after convection without correction. These intermediate concentrations X'_{t+} are then modified to be all non negative in one of the following ways

1. Cut all negative concentrations by setting the concentration to 0 (cutting method)

$$\tilde{X}_{t+} = 0 \; \forall \; X'_{t+} < 0 \tag{3.4}$$

   To avoid negative values by computational artifacts, instead of zero a very small value, e.g. 10^{-32}, can be chosen, in the test cases described below this did not lead to different results.

2. Shift all concentrations in the convective column by the absolute value of the lowest negative concentration (shifting method)

$$\tilde{X}_{t+} = X'_{t+} + |\min(X_{t+}; 0)| \tag{3.5}$$

The shifting method will require larger corrections on the column mass but does not change the pattern of the vertical profile by shifting it. Furthermore, it produces fewer levels with concentrations close to zero than the cutting method. If the correction of negative concentrations becomes effective, it "produces mass", so that the concentrations have to be downscaled afterwards for achieving mass conservation. The quantity $M(X)$ is introduced as a column mass summation operator. For mass

conservation a correction factor α is defined with $\alpha M(\tilde{X}_{t+}) = M(X_{t-})$. For the new concentrations X_{t+} mass conservation requires

$$M(X_{t+}) = M(X_{t-}) = \alpha M(\tilde{X}_{t+}). \tag{3.6}$$

As the mass summation is linear the new concentrations are

$$X_{t+} = \alpha \tilde{X}_{t+} \tag{3.7}$$

ECHAM5 applies changes to tracer concentrations through the tracer tendency. The new tendency caused by the corrected convection is then the difference of concentrations before and after convection.

$$\Delta X_{\text{conv.corrected}} = \left(\frac{M(X_{t-})}{M(\tilde{X}_{t+})} \tilde{X}_{t+} - X_{t-} \right) \frac{1}{\Delta t} \tag{3.8}$$

The correction routine considers only levels in which convection takes place. This avoids an erroneous correction of concentrations above the convective column. In all runs obtaining the results presented in Chapter 4 the "shifting"-method was chosen.

3.3.2 Tests of the correction routine

Several tests of the correction routine were conducted which are described in the adjacent paragraphs.

a) Spatially constant initial tracer field, no emissions

As the Tiedtke scheme keeps constant tracer fields constant, the correction routine does not modify the concentrations so that this condition is fulfilled and the tracer mass mixing ratios of a uniform tracer field remain constant in time. Of course the correction routine would intervene in the unphysical case of an initialization with constant but negative concentrations.

(a) Original Tiedtke

(b) Modified according to Brinkop

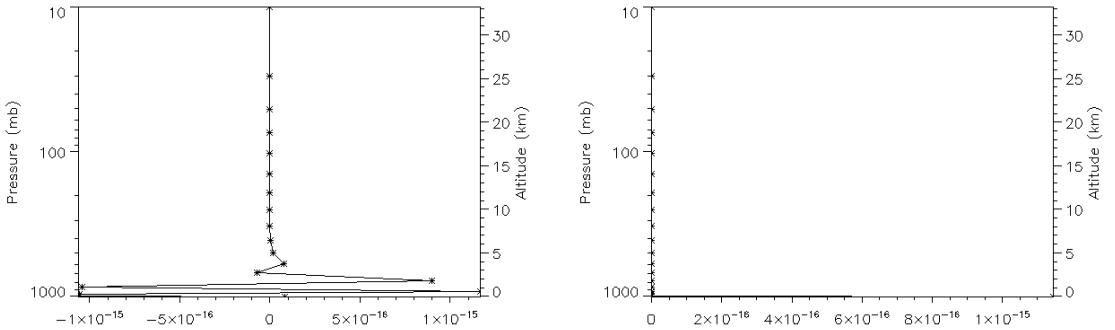

(c) Corrected, cutting method

(d) Corrected, shifting method

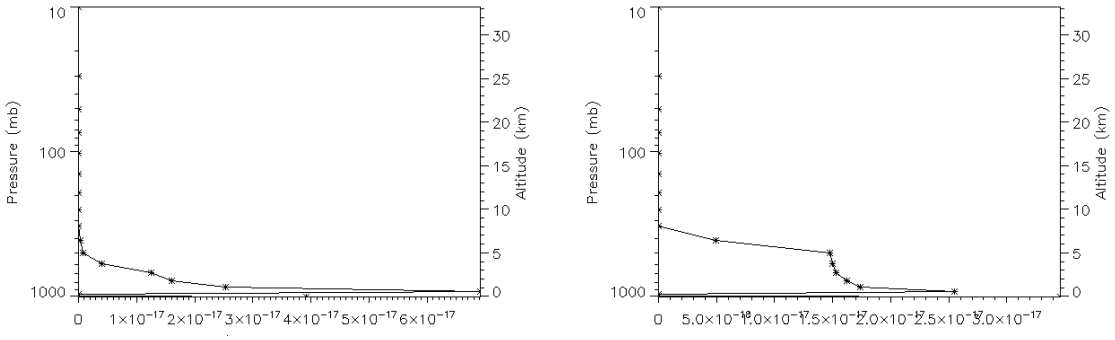

Figure 3.3: Vertical tracer mass mixing profile of convection in one column after 72 hours model run with emission source in the lowest layer and no initial concentration.

b) No initial tracer concentrations, single point source

In former tests the biggest problems occurred when an emission source was introduced in an atmosphere initially free of tracer concentrations. In these tests the emissions are introduced into the lowest box of one column by adding the emission flux to the tracer tendency. Here the emission flux is set to 10^{-7} kg/s which is comparable to the ^{85}Kr outflow of a big reprocessing facility. The next three paragraphs show the test case with various combinations of the single transport processes switched on.

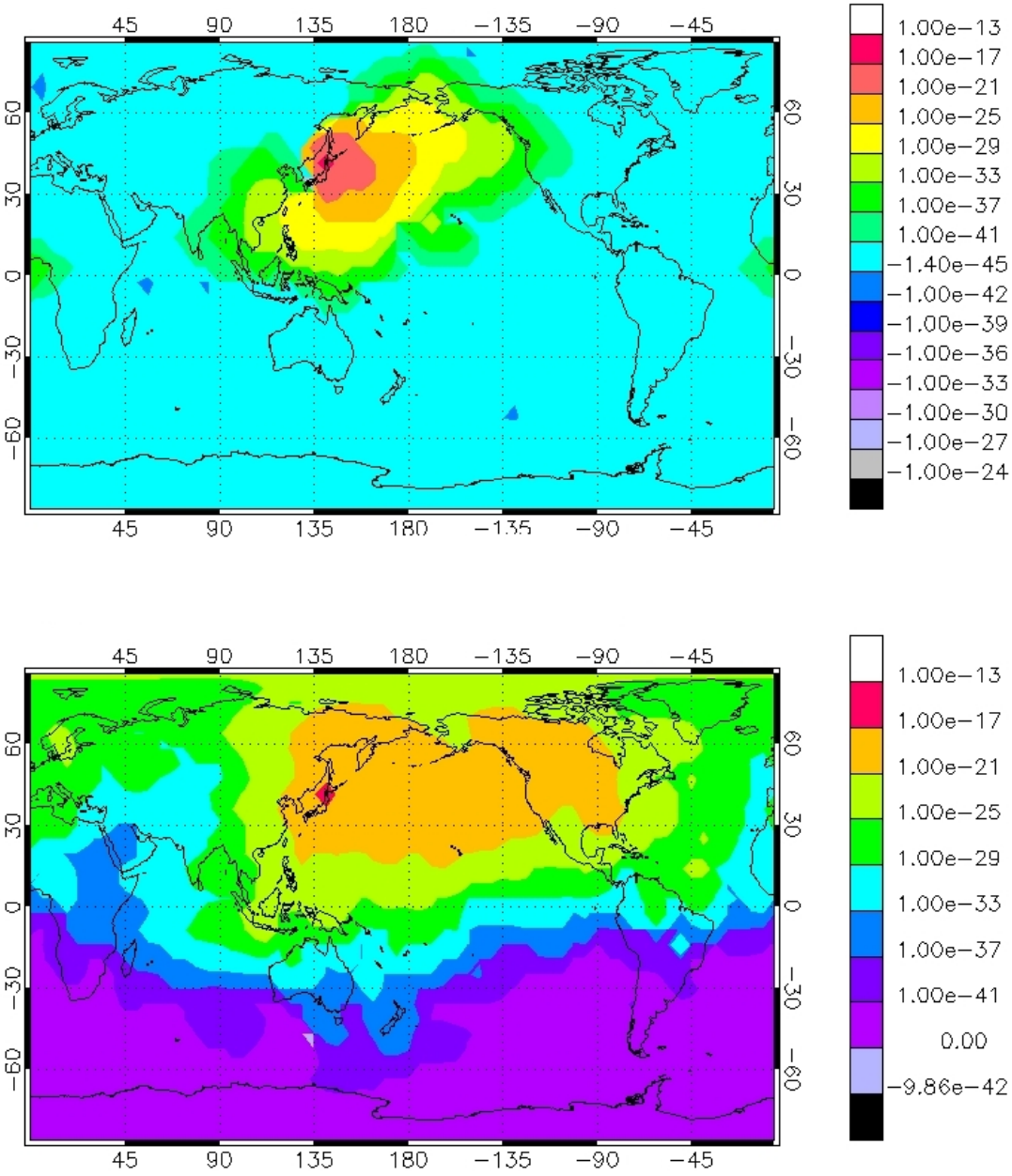

Figure 3.4: Tracer mass mixing ratio distribution at the lowest level, one day (top) and one week (bottom) after emission start. Mind the different color scales.

Convection only

Figure 3.3 shows a comparison of the vertical profiles of the different convection configurations. The original Tiedtke scheme (Figure 3.2(a)) shows strong oscillations in the concentration profile. The Brinkop correction admits no transport out of the lowest layer because the flux scheme would cause negative concentrations in the second lowest level. Therefore, the Brinkop scheme suppresses any tracer mass fluxes and a positive mass mixing ratio is only in the lowest level as hardly discernable in Figure 3.2(b). The two new correction routines differ in the way that the shifting method shown in Figure 3.2(d) leads to relatively high concentrations at the top of the convective column in comparison to the cutting method (Figure 3.2(c)). This is due to very low negative values in the second lowest level. It is not possible to analyze mass conservation except for convection itself, because variations in atmospheric pressure change the air mass in a column, but the advection associated with these pressure changes is not active.

All transport processes active

If all transport processes are switched on in the case of a single tracer source with no initial background concentrations no artifacts occurred at longitude zero which where observed with the uncorrected version. Nevertheless, still small negative concentrations occur. A possible reason for that is the way of operator splitting. In all processes the tracer concentrations of the time step before are entering. Then each process calculates its contribution to the tracer tendency based on the old concentration. In case of small concentrations, negative tendencies of the single processes can sum up and cause a tracer tendency which leads to a negative concentration for the next time step. As the convection correction allows very small positive values, negative tracer tendencies originating from other processes can occur although all processes for itself are positive definite in respect to the concentration of the time step before.

Only advection and vertical diffusion

If the convection is switched off there is transport into higher levels only through vertical diffusion. Therefore the upward tracer transport is weakened compared to runs with active convection. A comparison with vertical profiles produced with active convection shows no unexpected behavior. There occur still small negative concentrations which are supposed to be a consequence of the operator splitting as described in the Section 3.3.3.

c) Uniform initial tracer field with single tracer point source

For this experiment the initial tracer mass mixing ratio was set to 10^{-17}, a value which is comparable to the lowest ^{85}Kr concentrations occurring in the real atmosphere. In the case of convection being the only active transport process, the Tiedtke scheme produces results which are similar to the case with zero initialization because the gradients do not differ very much. If all transport processes are switched on, the misbehavior of the original convection scheme is partly compensated by the background concentration and the other processes. The new correction routine for the convection scheme fulfills the requirements of non negative tracer concentrations. Nevertheless, small negative concentrations occur in the combination with the other transport processes as for example shown in Figure 3.4 (top) in the Southern Pacific. A possible reason is the mode of independent application of all operators to the concentration of the time step before.

3.3.3 Modification of operator splitting

As in nature the processes of tracer transport happen in parallel, a first attempt in modeling is to apply all processes to the concentration of the time step before and adding up the tendencies of the single processes to an overall tendency. This only neglects the cross-terms of processes influencing each other. With large time steps this can lead to negative concentrations in the following way: Each single tendency of the subprocesses can assume a positive or a negative change. Consequently, the

overall ΔX may assume a negative value. In a more schematic way this parallel operating can be denoted as

$$\Delta X = \Delta_{\text{advection}} X_- + \Delta_{\text{diffusion}} X_- + \Delta_{\text{decay}} X_- + \Delta_{\text{convection}} X_-$$

In the standard version of ECHAM5 the operator splitting is more intricate. In principle it is parallel, but for the decay of radionuclides and the convection the model uses concentrations already updated by all previous processes. In the notation introduced above this means for the operator splitting performed in ECHAM5:

$$X_{\text{adv,diff}} = \Delta_{\text{adv}} X_- + \Delta_{\text{diff}} X_- + X_-$$

$$\Delta X = \text{decay}(X_{\text{adv,diff}}) - X_- + \Delta_{\text{conv}} X_{\text{adv,diff,decay}}$$

A consecutive operator splitting was introduced to avoid negative concentrations in any case. As the concentrations are already updated for entering the single processes, the overall tendency is reset to zero. The new tracer tendency is calculated in respect to the updated tracer mass mixing ratio after the last process, i.e. the corrected convection. On the one hand, a disadvantage of this method is the arbitrary order of the single processes in a single time step. On the other hand, it is absolutely safe against negative concentrations and double impacts of processes. Thus the finally implemented operator splitting calculates a tendency based on all processes performed one after another:

$$\Delta X = \text{convection}(\text{decay}(\text{diffusion}(\text{advection}(X_-)))) - X_-$$

The main advantage of this scheme is that negative concentrations are no longer possible as long as the single processes are positive semi-definite.

3.3.4 Global mass conservation

In order to achieve global mass conservation of ^{85}Kr, the global tracer inventory according to the emission data base is calculated for each time step and is compared with the global tracer content of the modeled atmosphere after application of the time filter of the time step before.

The entire tracer field is scaled by a respective factor. Thus the global tracer mass is conserved as it is globally prescribed at each time step. For the calculation of the time dependent inventory the analytical solution of the emission/decay function is used. The code implementation of the global mass fixer is described briefly in Appendix D.4. The tests of the global tracer mass fixer were successful, so that the model was ready to run the global background simulation.

3.4 Description of simulation experiment

The improved version of ECHAM5 was used for the simulations achieving the results on the global distribution of ^{85}Kr and its variability presented in Chapter 4. The following sections describe the basic parameters and conditions of the simulation experiment.

3.4.1 Model setup

For the simulation of global ^{85}Kr background concentrations in ECHAM5 the time period from 1971–2006 was chosen. On the one hand, for the investigation of detectability the main interest is the present time and the near past, on the other hand available continuous measurements for model evaluation started in the early 1970s. For initialization of the simulation from 1971 to 2006, a 3-dimensional concentration field was derived from the data of Winger (2002). The model output of ECHAM4 for December 1970 in T31 L19 resolution was interpolated to the T63 L31 resolution grid and the concentrations were scaled by a global factor consistently to the total ^{85}Kr content of the atmosphere at the end of 1970 according to the emission inventory. The resolution of T63 L31 was chosen because of the high model performance at this resolution as best compromise between accuracy and necessary computing time. T63 L19 is not used because of the coarse representation of vertical transport, T83 L31 as next highest resolution has been tested by Roeckner et al. (2006) and showed no large gain in model performance compared to T63 L31. The spectral truncation T63 results in a spatial grid resolution of 1.8° which corresponds at mid latitudes to approximately 200 km × 200 km grid boxes. The fixed time step length for the T63

L31–resolution is 12 minutes. The data output was stored for every six hours, so that there are four full 3-dimensional datasets per day of all model variables available.

3.4.2 Tracer implementation

The injection of the tracer from point sources is managed in the submodel `mo_transport` described in Appendix D.1, which was developed for this thesis. According to the locations of the facilities an emission mask was defined with entries scaled to the ^{85}Kr activity emission in PBq of each facility for the whole year. The emissions had a constant strength without any temporal variation or pulse characteristics within the year. The actual emission is introduced as lower boundary condition of vertical diffusion in the subroutine `mo_vdiff`. The modifications concerning mass conservation, convection and operator splitting described in Section 3.3 were active, so that the ^{85}Kr mass was conserved in every time step and negative concentrations could not be generated.

3.4.3 Nudging

To adapt the long term dynamic situations of the past, the prognostic variables in the model were constrained to ERA40 reanalysis data with a relaxation method (so called *nudging*) on all levels. ERA40 is a reanalysis product of the ECMWF, which assimilates various observational data to a fixed version of the global weather prediction model of ECMWF. The dataset is described in detail in the documentation (Uppala et al., 2005). For this study, the following parameters were nudged:

- temperature
- log surface pressure
- vorticity and divergence
- sea surface temperature

In order to sustain the global mean values, especially air mass conservation in the case of surface pressure, the spectral coefficient of order zero was not nudged. The ERA40 data is available for every six hours. For the time between the data points

the nudging data is interpolated time dependent with cubic splines. More details on the relaxation method can be found in the publication of Jeuken et al. (1996). As the ERA40 period ended in 2001 for the time after that ECMWF analysis data were used for nudging. These nudging data have erroneous wind fields for February 2006 as the global ECMWF model introduced a change in the number of vertical levels unrecognized by the nudging data generator for that month. For that reason the analysis of global dynamics in Chapter 5 end in December 2005.

3.4.4 Computing technology

The ECHAM5 model is parallelized and optimized for calculations on multi-processor architectures. It was operated on a NEC SX-6 vector high performance computer of the DKRZ. One computing node with 8 CPUs was used, the main simulation experiment over 36 simulated years needed approximately 2000 hours of wall clock CPU-time. Additionally several test and sensitivity studies were performed to check the tracer transport behavior in respect to the issues discussed above. In particular the rerun consistency and the independence of the number of processors were checked.

4 Evaluation of simulated global ^{85}Kr background concentrations

This chapter describes the results of the simulation experiment from 1971 to 2006. After the presentation of the temporal evolution of the global ^{85}Kr distribution, the simulated concentration time series at various measurement sites are evaluated against available measurements. Furthermore the variability of ^{85}Kr concentrations is analyzed.

4.1 Global distribution

The spatial distribution of the annual mean concentrations at the surface is shown in Figures 4.1 – 4.4. The maximum mean values found in the grid boxes in which strong sources are located exceed the color scale and are in the range from 7.7 Bq m^{-3} around Chelyabinsk in 1971 to 27.1 Bq m^{-3} around La Hague in 2006. Comparing the subsequent plots, strong changes in emission activities at various sites can be recognized. In particular, sites are observable which stopped or ramped up their operation in the simulated years. Some small sources cannot be seen in the chosen color scale since the concentration changes induced in the coarse model grid are not discernible. There is an overall longterm increase of ^{85}Kr concentrations and a transport into the southern hemisphere, which is discussed in more detail in chapter 5. Because of the fact that annual averages are presented in Figures 4.1 – 4.4, no actual synoptic patterns are recognizable except an eastward shape of the emissions plumes caused by the prevailing westerly winds near the surface in the latitudes where the strong sources are located.

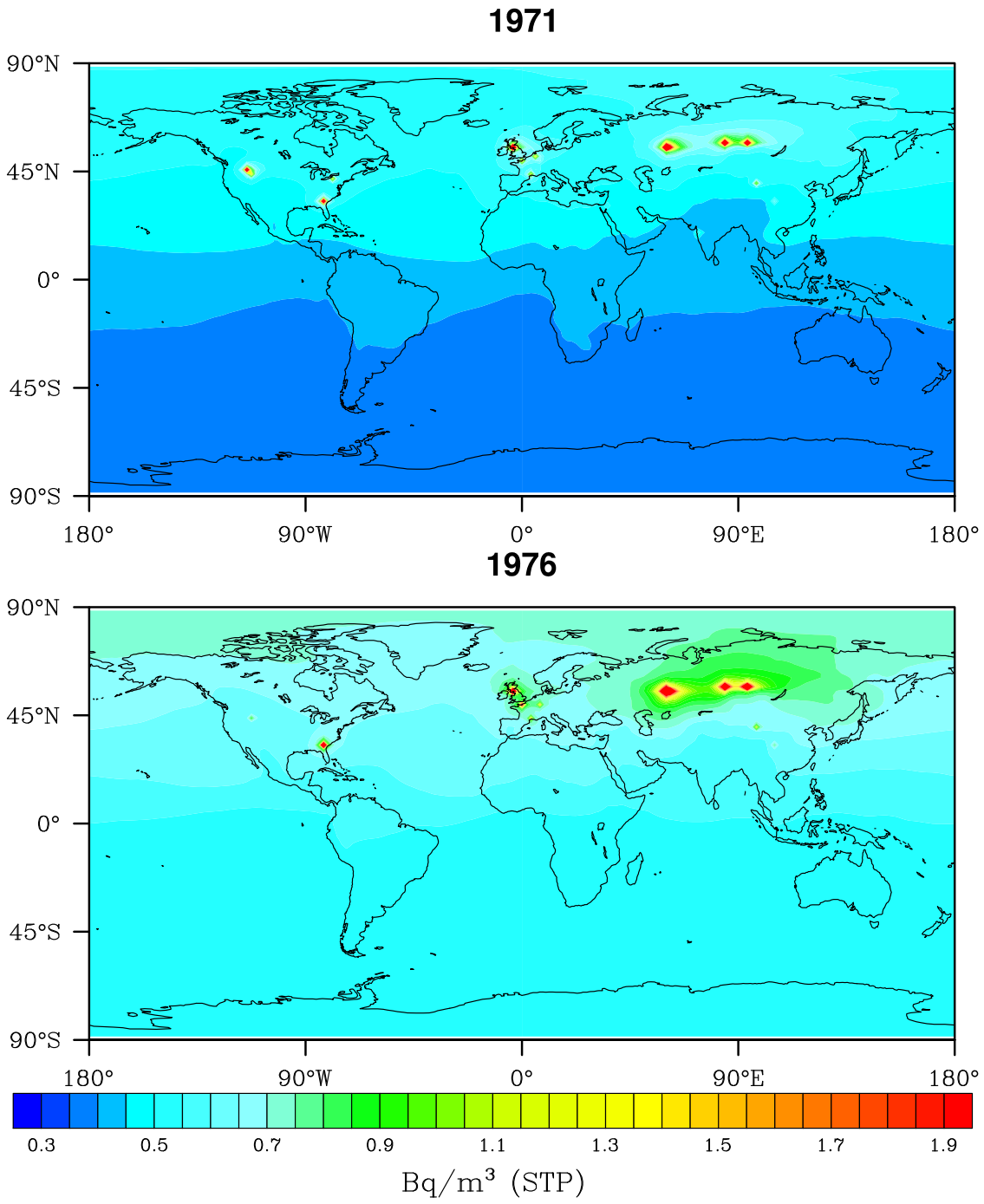

Figure 4.1: Annual mean ^{85}Kr concentration at thesurface 1971 and 1976.

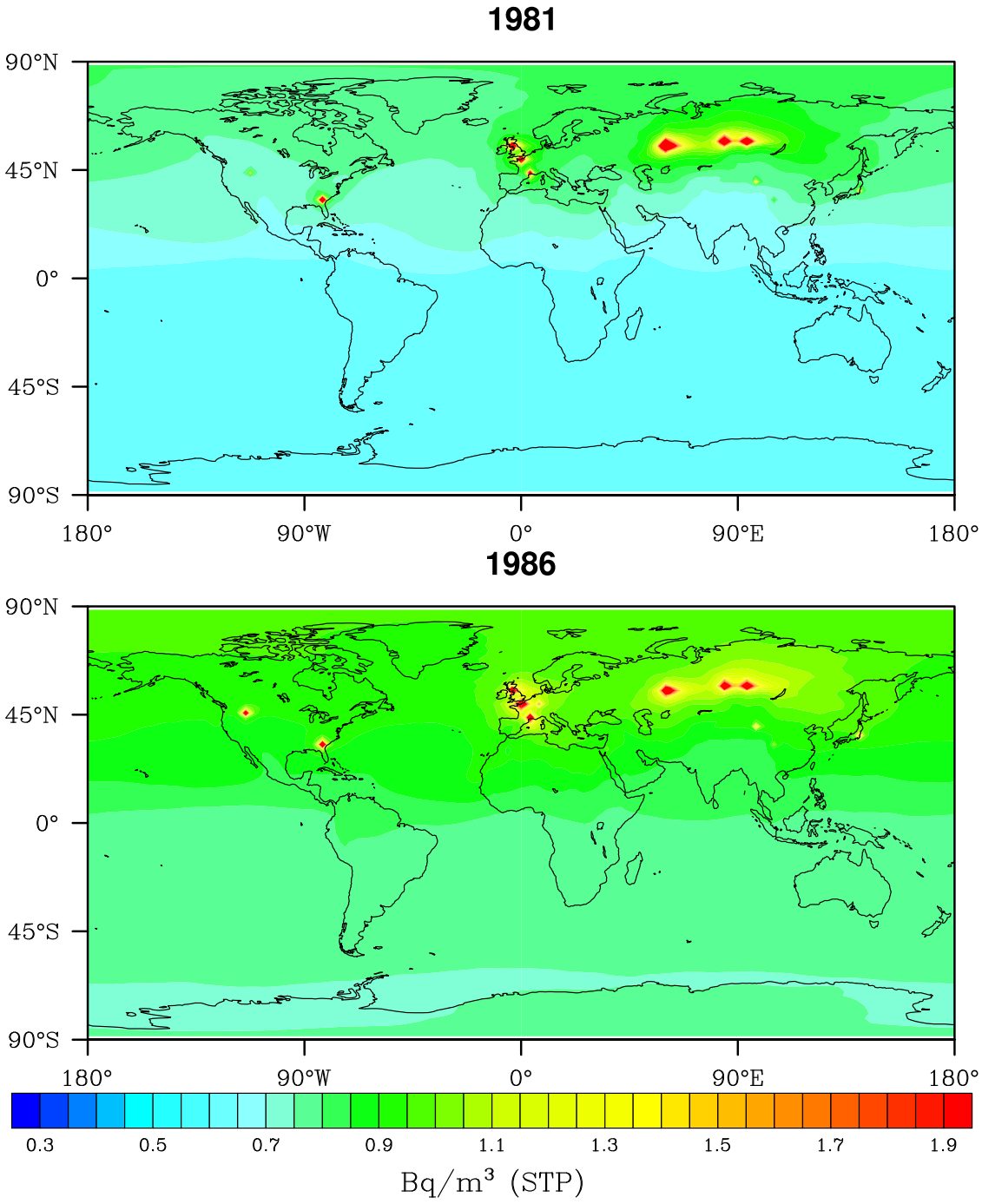

Figure 4.2: Annual mean ^{85}Kr concentration at the surface 1981 and 1986.

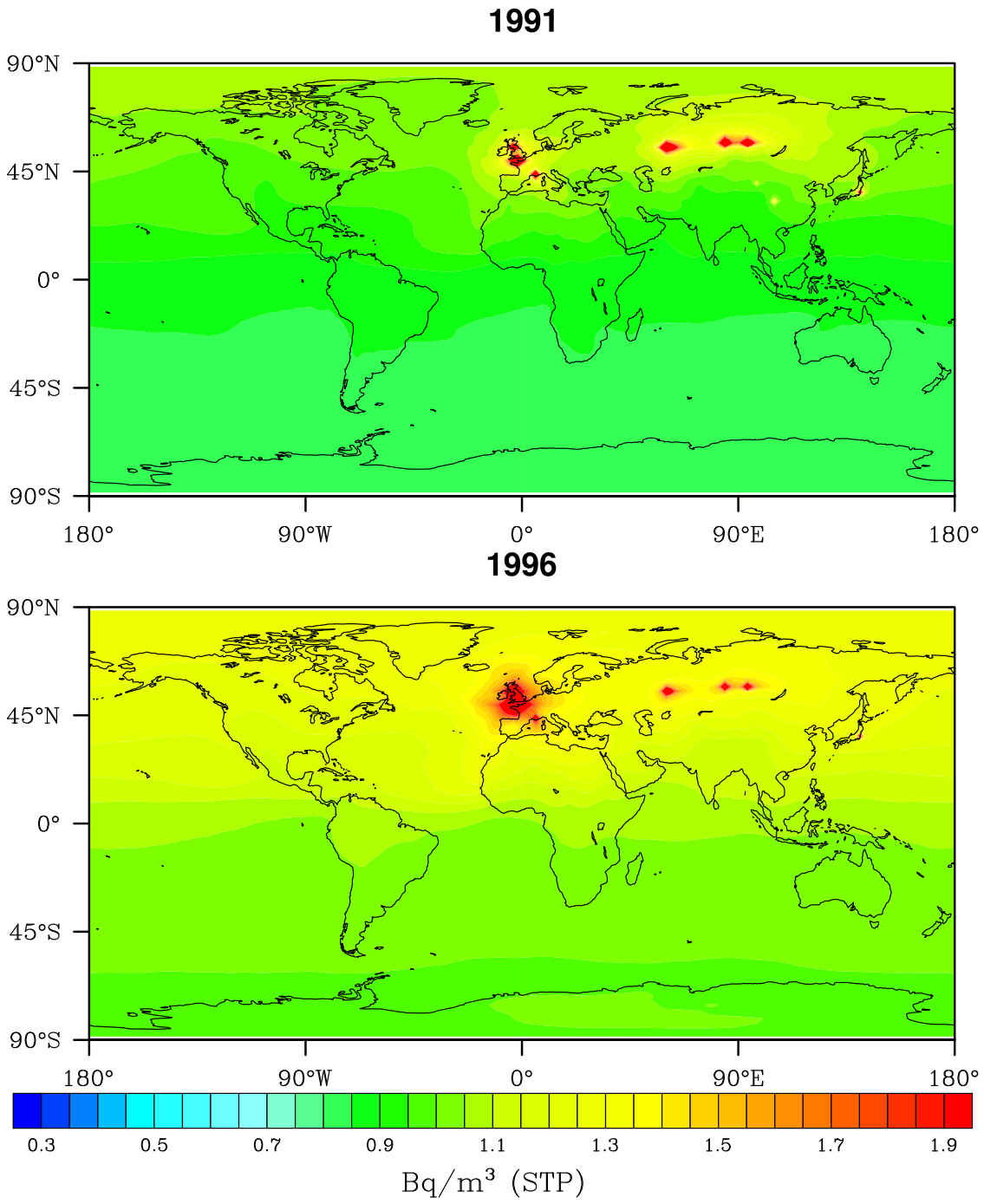

Figure 4.3: Annual mean ^{85}Kr concentration at the surface 1991 and 1996.

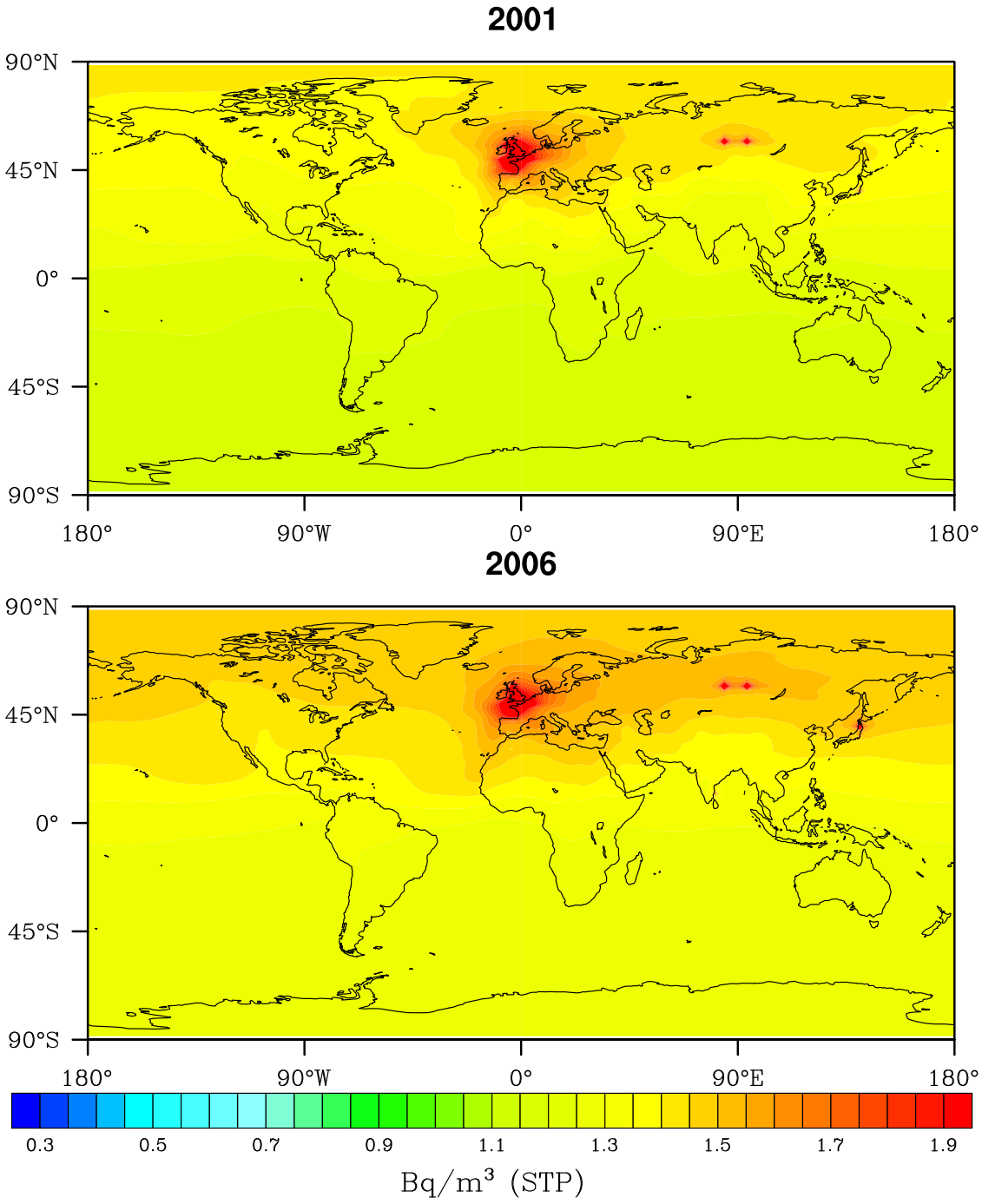

Figure 4.4: Annual mean ^{85}Kr concentration at the surface 2001 and 2006.

4.2 Comparison with measurements

The modeled concentration data were compared with measurement data provided by the German Federal Office for Radiation Protection. As described in Section 2.5, the measurements are usually performed on air probes of one week sampling time. As the air accumulated continuously in the sample, the evaluated ^{85}Kr concentration can be interpreted as a mean value over the sampling period. In the following evaluation two different reference time scales are chosen: first, monthly concentration means from the model are compared with the corresponding monthly means of the observation station, for which the values of the first and last week of the month were fractionally attributed to the respective month. This is only possible to be done correctly for measurement data from sites without interruptions in the observation time series. Secondly, the concentration values of the weekly samples were compared with the mean concentration of the actual sampling time extracted from the model results. The simulated concentrations were bilinearly interpolated to the location of the sampling station.

4.2.1 Time series at various sampling locations

In the following, the comparison between measurements and simulated concentration is presented for selected observation sites in various regions of the world. The figures of analyzed stations which are not shown in this chapter are attached in Appendix B. The station with the longest available record of weekly samples is in Freiburg, South-West Germany. Figure 4.5 shows the comparison between measured and simulated monthly means from 1973 to the end of 2006. The simulation overestimates concentrations in the early 1980s, but there is a reasonably good agreement for the rest of the time. Regularly measured peaks which are not represented in the model can be attributed to fresh plumes from Marcoule and La Hague which are not fully resolved in the model with constant emissions. Figure 4.6 shows the weekly samples taken at Schauinsland mountain near Freiburg but about 1200 meters above sea level, $\approx 900\,m$ higher than Freiburg. The measured concentrations in Freiburg tend to be lower. This could be explained by the channeling effect for wind directions in the Rhine valley, and sometimes strong inversions occur which keep low level air in

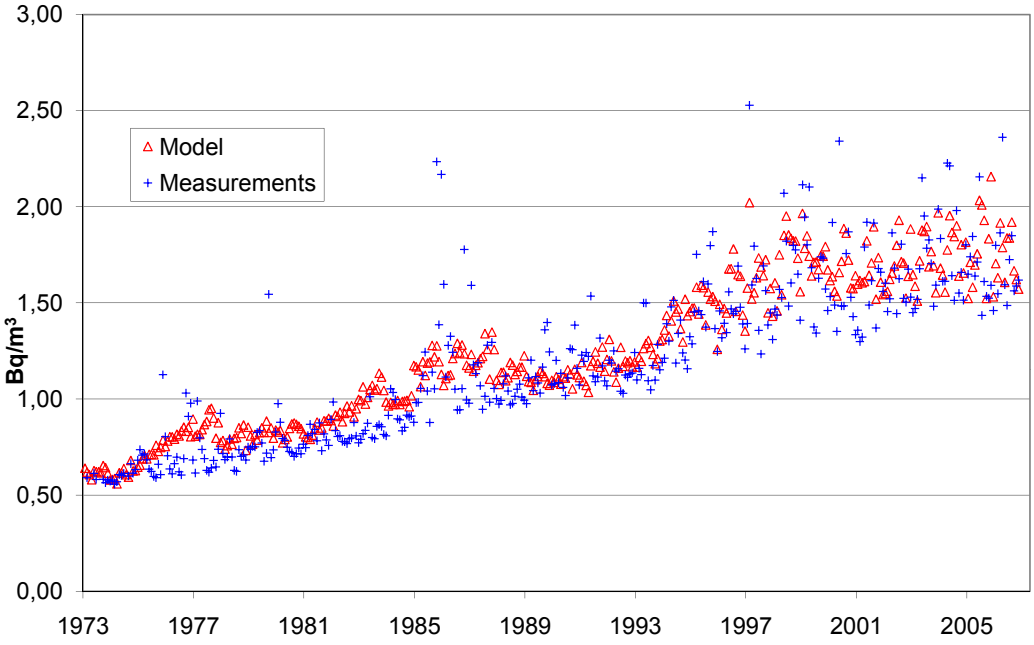

Figure 4.5: Comparison between simulated and observed monthly averaged ^{85}Kr concentrations in Freiburg.

Freiburg separated from air advected from France with higher ^{85}Kr concentrations. On the other hand, those inversions caused concentration peaks in the period when the reprocessing facility Karlsruhe (160 km north of Freiburg) was operating. They were observed in Freiburg but not at Schauinsland, as ^{85}Kr accumulated in the Rhine valley during inversion periods.

In Madrid (Figure 4.7) the concentrations are sometimes overestimated by the model for particular weeks - this may be a consequence of the high diffusivity of the model perpendicular to the main wind direction. A more detailed analysis shows that the simulated high concentrations occur mainly in the summer months when La Hague stops operation for the summer break. So the deviation can be explained with the yearly constant emissions used in the model.

Miami is an example of a observation site not directly influenced by ^{85}Kr sources in its vicinity. The data shown in Figure 4.8 indicate an overestimation by the simulated concentrations in the early 1980s which is a hint to errors in the emission inventory, most likely connected to the Russian emissions. Furthermore, there is an underestimation in 1990 and 1991 which can be most likely explained by additional

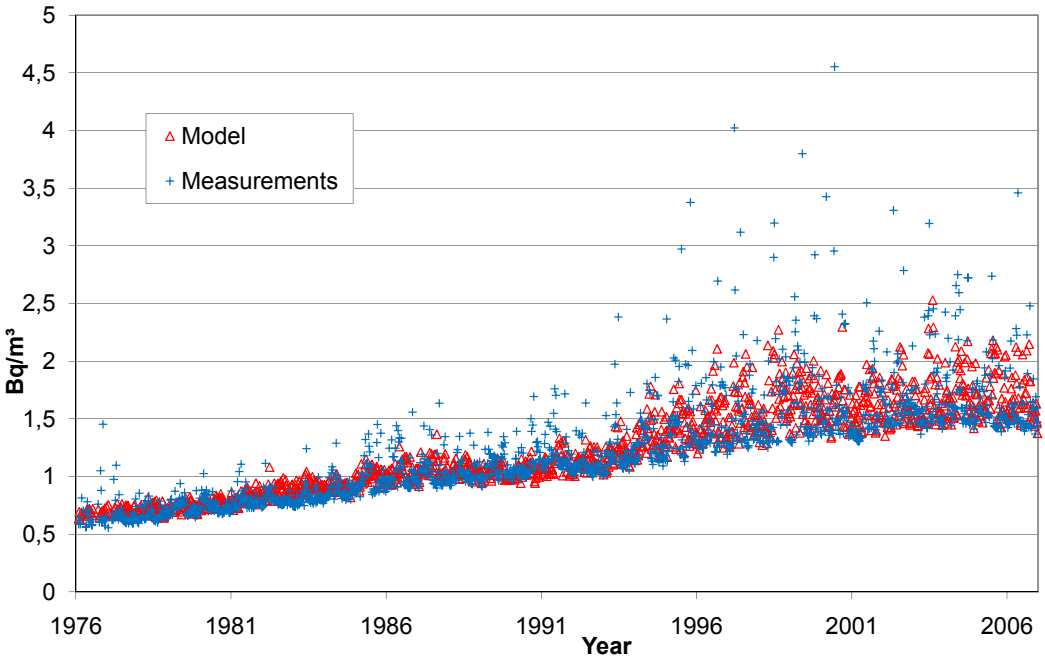

Figure 4.6: Comparison between ^{85}Kr concentration in week samples from Schauinsland and corresponding simulation results.

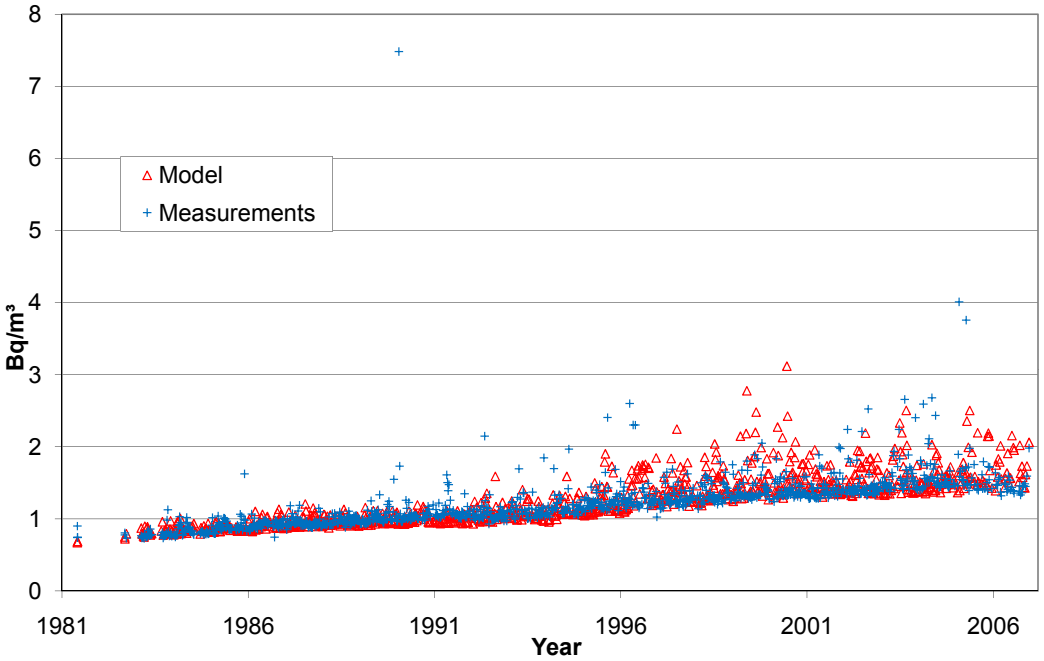

Figure 4.7: Comparison between ^{85}Kr concentration in week samples from Madrid and simulated concentrations average over the corresponding week.

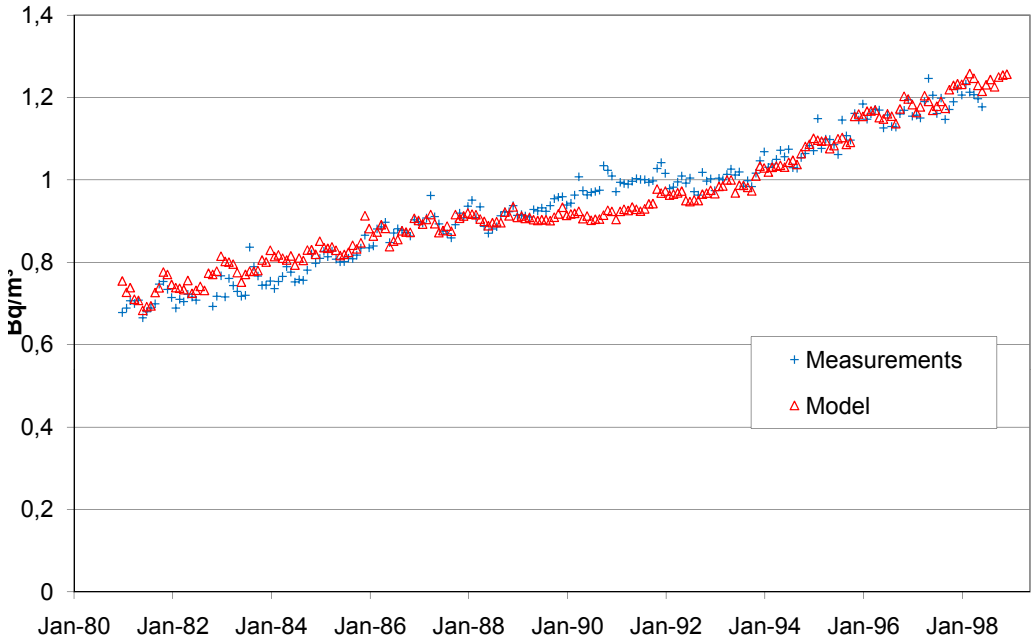

Figure 4.8: Comparison between ^{85}Kr concentration in week samples from Miami and corresponding simulation results.

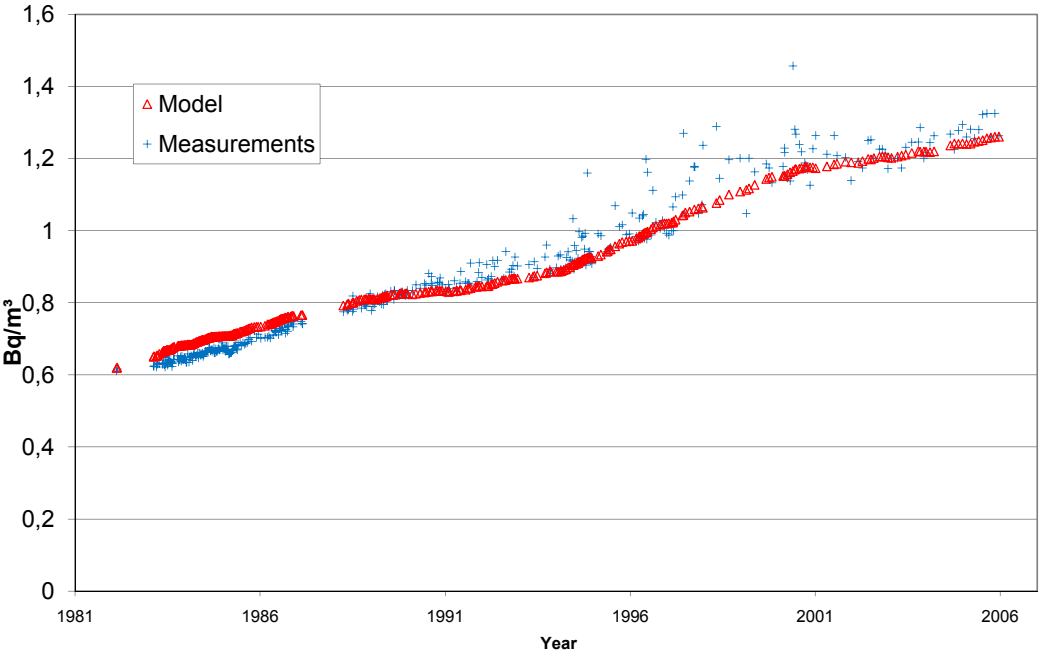

Figure 4.9: Comparison between ^{85}Kr concentration in weekly samples at Antarctica with up to one day sampling time and corresponding simulated values.

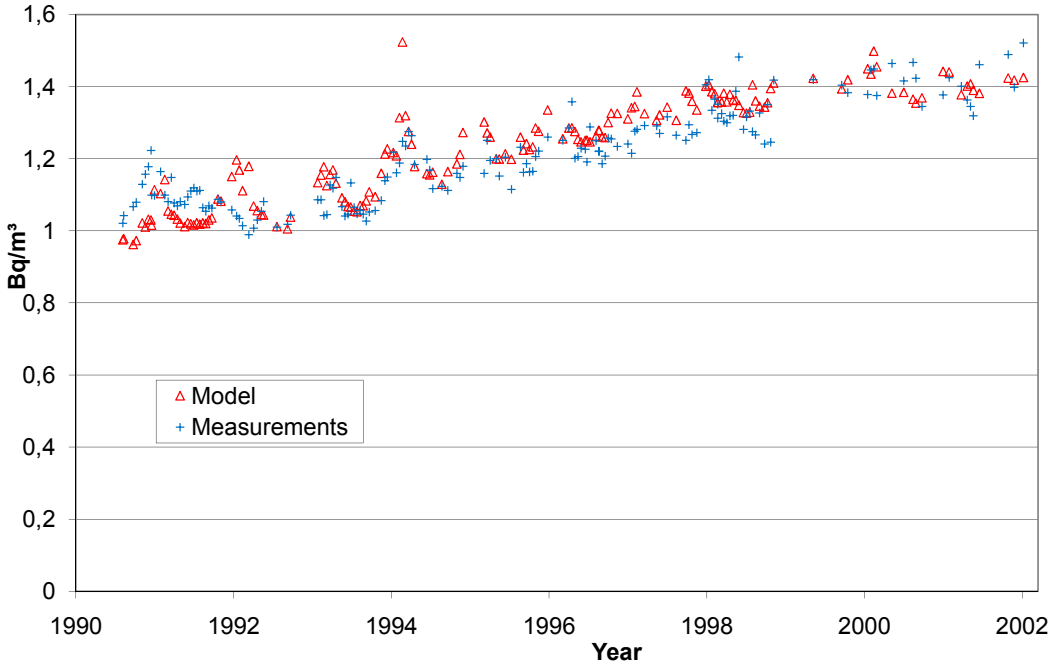

Figure 4.10: Comparison between ^{85}Kr concentration in week samples at Alert and corresponding simulated ^{85}Kr mean concentration.

Russian emissions as analyzed in Section 4.3.

For assessing high latitudes, the stations Alert at 85.5 °N and Neumayer station, Antarctica, at 70.6 °S are shown. For Alert only measurements since 1990 are available. They show good agreement with the simulation as presented in Figure 4.10. For Antarctica (Figure 4.9) the baseline is also well simulated, but the measurements show since 1990 a higher variability than the model indicates. The air samples at Antarctica are taken in a different way from the other stations operated by BfS: The sampling lasts only a few hours to one day and is performed once a week. In fact, the assumptions for the emission strength of the reprocessing facilities in the Southern Hemisphere in Pelindaba and Ezeiza are too weak to cause a significant signal in the global model. If the measurement results are correct, the variability of measured concentrations could hint to stronger ^{85}Kr sources on the Southern Hemisphere not included in the inventory. The medical isotope production facilities on the Southern Hemisphere can only partly explain this variability according to the estimations of their ^{85}Kr emissions mentioned in Section 2.4.2.

The comparison for the station of Tsukuba is shown in Section 5.2.2, the figures for

Cape Point, Cape Grim, Krakow, Heidelberg, Perl are attached in appendix B. They all show a good agreement between simulated and observed concentrations, partly disturbed by local sources close to the observation site.

4.2.2 Statistical measures for quality of model results

For a quantitative evaluation of the model results, the simulated concentration time series are compared to their observed counterparts in respect to different statistical parameters. The parameters from the COST Action 728 Report (Schlünzen and Sokhi, 2008) listed in Table 4.1 are applied.

	definition	name	ideal
AB	$= \overline{P} - \overline{O}$	absolute bias	0
ANB	$= \frac{\overline{P}-\overline{O}}{\overline{O}}$	normalized AB	0
MNB	$= \frac{1}{N}\sum \frac{P_i-O_i}{O_i}$	mean normalized bias	0
MNE	$= \frac{1}{N}\sum \frac{\lvert P_i-O_i\rvert}{O_i}$	mean normalized error	0
NMSE	$= \frac{\frac{1}{N}\sum (P_i-O_i)^2}{\overline{P}\overline{O}}$	normalized mean squared error	0
STDE	$= \sqrt{\frac{1}{N}\sum \left[(P_i-\overline{P})-(O_i-\overline{O})\right]^2}$	std of error	0
r	$= \frac{\frac{1}{N}\sum (O_i-\overline{O})(P_i-\overline{P})}{\sigma_O \sigma_P}$	correlation coefficient	1
CV	$= \frac{\text{stde}}{\overline{O}}$	coefficient of variation	0
IOA	$= 1 - \frac{\sum (P_i-O_i)^2}{\sum (\lvert P_i-\overline{P}\rvert + \lvert O_i-\overline{O}\rvert)^2}$	index of agreement	1

Table 4.1: Statistical parameters for model evaluation - P is the model "prediction", O the observation.

The values are given in Table 4.2 and the normalized errors are in the range of a few percent unless there is an active reprocessing plant in the same or neighboring grid cell. To point out the effect of sources close to the observation the monthly values for Heidelberg and Tsukuba are additionally divided in periods when the neighboring reprocessing facility (Karlsruhe and Tokai respectively) was operating or closed. The model errors for Tsukuba are dominated by measured young ^{85}Kr plumes from Tokai, but there is excellent agreement in 1998 and 1999 when the plant

at Tokai was completely shut down. For Heidelberg, the values in the downtime are not as excellent because there is still an influence of unresolved plumes from La Hague.

The overall very good agreement between measurements and simulations with errors in the range or even below the uncertainty of the emission inventory confirms the model calculations. As the emission data, the tracer transport by the model and the observations are independent from each other, it is very unlikely that the good results are due to different systematic errors compensating each other.

4.2.3 Measurements taken on ships

From 1980 to 1987, a total of 182 ^{85}Kr samples were taken on Atlantic ship cruises. The measured concentrations are reported by Weiss et al. (1983). The corresponding model results were calculated by interpolation of the simulated concentration to the ship position on the specific date. The absolute error for all available ship measurements is shown in Figure 4.11. The absolute model error is mostly below $0.1\,\mathrm{Bq\,m^{-3}}$, in the Southern Hemisphere even below $0.05\,\mathrm{Bq\,m^{-3}}$. The three outliers at northern mid latitudes occurred when the ships entered the grid cell where La Hague is located or directly neighboring cells, so that the modeled concentration exceeds the measurements easterly of the reprocessing plant due to numerical diffusion and in absence of a fresh plume. For one particular measurement the simulated concentration was by $0.1\,\mathrm{Bq\,m^{-3}}$ too low - in this case probably the sample was taken within a ^{85}Kr plume. The representation of the meridional ^{85}Kr distribution at the surface in ECHAM5 shows overall a very good agreement with the ship measurements.

4.2.4 Measurements of vertical concentration profile

There are only few ^{85}Kr measurements in higher altitudes reported. Balloon and aircraft campaigns from the 1980s are summarized by Weiss et al. (1983). Unfortunately, there was no corresponding surface sample taken and there were only few samples taken in lower altitudes so that a detailed analysis of the boundary layer is not possible with the data. Although the value measured at lowest altitude in

Monthly means at	Period	n	AB / Bq m^{-3}	ANB	MNB	MNE	NMSE	r	CV	IOA
Freiburg	1973-2000	329	0.05	0.04	0.07	0.13	0.027	0.87	0.16	0.93
Schauinsland	1976-2000	287	-0.02	-0.01	0.00	0.08	0.026	0.88	0.16	0.93
Madrid	1981-2000	201	0.04	0.04	0.04	0.08	0.026	0.73	0.16	0.84
Krakau	1981-1988	75	0.03	0.04	0.04	0.06	0.004	0.86	0.06	0.87
Miami	1981-1998	207	0.00	0.00	0.00	0.03	0.002	0.96	0.04	0.98
Cape Point	1985-1997	140	-0.03	-0.03	-0.03	0.04	0.003	0.92	0.05	0.94
Cape Grim	1987-1996	87	-0.03	-0.03	-0.03	0.03	0.001	0.91	0.03	0.91
Antarktis	1982-1993	106	0.01	0.01	0.01	0.03	0.001	0.98	0.04	0.97
Tsukuba	1995-2005	128	-0.27	-0.15	-0.02	0.20	0.323	0.39	0.52	0.20
	Tokai operat.	90	-0.41	-0.20	-0.05	0.26	0.389	0.25	0.56	0.02
	1998-1999	24	0.02	0.01	0.01	0.02	0.0004	0.85	0.02	0.96
Heidelberg	1985-1996	136	-0.15	-0.10	-0.01	0.18	0.245	0.09	1.19	0.04
	1985-1990	64	-0.36	-0.23	-0.07	0.27	0.480	0.10	1.35	-0.11
	1991-1996	72	0.04	0.03	0.04	0.10	0.015	0.66	0.98	0.79
Weekly samples at		**n**	**AB**	**ANB**	**MNB**	**MNE**	**stde**	**r**	**CV**	**IOA**
Freiburg	1973-2006	1697	0.05	0.04	0.08	0.15	0.32	0.77	0.26	0.85
Schauinsland	1976-2006	1558	-0.01	-0.01	0.02	0.11	0.26	0.82	0.21	0.89
Madrid	1981-2006	1061	0.01	0.01	0.02	0.12	0.34	0.54	0.28	0.69
Krakau	1981-1988	275	0.02	0.02	0.04	0.07	0.20	0.40	0.22	0.28
Miami	1981-1998	815	0.03	0.03	0.04	0.05	0.05	0.95	0.05	0.92
Cape Point	1985-1997	385	-0.03	-0.03	-0.03	0.04	0.04	0.89	0.04	0.88
Cape Grim	1987-1997	167	-0.02	-0.02	-0.02	0.03	0.03	0.91	0.03	0.93
Antarktis	1982-2006	385	0.00	0.00	0.01	0.04	0.05	0.98	0.05	0.90
Tsukuba	1995-2006	551	-0.30	-0.16	0.03	0.23	1.45	0.23	0.77	0.09
Heidelberg	1985-1999	666	-0.12	-0.08	0.05	0.21	1.23	0.09	0.82	0.07
Jungfraujoch	1987-2006	867	0.01	0.01	0.01	0.05	0.11	0.86	0.08	0.92
Alert	1990-2002	168	0.02	0.02	0.02	0.05	0.07	0.87	0.06	0.92
Perl	1989-2006	798	0.09	0.05	0.10	0.19	0.55	0.58	0.34	0.69
Wien	1988-2006	573	0.00	0.00	0.00	0.07	0.15	0.84	0.11	0.91

Table 4.2: Statistical measures for model evaluation, based on monthly mean values (upper half) and actual sampling weeks (lower half).

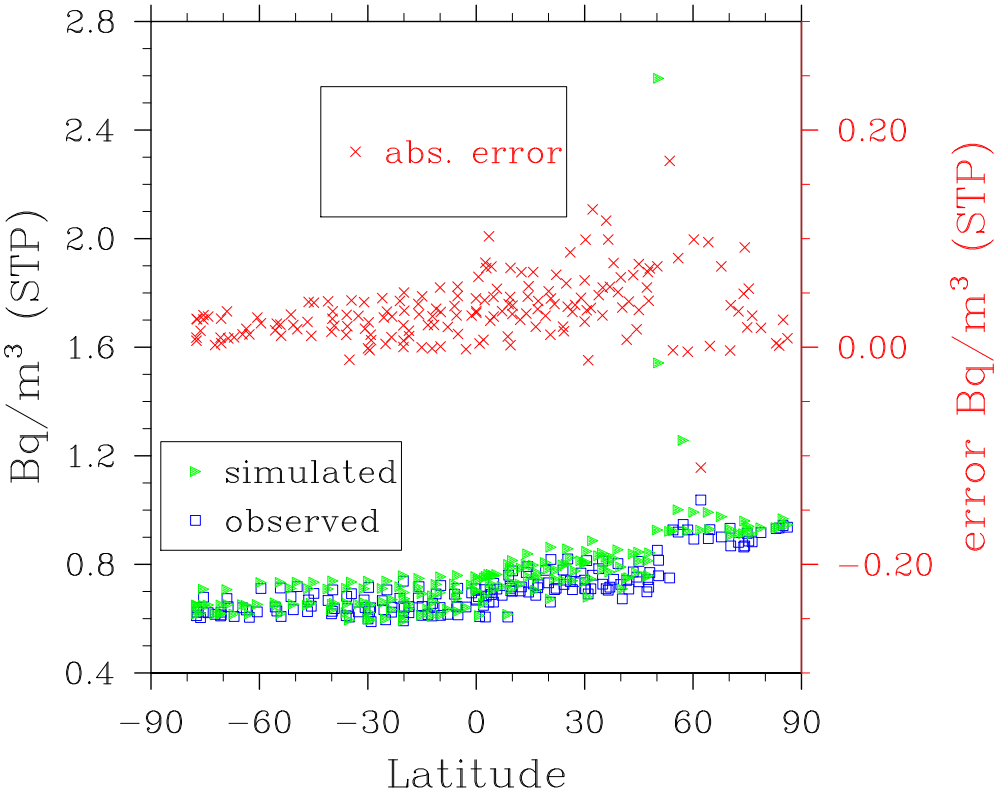

Figure 4.11: Meridional distribution of 182 measurements taken on ships, absolute simulated and observed concentrations (left scale) and absolut model error (red, right scale).

Figure 4.12 may indicate a slightly too high planetary boundary layer in ECHAM5, no general statement based on this single measurement is possible. The values for altitudes above 5 km fit better, in particular when taking the uncertainties of the measurements into account (Figure 4.13).

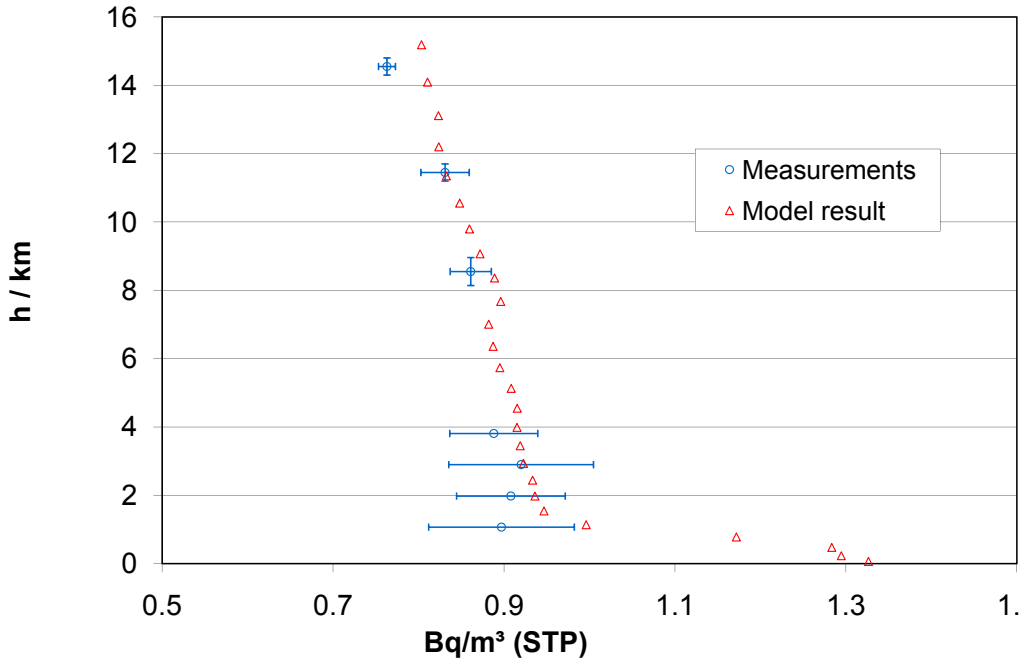

Figure 4.12: ^{85}Kr measurements in various heights taken at 44 °N, 1 °W on 28 Oct. 1987 and corresponding simulated concentrations.

4.3 Sensitivity to contributions of single sources in ECHAM5

In order to assess the contribution of single source locations to the concentration at a given sampling station, a version of the tracer implementation in ECHAM5 was developed in which the tracers emitted from various sources were defined and transported individually. Figure 4.14 shows the monthly mean ^{85}Kr concentration at four sites in February 1991 for emissions since January 1st, 1991. While the concentrations in Alert (Figure 4.14d) can be mainly explained by the Russian sources, the contributions to concentrations at Madrid (Figure 4.14b) and Vienna (Figure 4.14c) are dominated by La Hague. The concentrations in Miami (Figure 4.14a) are comparably strong influenced by emissions from Tokai although the other sources cause higher concentrations because of higher emissions. The discrepancy between simulated and observed concentrations in 1990 and 1991 is most evident in the data of Alert (Figure 4.10) and Miami (Figure 4.8). As the relative influence of the Russian

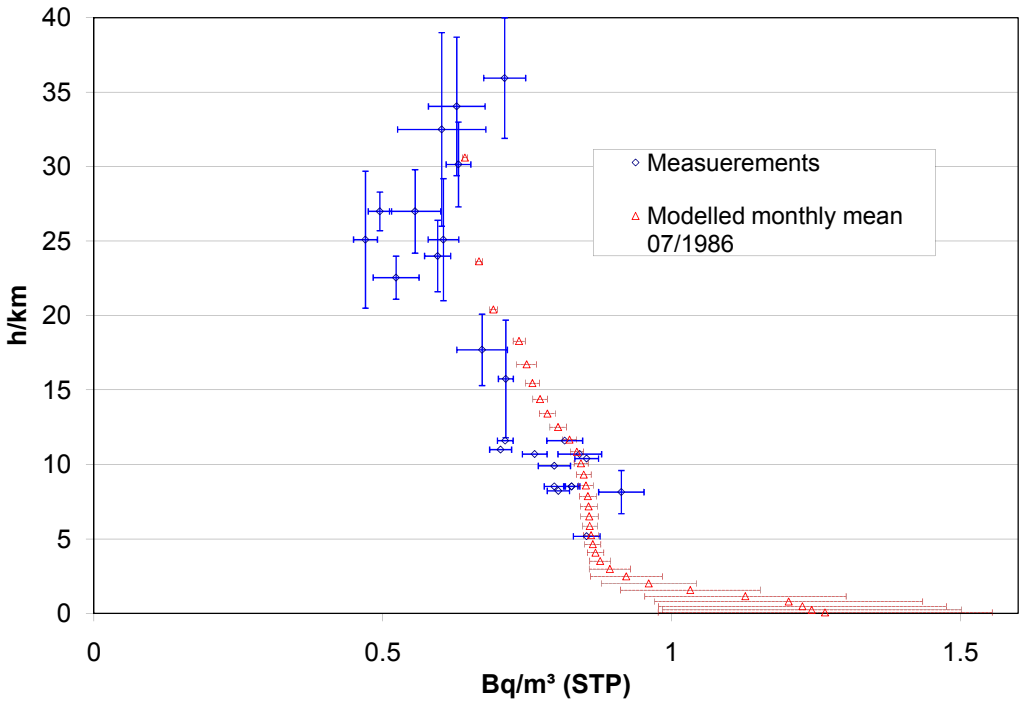

Figure 4.13: Vertical profile of ^{85}Kr measurements from various campaigns linearly extrapolated to 1 July 1987 and simulated mean values of July 1987 - the dashed horizontal error bars at the model results indicate the corresponding standard deviation in the model.

sources is strong at those sites this indicates too low emissions from Russian sites in the inventory for 1991 and 1992.

4.4 Variability of concentrations

Of particular importance for the detectability of additional ^{85}Kr sources is the variability of the background. As a measure of the variability of the modeled concentrations the standard deviation of the 6-hourly stored concentrations was studied. Figures 4.15 and 4.16 show the spatial distribution of the standard deviation for each month in 2005. Although yearly constant emissions are applied in the simulation, there are large variations in the vicinity of La Hague. In the Southern Hemisphere variability of concentrations is very low. No distinct seasonality of the variability can be derived from the maps.

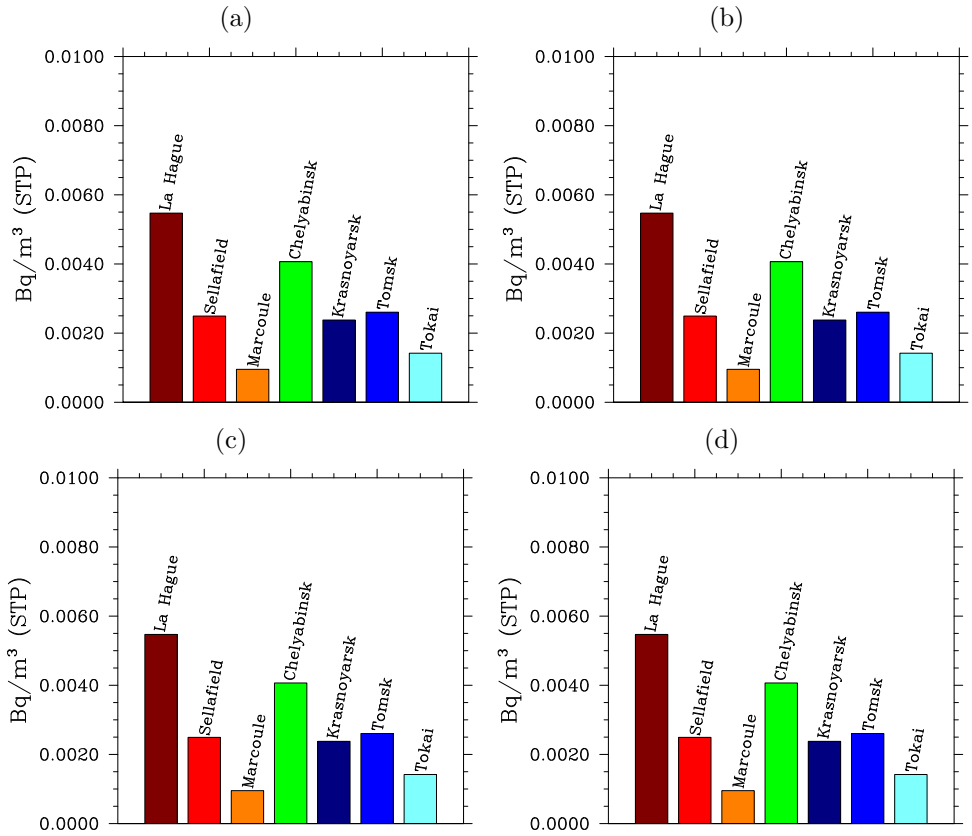

Figure 4.14: Impact of emissions released less than two months before from 7 different reprocessing facilities on simulated mean concentration in February 1991 at Miami (a), Madrid (b), Vienna (c) and Alert (d) - different scales.

The evaluation of the modeled variability is limited by the lack of sufficient short term measurements of ^{85}Kr concentrations available. Thus, only the variance of weekly means can be compared. The standard deviation of the weekly means is well reproduced by the model far from ^{85}Kr sources but intrinsically underestimated in the direct vicinity of reprocessing plants. In addition, the simulated variability of week samples is systematically lower than measured in the Southern Hemisphere. Figure 4.17 shows the coefficient of variation CV introduced in Table 4.1 dependent on the horizontal distance of the used measurement stations from La Hague. The distance was obtained using Google-Earth. The CV values decrease with increasing distance from the strongest ^{85}Kr background source. The two points at CV$\approx$ 0.8 are at Heidelberg and Tsukuba, where local sources in the same grid box dominate.

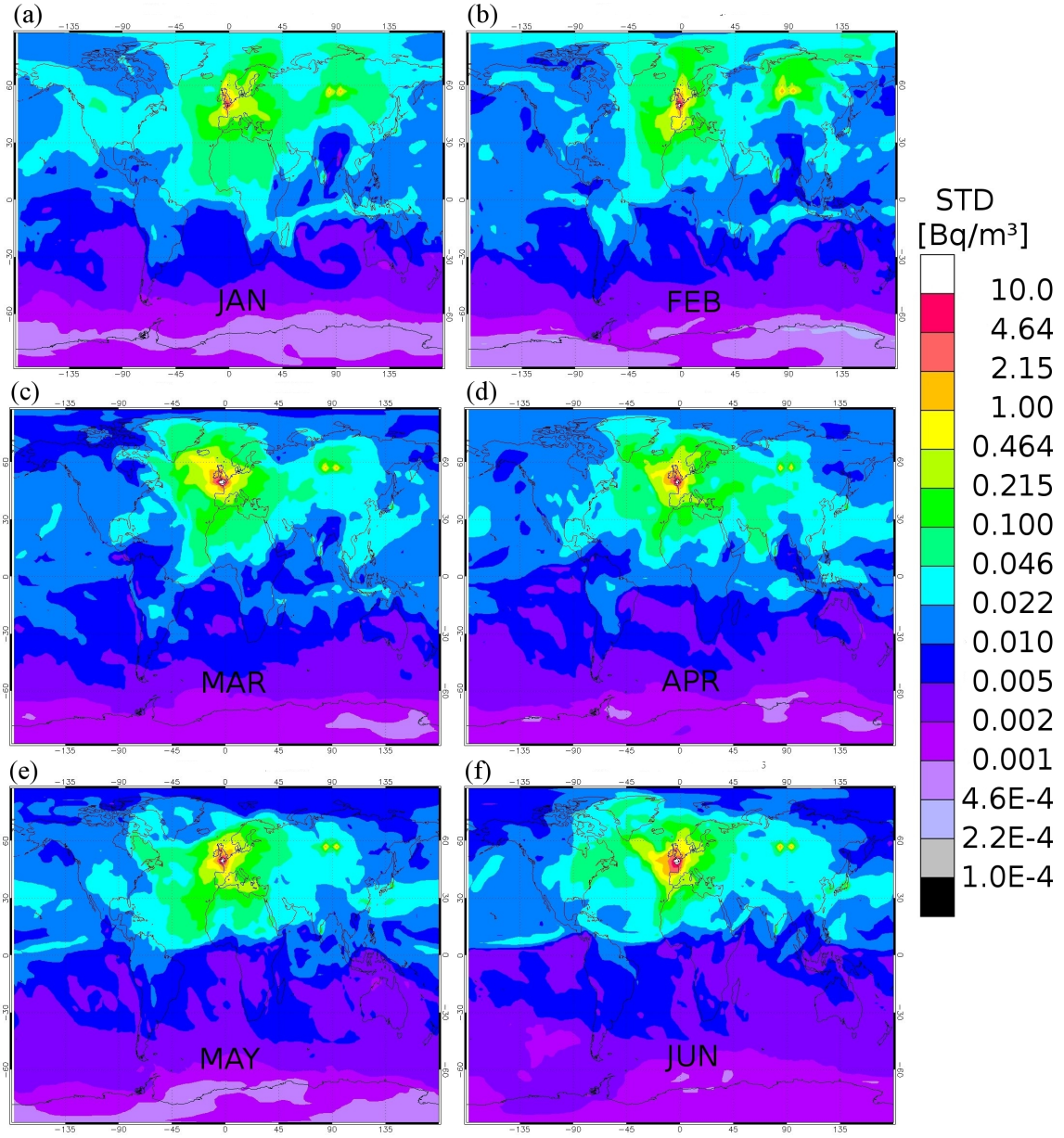

Figure 4.15: Standard deviation of simulated 6-hourly concentrations for January (a) to June (f) 2005.

4.4.1 Analysis of variability of time series

For analysis of concentration time series over several years, the long term trend was subtracted to investigate the unbiased variability of the concentrations in the

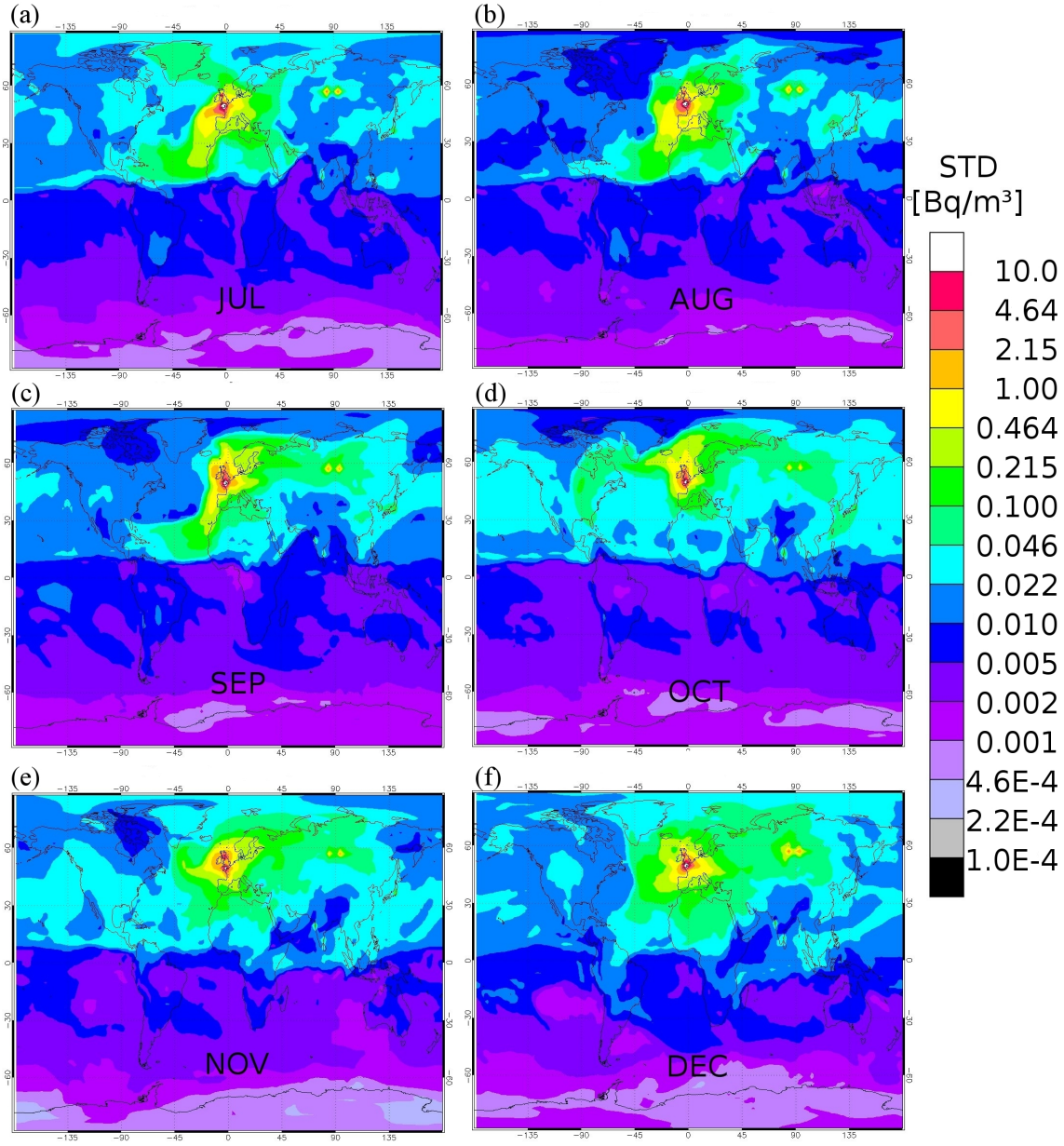

Figure 4.16: Standard deviation of simulated 6-hourly concentrations for July (a) to December (f) 2005.

model. The standard deviation of the 6-hourly concentration values was used as main measure. For comparison with the measurement data from weekly cumulative air samples also the variability based on the weekly means values was calculated.

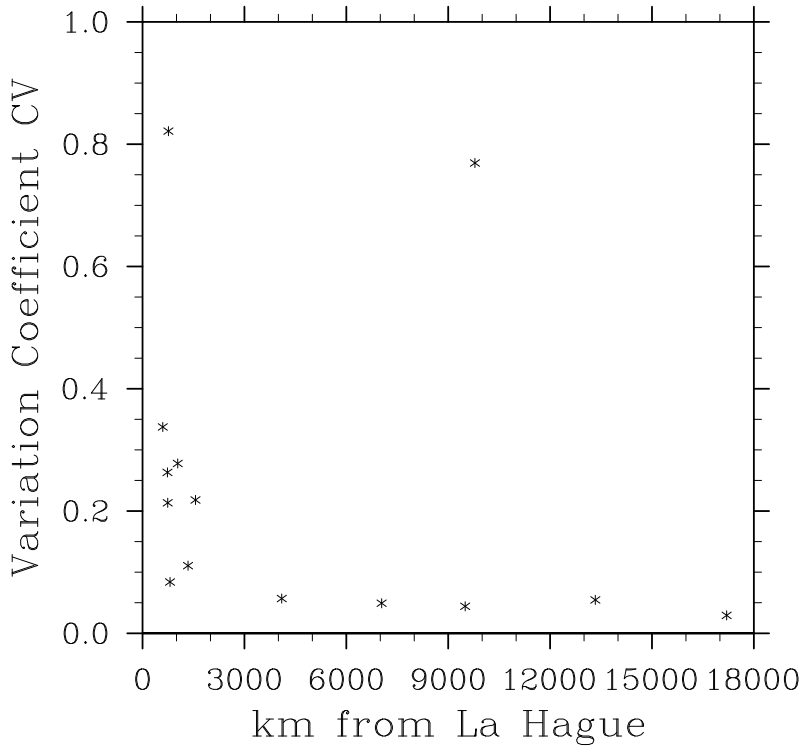

Figure 4.17: Variation Coefficient CV against distance from La Hague.

Time series decomposition by the LOESS method

A fitting method developed by Cleveland and Devlin (1988) is the so called LOESS method. It performs a polynomial regression around each data point considering only a subset of the data. The local subset is defined with a nearest neighbor algorithm and a weight function gives more influence to the points close to the central point. As result the polynomials are merged and a long term trend is obtained, a deterministic seasonality, and the remaining variability not captured by the fit. The LOESS method is implemented in the statistical analysis software R (R Development Core Team, 2009) with the function `stl`. Figure 4.18 shows the output for the monthly mean values of measurements, Figure 4.19 for the simulated monthly means.

The amplitude in the seasonal cycle of the measured concentration is about three times higher than that of the simulated seasonal cycle which is due to the regular operation break of La Hague in summer. Nevertheless, the seasonal cycle of the model with constant La Hague emissions has its minimum also in summer because stable

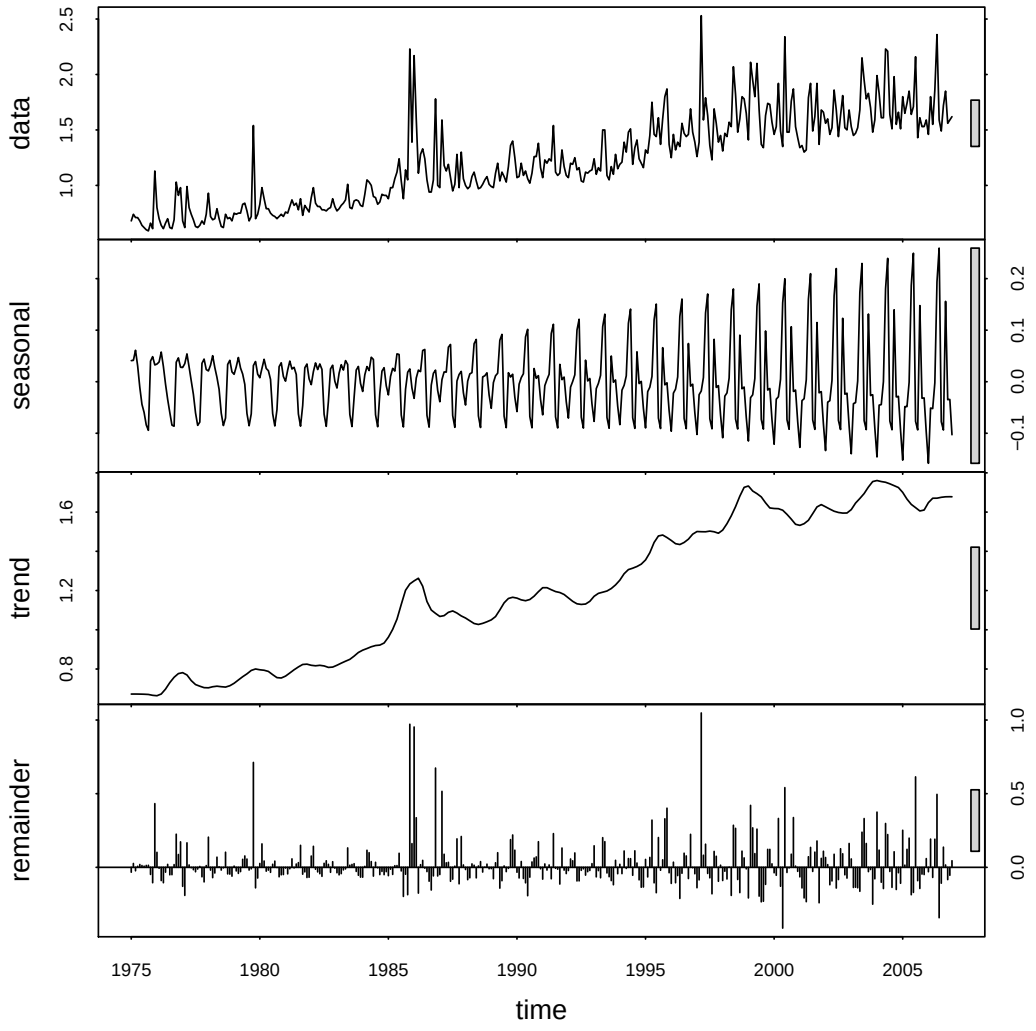

Figure 4.18: Time series decomposition of measured monthly values in Freiburg from 1975 to 2006.

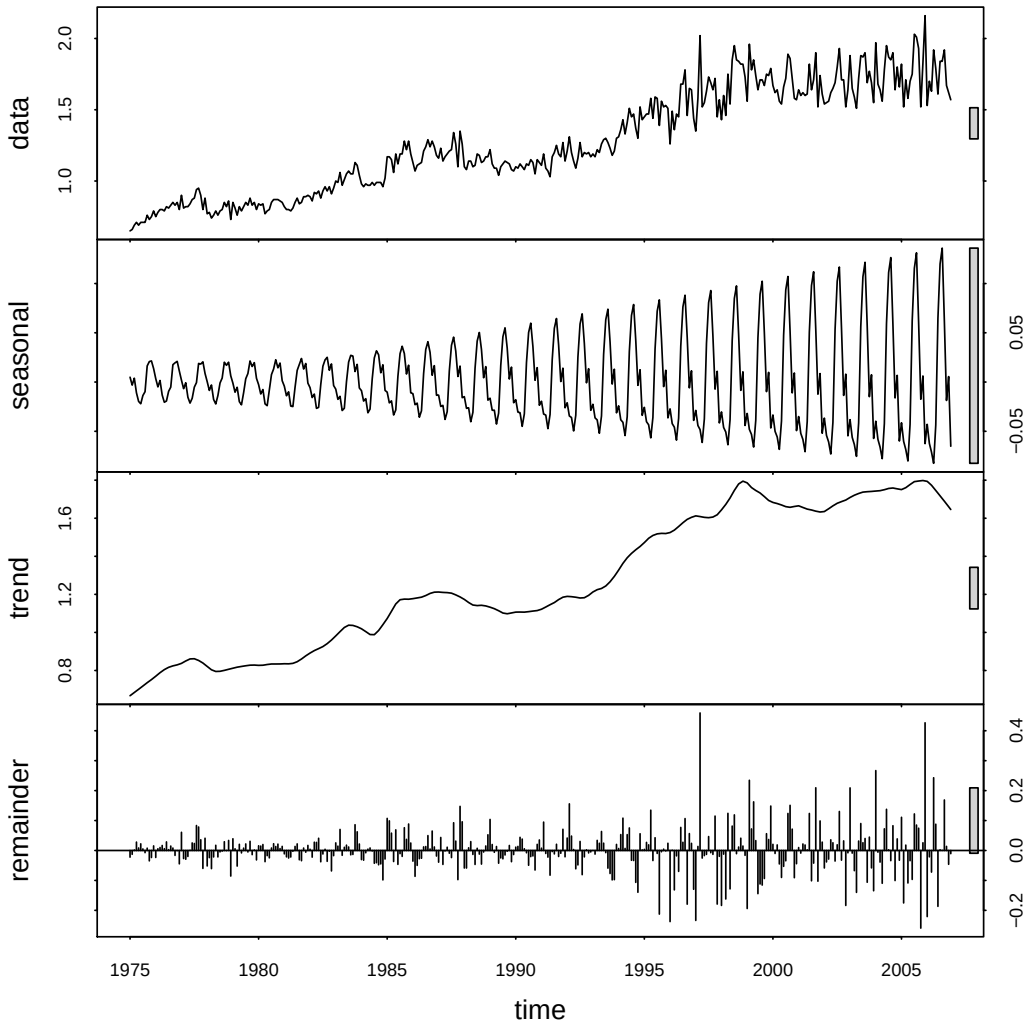

Figure 4.19: Time series decomposition of modeled monthly values in Freiburg from 1975 to 2006.

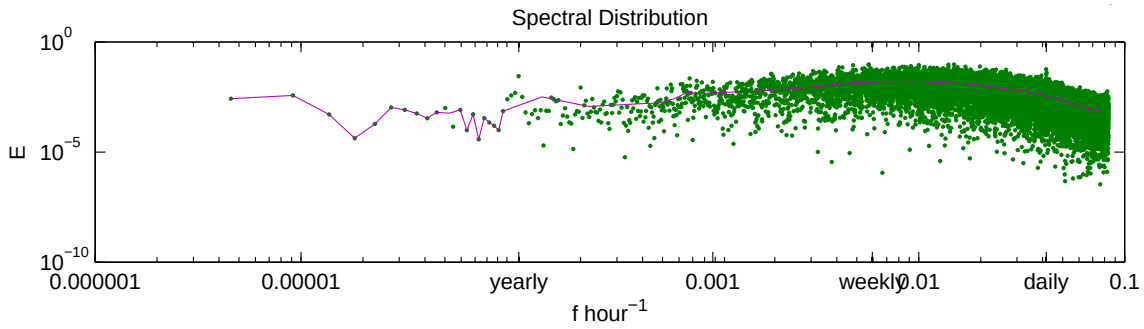

Figure 4.20: Spectral decomposition of time series of 6-hourly modeled concentrations at Schauinsland (linear trend subtracted) E corresponds to squared concentration variations.

continental high pressure and atmospheric blocking situations are often present and inhibit the transport in easterly direction. In the time series of the measurement there is an additional peak in 1986 caused by the Chernobyl accident, which was not included in the model.

Spectral analysis of concentration time series

The Fourier transformation of time series allows for an analysis of characteristic time scales and was performed for various sampling stations. As the time resolution of measurements was one week, it was not possible to derive meaningful conclusions from the spectral decomposition of the observed time series. The features of interest are rather on frequencies higher than weekly.

Figure 4.20 shows the spectral distribution of the time series of 6-hourly simulated concentrations at Schauinsland from 1976-2000. The maximum is at a frequency of some days (synoptic time scale). Additionally a tiny peak on the seasonal scale around one year can be distinguished in the data points which is not kept by the averaging interval of the trend line.

In July 2009, the Centre for Science and Peace Research received emission data from La Hague in hourly resolution which were provided by the operator Areva for 2007 and 2008. That data will be subject to a further study. A first evaluation of the data shows, that during periods when the facility is in operation ^{85}Kr emitted continuously

with rather constant strength for reprocessing campaigns lasting several weeks. This justifies the approach of yearly constant emission fluxes in the background simulation to some extent, although the summer break was not represented correctly.

4.5 Conclusions for detectability of additional sources

The long term simulation of the global ^{85}Kr background distribution with ECHAM5 in its modified version concerning mass conservation and non-negative concentrations was performed and evaluated. The model results show very good agreement with measurements in absence of close sources and plausible characteristics where ^{85}Kr sources are nearby. In spite of the assumed constant emissions also the variability of concentrations shows realistic characteristics in the Northern Hemisphere. Only the measured variability of ^{85}Kr concentrations on the Southern Hemisphere after 1988 is not represented in the model results. Possible explanations for that are on the one hand reasons in the model as high diffusivity, on the other hand, unknown or underestimated ^{85}Kr releases in the Southern Hemisphere could cause the disagreement. The statistical error of the ^{85}Kr measurements are below 1%. Nevertheless, systematic errors in the sampling process cannot be fully excluded.

For the assessment of detectability of small ^{85}Kr sources the global model ECHAM5 in the T63 horizontal resolution is not sufficient as the initial numerical diffusion dilutes emissions immediately without any transport. For sampling and detection scenarios the area of regard would cover only very few ECHAM5 T63 grid cells. Thus, for the investigation of sensitivity to individual plumes the Lagrangian Particle Dispersion Model HYSPLIT was used. The results will be presented in Chapter 6.

5 Analysis of air mass exchange between the hemispheres

As nearly all reprocessing plants are located at mid latitudes on the Northern Hemisphere, ^{85}Kr is suitable to analyze the transport of air between the Northern and Southern Hemispheres. The characteristic time scale of this transport process is investigated by the use of a two box model and compared with results of previous studies.

5.1 Interhemispheric exchange in a box model

For the analysis of interhemispheric transport we consider a two box model dividing the atmosphere into Northern and Southern Hemisphere. In this concept the tracer masses are denoted m_1 and m_2 in the Northern and Southern Hemisphere, with a source emission rates S_1 and S_2. Assuming that the rate of tracer increase in the Southern Hemisphere due to mass flux from the Northern Hemisphere is proportional to the present tracer mass in the Northern Hemisphere the proportional factor φ_{12} is defined. The factors φ_{12} and φ_{21} are also called air mass exchange coefficients and give the fluxes across the equator as fraction of the tracer mass in the box of origin. Thus, the mass change rates in the two boxes (with $\lambda = \frac{1}{\tau_{\text{decay}}}$ being the exponential radioactive decay constant of the tracer) are described by the following equations:

$$\dot{m}_1 = -\lambda m_1 - \varphi_{12} m_1 + \varphi_{21} m_2 + S_1 \tag{5.1}$$

$$\dot{m}_2 = -\lambda m_2 - \varphi_{21} m_2 + \varphi_{12} m_1 + S_2 \tag{5.2}$$

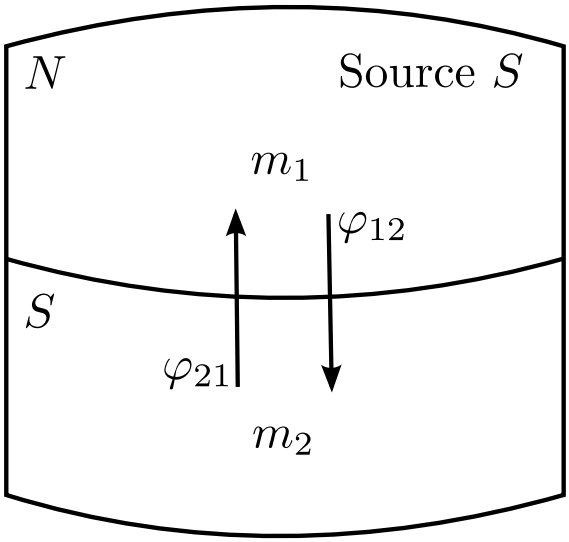

Figure 5.1: Two box model with source S, masses m_1 and m_2, and relative fluxes $\varphi_{12}/\varphi_{21}$.

The solution of the differential equation system is given in Appendix C. As in our simulation the sources on the Southern Hemisphere are only active from 1986 to 1992 and contributed, at maximum in 1989, $4 \cdot 10^{-5}$ of the total emissions, in this study S_2 equals 0 and there is only the northern source rate $S_1 = S$ as drawn in Figure 5.1. The air mass exchange coefficients φ_{12} and φ_{21} are independent of the actual tracer mass distribution (m_1 and m_2), and the air mass is not growing on one hemisphere, thus $\varphi_{12} = \varphi_{21} = \varphi$ as shown for a special case in Appendix C. With $S_2 = 0$ and $S_1 = S$ from equation (5.2) the relative mass flux rate φ over the equator is:

$$\varphi = \frac{\dot{m}_2 + \lambda m_2}{m_1 - m_2} \tag{5.3}$$

The characteristic exchange time of the interhemispheric transport is defined as the inverse of φ:

$$\tau_{\text{ex}} = \frac{m_1 - m_2}{\dot{m}_2 + \lambda m_2} \tag{5.4}$$

An alternative equation obtaining an instantaneous τ_{ex} with sources in both boxes is given by Lintner et al. (2004):

$$\tau_{\mathrm{ex}} = \frac{2\Delta M}{\Delta S - d\Delta M/dt - \lambda \Delta M} \tag{5.5}$$

with $\Delta M = m_1 - m_2$ and $\Delta S = S$ in absence of sources on the Southern Hemisphere. Equation (5.5) can be obtained by subtracting equation (5.2) from (5.1) with $\varphi_{12} = \varphi_{21} = \varphi$. To avoid the explicit dependence on the source strength and the difference of mass difference in the denominator, equation 5.4 was used in the analysis. A cross check applying (5.5) on the data gave a by 2% faster mean τ_{ex}, which can be due to the discretisation of differences and monthly source strength, especially the change of S at the turn of the year to the next year's value. The equivalence is only valid for constant S.

For big times t with constant source strength S, the mass difference between the tracer masses in the hemispheres approaches according to (C.10) the constant $m_1 - m_2 = \frac{S}{2\varphi+\lambda}$. The absolute masses approach linear asymptotes with the slope $\frac{1}{2}S$ for long times with constant source strength as shown in (C.13). Having a constant northern source strength S, in the two box model τ_{ex} is equal to the time lag until a certain tracer mass m_1 is reached on the other hemisphere so that $(m_1(t) = m_2(t+\tau_{\mathrm{ex}})$ as shown in appendix C in (C.15). A first signal time of interhemispheric transport is much faster than the characteristic mixing time τ_{ex}. Measurements of radioactive fallout from nuclear tests conducted at 21°S, 137°W in late summer 1968 for instance showed a first detection of ^{131}I ^{140}Ba at 34°N, 94°W three weeks later (Palmer, 1969).

In this thesis, the interhemispheric exchange time τ_{ex} was analyzed from two data sets: One climatological test simulation over 10 years in T21 L19 resolution and the data of the nudged ^{85}Kr background study in T63 L31 resolution described in Chapter 4 from 1971-2005. For the calculation according to equation (5.4) the amount of ^{85}Kr in each grid column was calculated according to present mixing ratios and pressure levels. This burden field was summed up for each hemisphere using monthly mean values.

The averaged τ_{ex} was calculated to 11.7 months in the T21 test simulation and to 10.5

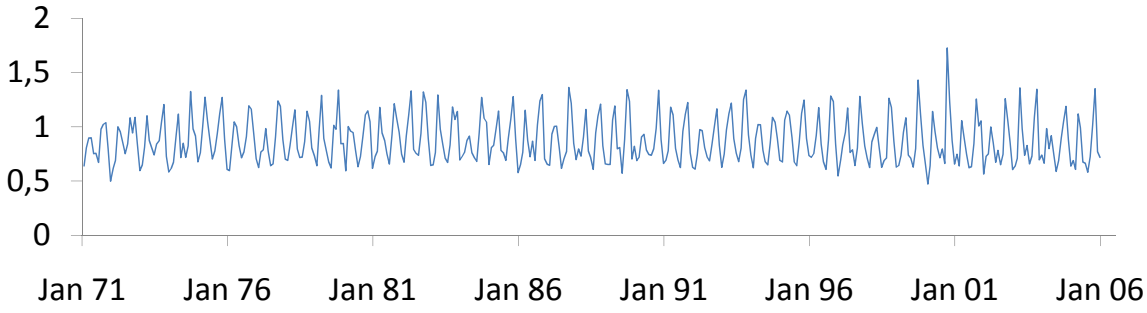

Figure 5.2: Monthly calculated τ_{ex} in years from 1971 to 2005.

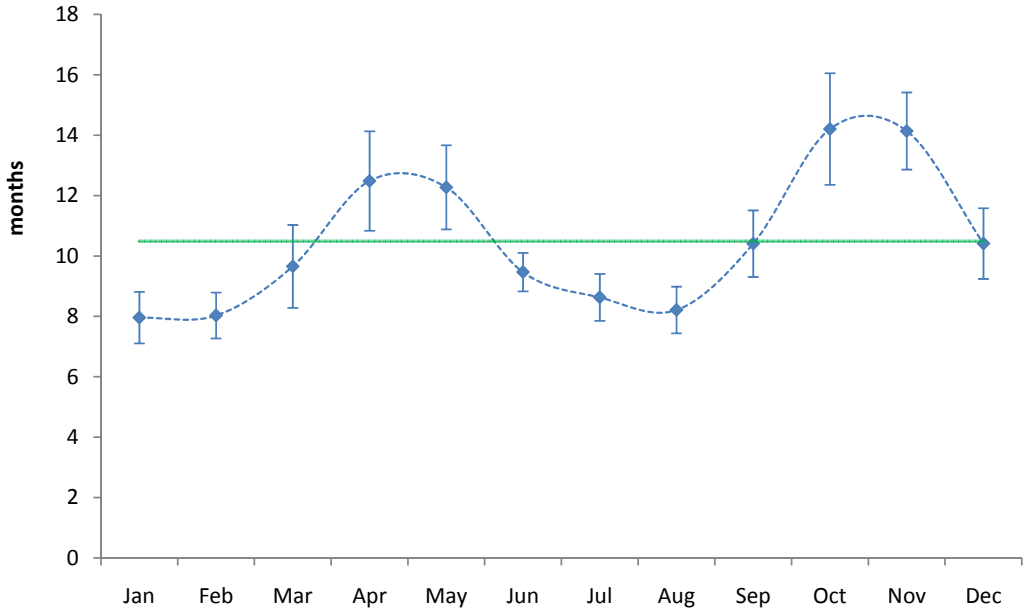

Figure 5.3: Seasonal mean of characteristic ^{85}Kr exchange time between the hemispheres in ECHAM 5 averaged from 1971 to 2005. The error bars show the sample standard deviation of the respective month.

months in the high resolution data over 35 years nudged simulation. In the following the data of the 35 years simulation in higher resolution are used. The time series of the monthly calculated τ_{ex} values is shown in Figure 5.2. In Figure 5.3 the seasonal dependence of the interhemispheric exchange time averaged over the simulated 35 years is shown. The values of τ_{ex} have maxima in April and October when the ITCZ lies over the geographical equator. They have minima in winter and summer when the circulation of the winter–hemisphere is crossing the equator and induces a faster mixing between the geographical hemispheres.

Author (year)	Tracer	Exchange time (years)
Nydal (1968)	$^{14}CO_2$	1.0
Newell et al. (1969)	Air	0.9
Czeplak and Junge (1974)	^{85}Kr	1.8
Maiss and Levin (1994)	SF_6	1.4
Jacob et al. (1987)	^{85}Kr	1.1
Levin and Hesshaimer (1996)	$SF_6/^{85}Kr$	1.6 (obs.)/1.2 (2-d-model)
Geller et al. (1997)	SF_6	1.3
Bowman and Cohen (1997)	CFC-12	0.75-1.0
Gilliland (1997)	CH_4,CH_3,CFCs	0.99-1.11
Lintner et al. (2004)		1.3/0.86
Denning et al. (1999)	SF_6	0.55-1.26
Kjellström et al. (1999)	$SF_6/^14CO_2$	0.9
Aghedo et al. (2008)	idealized	0.7
This study	^{85}Kr	0.9

Table 5.1: Exchange times between hemispheres from previous studies.

In several previous studies interhemispheric exchange was analyzed using different trace species. The resulting interhemispheric transport times are presented in Table 5.1. Jacob et al. (1987) used a Chemical Transport Model with a horizontal resolution of $8° \times 10°$ that is forced by a 3D-GCM with a resolution of $4° \times 5°$ horizontal resolution and nine vertical levels. An average interhemispheric exchange time of 13.2 months was found. That is 26% longer than the result of this ^{85}Kr – study. Levin and Hesshaimer (1996) studied the interhemispheric transport of ^{85}Kr by evaluating measurements in a two box model approach. They calculated mean concentrations from weighted measurements and derived exchange times from 18 up to 20 months, which is 80% longer than in our model results. A possible reason for those long exchange times is the fact, that the vertical distribution of ^{85}Kr differs between the hemispheres. As the sources on the Northern Hemisphere are close to the ground, the concentration decreases with height. The interhemispherical transport takes place in higher levels of the atmosphere, the slow downward mixing in the southern box is a possible reason for the slow exchange derived from ground based measurements. Evaluating a 2D transport model, Levin and Hesshaimer obtained lower exchange times similar to those derived by Jacob. Kjellström et al. (1999) analysed the transport of SF_6 and $^{14}CO_2$ in ECHAM4. They calculated a τ_{ex} of 10.8 months which is only 3 % above the exchange time of 10.5 months derived in this study. Aghedo et al.

(2008) investigated the resolution dependence of the interhemispheric transport of idealized tracers with different lifetimes in ECHAM5 and obtained a dependence on model resolution finding decreasing exchange time with increasing resolution. For the resolution T63L31 (nudged with ERA-40) the mean exchange time found by Aghedo et al. (2008) was with 8.5 months by two months faster than derived in this thesis.

5.2 Connection between exchange time and circulation phenomena

The main processes causing the interhemispheric transport are divergent outflow from tropical deep convection and the positioning of the ITCZ. The seasonal variation of the Hadley circulation also contributes to interhemispheric transport (Bowman and Cohen, 1997).

5.2.1 El Niño Southern Oscillation

The El Niño Southern Oscillation (ENSO) with its warm phase El Niño and the cold counterpart La Niña is subject of many research studies in Earth system science. The oscillation occurs with an irregular period. Gilliland (1997) investigated possible connections between τ_{ex} and ENSO and stated an interdependence between 1988/89 La Niña events and slightly faster interhemispheric transport. Lintner (2003) also evaluated the phase relationship between ENSO and τ_{ex} anomaly from 1981 to 1994 and supposed a connection. Based on the monthly τ_{ex} values processed over 35 years from 1971 to 2005 such connections between circulation phenomena and the interhemispheric transport time are investigated. The definition of the Southern Oscillation Index (SOI) describing ENSO uses the atmospheric surface pressure difference between Tahiti and Darwin. The difference Δp of the monthly means at the stations and $\overline{\Delta p}$ is the climatological average for the respective month while the standard deviation of that average stands in the denominator.

$$\mathrm{SOI} = 10\frac{\Delta p - \overline{\Delta p}}{\sigma(\Delta p)} \tag{5.6}$$

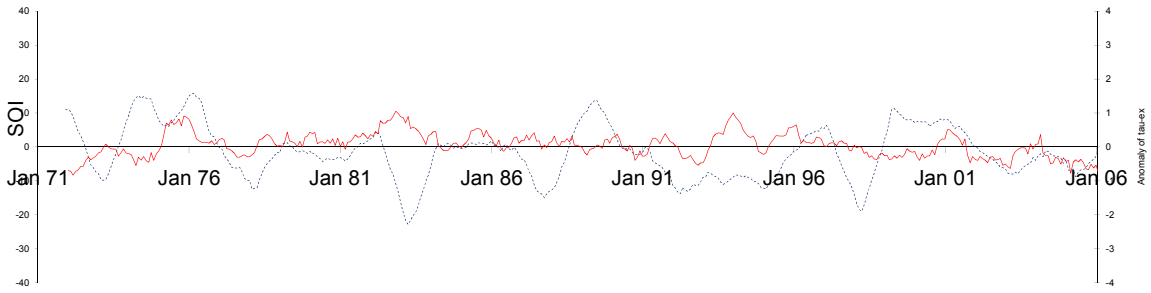

Figure 5.4: Running means of SOI (blue dashed line) and anomaly of τ_{ex} (red solid line) from 1971 to 2005.

Negative SOI values indicate El Niño conditions, positive SOI values occur during La Niña phases. Interpolating the surface pressure field in the results of the ^{85}Kr background simulation to Tahiti and Darwin gives an ECHAM5 internal SOI. The correlation coefficient between the monthly SOI calculated from model data and SOI from observations from 1971 to 2005 published by the Australian Government's Bureau of Meteorology is $r = 0.95$ (Bureau of Meteorology,Australian Government, 2009). However, in this simulation the nudging probably enforces the corresponding atmospheric pattern. Nevertheless ECHAM5 is capable of simulating ENSO phases correctly on its own in the coupled version with the ocean circulation model MPI-OM as evaluated by van Oldenborgh et al. (2005) which was not used for this study.

Figure 5.4 shows the running mean of the SOI and τ_{ex}. Although there seems to be a slight anticorrelation in some phases, there is no unique and general connection recognizable for the whole period. A correlation analysis of this kind between the anomaly of the monthly τ_{ex} from the 35-year average of the respective month in ECHAM5 nudged with ECMWF data and a various available circulation indices (list in Table 5.2) gives no significant connection of those indices to interhemispheric transport. Only the Antarctic oscillation index gives with $r = 0.17$ a weak positive correlation while the so called East Atlantic/West Russian pattern shows with $r = -0.17$ a weak negative correlation.

5.2.2 Asian Monsoon

Monsoon systems are seasonal circulation phenomena building up in response to different heating of continental land mass and the surrounding oceans. The strongest

index	name	corr. with τ_{ex} ano.
NAO	North Atlantic Oscillation	0.0
EA	East Atlantic Pattern	0.02
WP	West Pacific Pattern	0.01
EP/NP	EastPacific/North Pacific Pattern (EP/NP)	0.09
PNA	Pacific/North American Pattern	0.07
EA/WR	East Atlantic/West Russia Pattern	-0.17
SCA	Scandinavia Pattern	0.05
TNHT	Tropical/Northern Hemisphere Pattern	-0.05
POL	Polar/Eurasia Pattern	0.07
PT	Pacific Transition Pattern	0.1
AAOI	Antarctic Oscillation index	0.17

Table 5.2: List of circulation indices which show no distinct correlation with interhemispheric transport time anomaly (NOAA, National weather service, 2009, provided index data).

monsoon is situated between the continental land masses of Asia and Australia, consisting of the Indian Monsoon, South East Asian Monsoon, and East Asian Monsoon. The East Asian monsoon has two phases: Winter monsoon with northeasterly dry winds and summer monsoon with warm humid southwesterly winds bringing much precipitation to East Asia. The southwesterly current from the subtropical high forms a frontal convergence zone when meeting the westerly jet causing a distinct rain band over East Asia. This band moves northwards until summer monsoon season ends in August and then retreats to the south. Figure 5.5 shows the model evaluation for the observations in Tsukuba, Japan - the observation site is heavily influenced by ^{85}Kr emissions from Tokai reprocessing plant at 60 kilometers distance. But from March 1997 to May 2000 the reprocessing plant was not operational due to two accidents in the facility. As the model applied annual emission data, only in the years 1998 and 1999 Tsukuba was not influenced by close emissions neither in reality nor in the model. The seasonal variation of the ^{85}Kr background concentrations is simulated with excellent agreement. This annual cycle can be explained by the East Asian Monsoon. The southwesterly winds in summer transport air with low ^{85}Kr levels from the south to Tsukuba in summer while the in winter the north-easterly current carries air with raised ^{85}Kr concentrations from Russian and European sources. The presence of meridional flows during monsoon season leads to the hypothesis of a connection between monsoon intensity and interhemispheric transport.

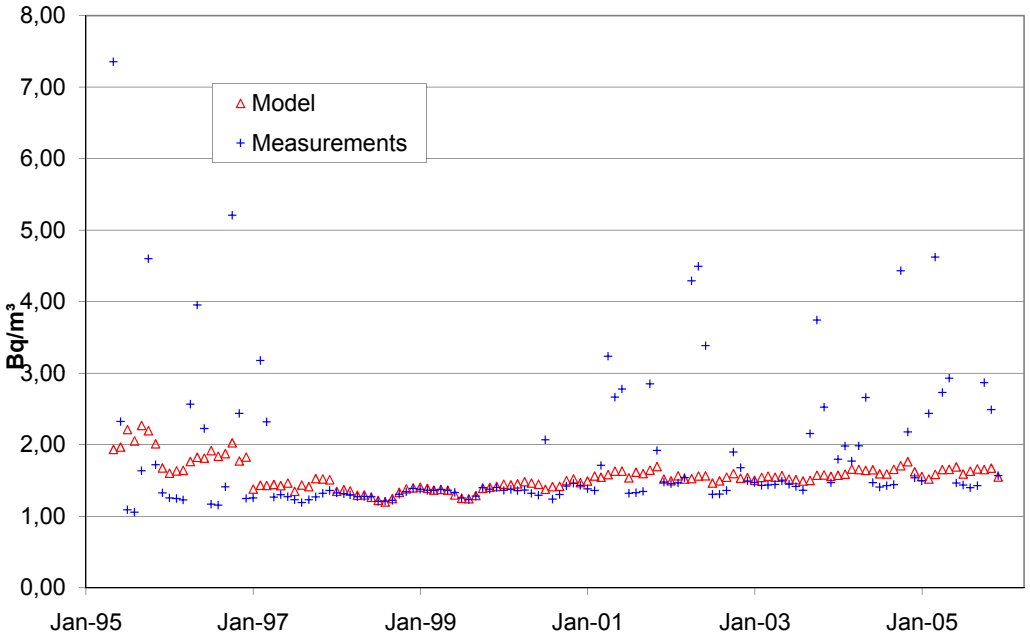

Figure 5.5: Simulated monthly mean concentrations at Tsukuba. The reprocessing plant Tokai was not operational from June 1997 to May 2000.

Monsoon indices

For quantifying the strength of Asian monsoon Webster and Yang (1992) developed a circulation index (called Webster-Young monsoon index- WYMI) which is calculated as the vertical shear in zonal wind u between the 200 hPa and the 850 hPa level averaged over the area from 0°N to 20°N latitude and from 40°E to 110°E longitude.

Wang and Fan (1999) proposed to treat the Indian monsoon and the East Asian monsoon indices separately and developed the Indian Summer Monsoon index (ISMI) and for the East Asian Monsoon the "Western North Pacific Monsoon Index" (WNPMI). For the Australian monsoon the index (AUSMI) is defined by Kajikawa et al. (2009).

$$\begin{aligned}
\text{WYMI} &= u_{200\text{hPa}} - u_{850\text{hPa}}\ (0°\text{-}20°\text{N}/40°\text{-}110°\text{E}) \\
\text{ISMI} &= u_{850\text{hPa}}(5°\text{-}15°\text{N}/40°\text{-}80°\text{E}) - u_{850\text{hPa}}(20°\text{-}30°\text{N}/70°\text{-}90°\text{E}) \\
\text{WNPMI} &= u_{850\text{hPa}}(5°\text{-}15°\text{N}/100°\text{-}130°\text{E}) - u_{850\text{hPa}}(20°\text{-}30°\text{N}/110°\text{-}140°\text{E}) \\
\text{AUSMI} &= u_{850\text{hPa}}(15°\text{-}5°\text{S}/110°\text{-}130°\text{E})
\end{aligned}$$

index	month	τ_{ex}-month	r	p-value
WYMI	Jun	Jun	-0.29	9.5%
	Sep	Oct	-0.26	12.7%
ISMI	Jun	Jul	-0.45	0.6%
	Aug	Aug	0.35	4.0%
	Sep	Sep	-0.32	5.9%
WNPMI	Jun	Jun	-0.27	13.6%
AUST	Jan	Feb	-0.32	6.0%
WASMI	Jun	Jun	-0.31	6.6%
	JJA	JJA	-0.26	13.4%
	JJA	JAS	-0.35	3.8%
	JJAS	JJAS	-0.43	0.9%

Table 5.3: Correlation coefficient between 35 years of the listed monsoon indices and τ_{ex} for the respective month or the following month and t-test p-value.

There is also a monsoon cycle at western Africa. The West African Summer Monsoon Index (WASMI) is defined at the 850 hPa level using a so called *dynamical normalized sasonality (DNS)* averaged over the area 5°-17.5°N/20°W-40°E (Li and Zeng, 2003). The DNS is calculated building the differences between the climatological mean of the wind vector of each month and the current wind vector of that month.

Monsoon correlation with interhemispheric transport

The indices introduced above are available from the International Pacific Research Center, Hawaii (Kajikawa and Wang, 2009) from 1948 to 2008 derived from NCEP/NCAR reanalysis data. The normalized index series are provided for the monsoon season June, July, August, and September and the derived seasonal means JJA/JJAS. A correlation analysis was performed using the τ_{ex}-data of the respective months to investigate interdependencies with the interhemispheric exchange time τ_{ex} of the respective months. As the τ_{ex} values were calculated from month to month and as means at the middle of the month, also the following month was taken into account, i.e. the τ_{ex} value is valid for the beginning of the month. Table 5.3 shows all combinations from which a correlation coefficient $|r| > 0.25$ resulted. In general, only the August datasets led to a positive correlation. The negative correlation indicates that when strong monsoons are present, τ_{ex} is small and the interhemispheric transport

is fast. The highest correlation occurs with Indian Summer Monsoon at its beginning, also the mean seasonal African monsoon shows a anti-correlation of $r = -0.43$ with mean τ_{ex}–season from June to July. The only significant positive correlation is found between South Asian Monsoon and τ_{ex} in August, when the monsoon system reaches its maximum northern extent. For analyzing the statistical significance of the correlation coefficients a t-test was performed. This test is only valid strictly if the samples follow a Gaussian distribution. The resulting p-value is the probability of the hypothesis of uncorrelated samples (r=0) being true. Only the correlations of Indian Summer Monsoon and seasonal average of West African Summer Monsoon with the respective τ_{ex} values fulfill the requirement of a 95% significance level. The results show that there is an interdependence between the monsoon systems and interhemispheric exchange. This is to the authors knowledge the first systematic study investigating the correlation of simulated interhemispheric exchange time and monsoon indices over a long time series. The advection of southern air with lower ^{85}Kr concentrations during monsoon season influences the background concentrations in the corresponding regions and has a positive influence on the detectability of additional ^{85}Kr sources. The more dominant process related to interhemispheric transport, strong convection updrafts in the ITCZ, can impede the detection of secretly operated ^{85}Kr sources in the ITCZ with ground based measurements.

6 Detectability of additional ^{85}Kr releases

The potential of detection of the ^{85}Kr signature from clandestine plutonium separation activities in atmospheric air samples is studied in this chapter. The minimum strength of the hypothetical sources (Figure 6.1) to cause concentrations significantly exceeding the variability of the background concentrations is calculated using the Lagrangian Particle Dispersion Model HYSPLIT. The possible sampling approaches for ^{85}Kr inspection procedures are discussed in Chapter 2.

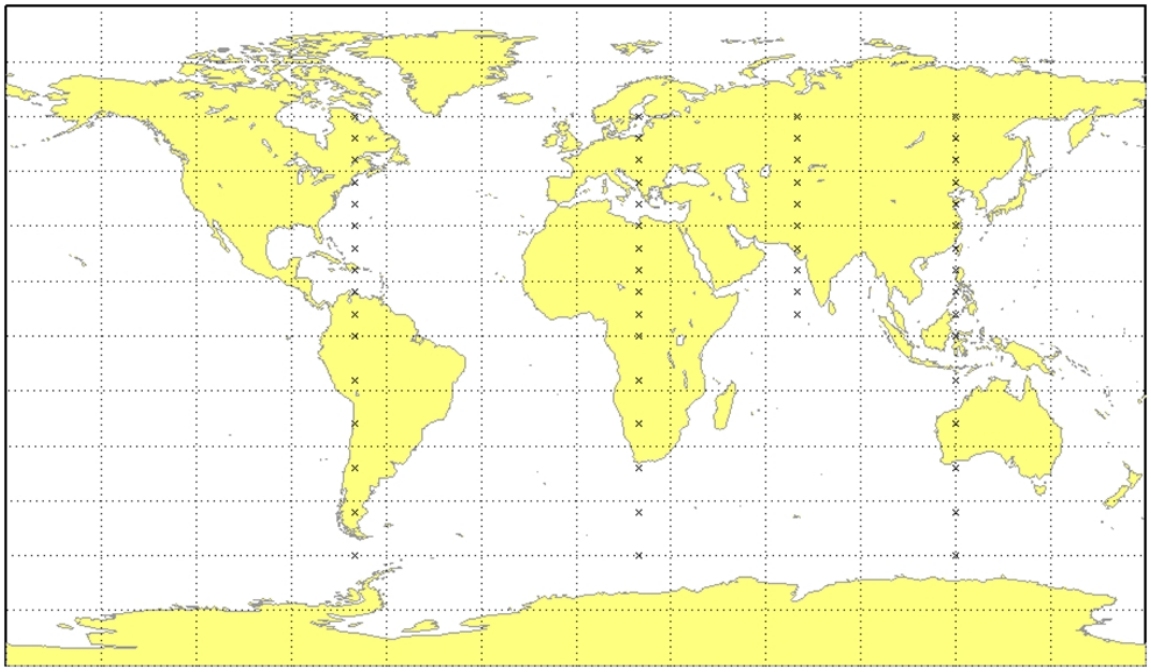

Figure 6.1: Geographical distribution of hypothetical ^{85}Kr release locations.

6.1 Sensitivity to hypothetical ^{85}Kr sources

This study investigates the potential to detect additional ^{85}Kr plumes released from a grid of hypothetical release points above the simulated background variability given by the ECHAM5 study (Chapter 4). The investigation refers to the simulated maximum concentration in the plumes which implies the optimistic assumption, that it is possible to take samples close to the center of the plume. Thus, the results are only strictly valid, if a fixed sampling station is hit by the plume or if the inspector gets to the right place at the right time in the "Catch the plume"–scenario. Therefore, this study investigates the theoretically highest potential for detection. The quantification of detection probabilities in real situations with real sampling equipment is beyond the scope of this model study.

6.1.1 The HYSPLIT model and simulation setup

The Lagrangian particle dispersion and trajectory model HYSPLIT ("Hybrid Single-Particle Lagrangian Integrated Trajectory") was developed jointly by the US National Oceanic and Atmospheric Administration (NOAA) and the Australian Weather Service. The model is described by Draxler and Rolph (2003). For this study, gridded meteorological data from the Global Data Assimilation System (GDAS1) archive hosted by NOAA's Air Resources Laboratory (ARL) for the year 2005 has been used. The resolution of the meteorological data was $1^\circ \times 1^\circ$, the resolution of the model grid for concentration calculations was set to $0.1^\circ \times 0.1^\circ$. As the precision of the concentration field is therefore not fully supported by the applied wind field data the meteorological interpretation of the plume shape is limited. The height of the atmosphere was set to 10 km and the vertical winds were taken from the input data. The simulation domain was restricted to an area of $50^\circ \times 50^\circ$ with the source location in its center.

6.1.2 Release points and emission scenario

For this study a source location setup was defined comprising 58 stations globally grouped in 4 clusters: Atlantic/South America, Europe/Africa, Central-East, and

Far East/Australia. All except the Central East cluster includes 16 sources, the latter one 10. Their geographical distribution is shown in Figure 6.1. In order to calculate the ^{85}Kr concentration at surface level the HYSPLIT Model has been used. For each source a constant ^{85}Kr emission signal of 6 hours has been assumed released at an elevation of 10 meters (a.g.l.). The emission flux had been set to 1 in arbitrary units in order to be scaled in subsequent analysis. The propagation of the concentration plume for the subsequent 144 h (6 days) has been calculated. Every 6 hours a concentration output has been stored, averaging concentration levels of the preceding 6 hours. The starting time of emissions was 9:00 a.m. at 8th day of each month in 2005 except for the months January and March where the starting time was set to 9:00 a.m. at 15th because of missing meteorological data. A number of 16704 data fields have been generated, thereof 8532 were used for the analysis. The difference is due to plumes that left the model area of $50° \times 50°$ within the simulated time of 6 days because of high wind velocities. The first three days after release which are of particular interest for the detection of small sources are not affected by this effect of plumes leaving the model area.

6.2 Results on detectability

For the assessment of detectability the concentration maximum in the plume was evaluated for each stored time step. The criterion for possible detection in this model study was that the concentration in question has to be at least three sigma of the background concentrations of the month in question. Thus, only if the potentially measurable signal exceeds three standard deviations of the background, the signal is assumed to be detectable. For the variability the standard deviations of the monthly means from ECHAM5 were taken as presented in Chapter 4. The values represent the variability of the instantaneous six hourly surface concentrations in the global model. As the specific time patterns of the emissions from reprocessing plants were not included in the global model, the variability may be higher in regions directly influenced by active background sources. In the HYSPLIT runs a standard emission strength of 1 unit was assumed. It is easily possible to scale the source strength linearly according to a specific expected concentration. For that, the quantity of the minimum detectable release was defined: The minimum detectable release (S_{MDR}) is

calculated according to (6.1) with σ_g being the location specific standard deviation of the global background calculated by ECHAM5, E the emission scale factor in HYSPLIT determined by source strength and pulse length, and c the local concentration output of HYSPLIT.

$$S_{\mathrm{MDR}} = \frac{3\sigma_g E}{c} \tag{6.1}$$

Taking three standard deviations as threshold accounts for the fact that the temporal pulse patterns of the background sources were not resolved in the global model and that measurements indicate a higher variability of concentrations than simulated by ECHAM5. That way of definition of S_{MDR} (6.1) implies that low sensitivity leads to high minimum detectable releases and high sensitivity - thus good detectability - is expressed by low minimum detectable release values.

For the analysis three thresholds for the minimum detectable release are of special interest for the application: A release of

- 3.2 TBq according to the emission scenario for one dissolution campaign out of fifty campaigns during one year for retrieving one significant quantity plutonium (8 kg).
- 10 TBq assuming a more active plant.
- 100 TBq corresponding to the emissions of an industrial facility.

For comparison it has to be considered that daily emissions of the reprocessing plant La Hague exceed occasionally 1000 TBq and have daily mean values of several hundred TBq (e.g. 650 TBq per day in 2007). Figure 6.2 shows as example the results for one plume from the Far East longitude band. In the pictures the blue filled area indicates, where the minimum detectable release is below the threshold of the corresponding row and therefore detection is possible. The columns indicate the situation 24, 48, and 72 hours after end of the 6 hour release phase. In this example, only for the big threshold, detectability is still given after 72 hours (Figure 6.2i). The small release of 3.2 TBq is detectable after 24 h (Figure 6.2a) but not after 48 hours, when a 10 TBq release would still be detectable (Figure 6.2e).

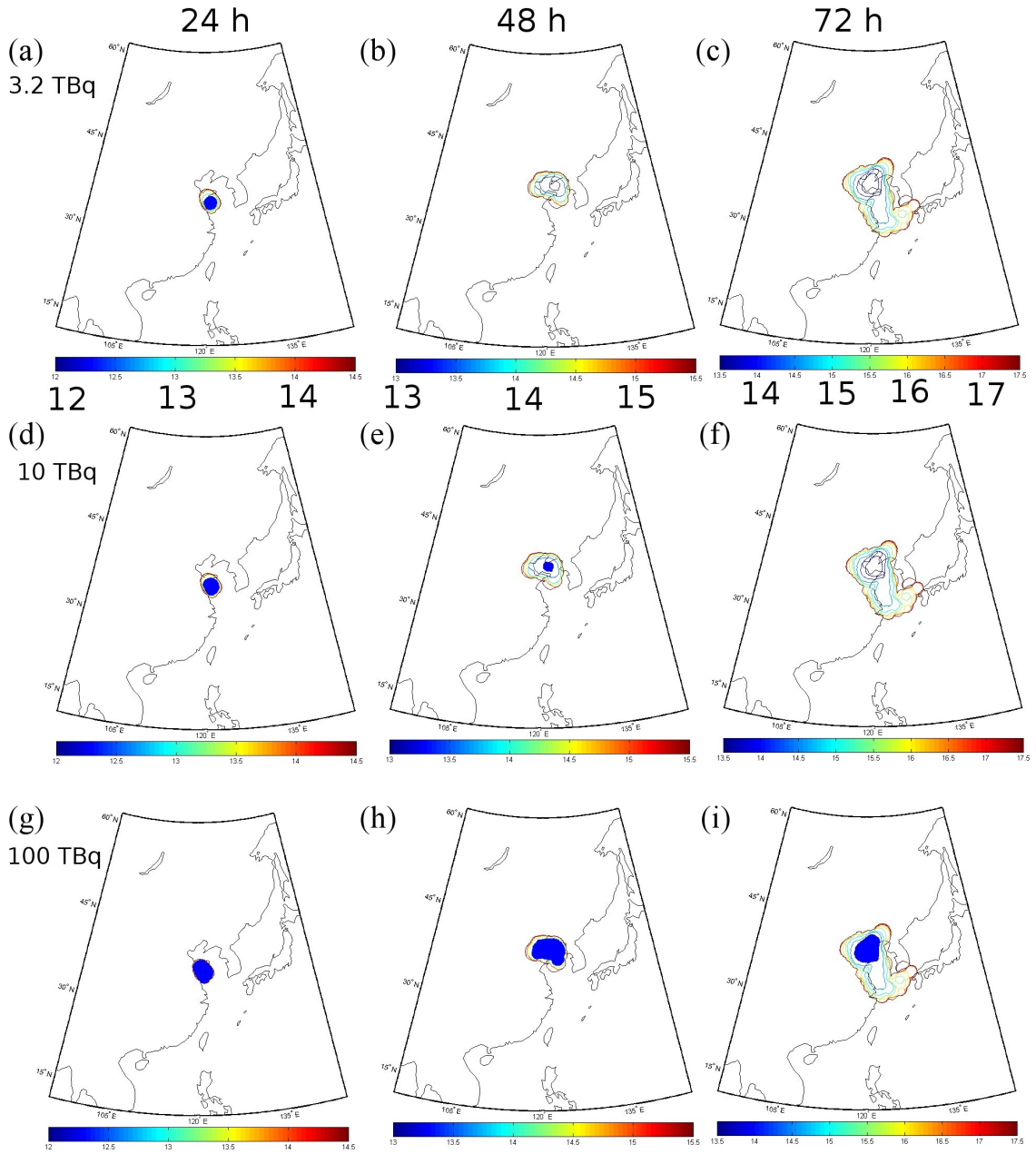

Figure 6.2: Example for detectability situation 24 (a, d, g), 48 (b, e, h) and 72 (c, f, i) hours after release. The blue filled area indicates the area where a 3.2 TBq (a, b, c) , 10 TBq (d,e,f) and 100 TBq (g, h, i) release would be detectable. The contour lines indicate the power of ten of the dilution factor.

Figure 6.3 shows how detectability evolves in time after the end of the 6-hour release.

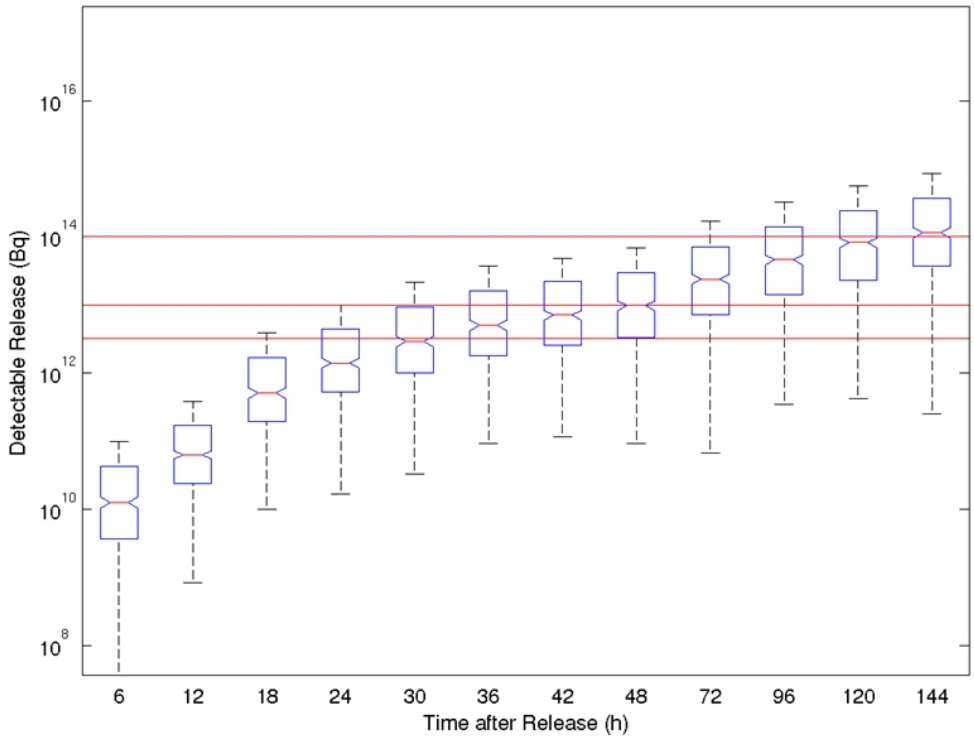

Figure 6.3: Minimum detectable release against time after release stop. The horizontal lines indicate the 3.2, 10 and 100 TBq threshold.

The median and the lower and upper quartile are indicated by the boxes. Thus, for example a release of 3.2 TBq was detectable in nearly half of the cases after 30 hours. About 25% of the 3.2 TBq releases are still detectable 48 hours after release. The time passed after release is clearly a critical factor for the detection as after 72 hours the releases have to be bigger than 3.2 TBq to remain detectable.

Figure 6.4 shows the detectable release in dependence of the distance of the plume centre, i.e. the maximum concentration in the plume, from source. Under very suitable conditions, a plume can still be detectable at more than 1000 km distance from the source. For most cases, the detectability is limited to 500 km distance. The shape of the maximum of a plume is in general occurring as a rather broad peak so that small deviations from the plume center affect the detectability only marginally.

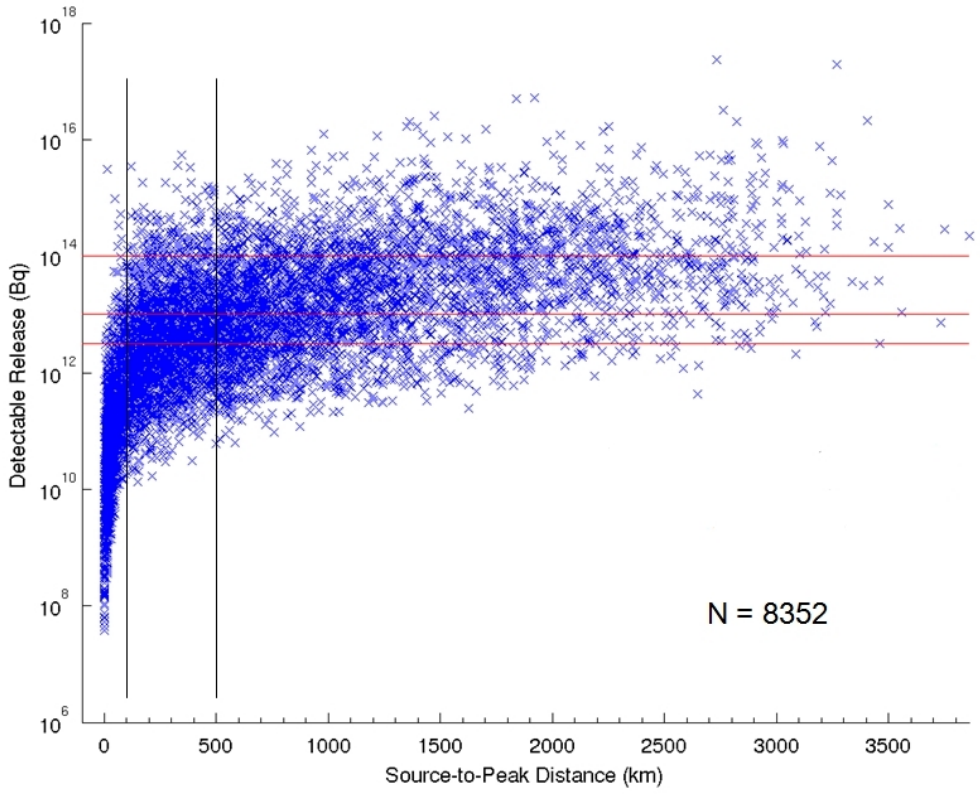

Figure 6.4: Minimum detectable release against distance of plume maximum from source location. The vertical lines are at 100 and 500 km distance.

Nevertheless quantifying the probability of catching a plume under real conditions would have to account for a prediction error.

An analysis of the seasonality of the minimum detectable releases showed no characteristic dependence. Table 6.1 summarizes the detectability for the considered regions and emitted activities concerning detectability after 24, 48 and 72 hours after stop of release. As expected the results show large differences between the hemispheres and depend on the distance to western European background sources. The results on the Southern Hemisphere are quite promising with detection of even the small release of 3.2 TBq in 93% of the analyzed cases 24 hours after end of a 6-hour release and still more than 50 percent after 48 hours. However, at 20°East, Northern Hemisphere, only 100 TBq releases reach high detection probabilities. Remarkable is the reduction of potential detectable situations between 24 and 48 hours after release.

LON	Time	3.2 TBq	10 TBq	100 TBq
Northern Hemisphere				
70°W	24 h	71 %	93 %	100 %
	48 h	8 %	50 %	90 %
	72 h	3 %	19 %	79 %
20°E	24 h	23 %	55 %	97 %
	48 h	3 %	8 %	77 %
	72 h	1 %	4 %	45 %
70°E	24 h	71 %	94 %	100 %
	48 h	14 %	48 %	94 %
	72 h	5 %	24 %	88 %
120°E	24 h	72 %	93 %	100 %
	48 h	20 %	45 %	95 %
	72 h	10 %	29 %	81 %
Southern Hemisphere				
70°W	24 h	89 %	97 %	100 %
	48 h	54 %	78 %	93 %
	72 h	39 %	62 %	90 %
20°E	24 h	93 %	99 %	100 %
	48 h	51 %	75 %	94 %
	72 h	25 %	54 %	83 %
120°E	24 h	93 %	100 %	100 %
	48 h	49 %	76 %	97 %
	72 h	25 %	54 %	90 %

Table 6.1: Percentage of cases fulfilling the detection criterion for the three reference emission quantities 24, 48, and 72 hours after stop of release listed per region (100% corresponds to a sample 120 plumes on the northern and 72 plumes on the southern hemisphere).

7 Conclusions and outlook

The goal of this thesis was an assessment of the detectability of ^{85}Kr releases from undeclared nuclear reprocessing for the separation of plutonium for nuclear weapons. This supports the IAEA in the effort to develop novel technologies for the detection of clandestine nuclear activities violating the Non-Proliferation Treaty.

For the analysis of the ^{85}Kr background and its variability, the long term global distribution caused by emissions from known reprocessing plants was simulated using the general circulation model ECHAM5. To investigate the potential detectability above the variability simulated by ECHAM5, hypothetical ^{85}Kr plumes were simulated using the Lagrangian particle dispersion model HYSPLIT.

In first tests of ECHAM5 with tracer point sources negative concentrations caused by the convective transport and an increase of total tracer mass caused by the advection scheme occurred. The code was successfully modified to prevent negative concentrations and a mass fixing routine was applied scaling the atmospheric ^{85}Kr content according to the actual ^{85}Kr budget for every single time step.

The evaluation of the simulated concentrations against measurements provided by the German Federal Office for Radiation Protection shows very good agreement. The deviation of model results in terms of mean normalized bias is smaller than 0.05 at most observation sites. Only in the direct vicinity of sources the agreement of the coarse Eulerian Model with the observations is worse as the sub-grid scale shape of the plumes cannot be resolved in ECHAM5. The comparison of the simulated concentrations with a small set of balloon and aircraft measurements as well as measurements on Atlantic ship cruises shows a very good agreement with relative model errors below 10%.

The further analysis of ^{85}Kr concentration time series at various observation sites shows a realistic behavior of the variance of weekly averaged concentrations in the Northern Hemisphere. The simulated variability of concentrations in the Southern Hemisphere is much lower than indicated by observations.

Further analysis was performed on global atmospheric circulation. With the known ^{85}Kr sources located nearly exclusively on the Northern Hemisphere the air mass exchange across the equator was investigated in the simulation data. The calculated characteristic exchange time τ_{ex} of 10.5 months is similar to values obtained in previous studies. The analysis of the 35 year series of monthly calculated τ_{ex} shows negative correlations between interhemispheric transport time and certain monsoon indices in the respective months of monsoon season. Hence, strong monsoon events accelerate the interhemispheric transport.

For the analysis of the hypothetical ^{85}Kr plume simulations using the Lagrangian particle dispersion model HYSPLIT, minimum releases are determined causing concentrations in the plume center three times as high as the location specific background variability simulated by the global model ECHAM5. The smallest reference release was 3.2 TBq, which is the amount of ^{85}Kr released per batch if separating one significant quantity plutonium in 50 weekly dissolution batches. The results show that in particular for the detection of such a 6-hour release of 3.2 TBq the measurement should take place within 24 hours after the stop of release. On the Southern Hemisphere the chances of detection are higher because of the less variable background situation. The release on industrial scale of 100 TBq in 6 hours stays detectable for more than two days under most conditions.

Although the probabilities for definitive detection of small releases are limited in the current situation there would be a deterrent effect of the possibility of detection. Even a method with a detection probability of only $p = 5\%$ for a single plume leads to considerable chances of detection when applied over a longer period. Thus in the reference scenario of 50 plumes the probability of at least one detection is $1 - (1 - p)^{50} = 92\%$. Of course this reasoning is only valid if there is a very low false alarm rate which again brings the background variability into the focus.

The next steps for the project to which this thesis provides a major contribution are further background modeling studies on regional scale or global scale in higher

spatial and temporal resolution with improved information about the emission times of the strong background sources. Furthermore, the potential of localization of unknown ^{85}Kr sources is planned using inverse Lagrangian modeling applying source-receptor-sensitivity matrices. For the IAEA an estimation of the expected costs of the application of various inspection approaches has to be done.

A further investigation of the variability of the ^{85}Kr concentrations on the southern hemisphere is desirable to clarify the discrepancy between simulations and observation. For the final quantification of detection probabilities sufficient measurement data with short sampling times are needed. The limitation to mostly week samples so far limits the possible conclusions on hypothetical detections applying air samples over only few hours or even taking grab samples. For that, case studies with short term measurements in the field are necessary.

In this thesis, the information on the short term characteristics was derived from model results exclusively. Although the good agreement of model results with measurements on a weekly base builds confidence in the capability of the global model, it is not possible to evaluate the model on shorter time scales. The evaluation situation for the model study performed with HYSPLIT is even less satisfying. There were neither real emissions nor measurements, hence, there is nothing to compare with for evaluation. In this case one has to rely on HYSPLIT being tested and evaluated for many plume dispersion cases and therefore the simulated plumes evolve in a realistic way. The practical challenge will be to develop inspection strategies that maximize the probability of getting concentrations close to the plume maximum in the field. Aircraft measurements could improve the coverage of larger regions but are not foreseen in the current IAEA safeguard procedures.

The applicability of the ^{85}Kr method for IAEA safeguards also depends strongly on the future development of civilian nuclear reprocessing. If the commercial facilities ended their ^{85}Kr releases the background variability would shortly be suitable for the detection of illicit ^{85}Kr sources. Although the ^{85}Kr emissions of commercial plants seem to be irrelevant under environmental aspects, the verification of the NPT and a future ban of fissile material production for nuclear weapon construction could serve as an argument for efforts to minimize civilian ^{85}Kr emissions in order to achieve an more advantageous background situation.

In the IAEA report STR-321 IAEA (1999) a grid of only 25 km spacing between the measurement stations was considered necessary to utilize ^{85}Kr for the detection of the separation of small plutonium quantities. The case study concerning the Karlsruhe reprocessing plant (Kalinowski et al., 2004) showed for the specific situation with a stronger source, that an operation at 100 km distance could be detected in weekly cumulative samples without applying atmospheric transport models. In this thesis it is shown that ^{85}Kr detections may be possible up to 500 km from the source if support by atmospheric transport models and a qualified understanding of the specific background situation.

The knowledge about the ^{85}Kr background and its variability was considerably improved by the results of this thesis. Furthermore the first quantitative analysis of the potential detectability of additional ^{85}Kr sources taking the location specific background into account was achieved.

There is still a long way to go to the final application with technical requirements for facilitating measurements as well as severe challenges in the field of atmospheric transport modeling to be solved. In spite of those open questions and the limitations of the method under current background conditions, ^{85}Kr is according to present knowledge the best signature for long range detection of clandestine plutonium production.

Acknowledgements

I would like to thank everybody who contributed to my work in the last 3 $\frac{1}{4}$ years.

I am very grateful to Prof. Dr. Martin Kalinowski for giving me the opportunity to start the project as well as for wise advices, his motivated and motivating drive, and many ideas. It was a great pleasure to accompany the impressive grow up of the interdisciplinary Centre for Science and Peace Research (ZNF).
Prof. Dr. Heinke Schlünzen is warmly acknowledged for her judicious support and structural guidance keeping my work on the right track.
I was very fortunate to be kindly invited by Dr. Johann Feichter to the Max Planck Institute for Meteorology - thanks for the generous integration into the ACC working group and for providing access to the institute's infrastructure.
I'm very thankful for the conscious supervision of my work with ECHAM5 and beyond by Dr. Sebastian Rast who was sharing his office for nearly one year with me and gave constructive and detailed remarks on the thesis draft. I appreciate his unselfish commitment extraordinary.

It was very fruitful for me to participate in the IMPRS on Earth System Modelling benefiting from the Advisory Panel System and learning much in courses and at the annual retreats.

Because of their particular work for the project at the ZNF I thank the assistants Jochen Ahlswede (emission inventory update), Robert Annewandter (creating and running MATLAB scripts controlling the HYSPLIT study) and Robert Schoetter (support in data evaluation and discerning –and sometimes concerning– remarks).

For providing data and models I would like to thank Clemens Schlosser and Hartmut Sartorius at BfS, the ECMWF for the ERA-40 and analysis data, and Roland Draxler from the HYSPLIT development team.
In computer issues there was always reliance on the DKRZ and the CIS team as well as the IT-Service of the Chemistry Department.

I thank the German Foundation for Peace Research for founding and funding the ZNF and my position. Further funding for the project was provided by the joint program of the Federal Government of Germany and the IAEA. I thank the German program committee and Andrew Monteith and Julian Whichello at the IAEA for the good collaboration.

For proof-reading under severe time constraints thanks to Benni, Christian, Jana, Markus, and Simon.

I would further like to acknowledge all colleagues at the Centre for Science and Peace Research, at the Max Planck Institute for Meteorology and the Meteorological Institute for the delighting and peaceful working environment and many interesting discussions. I enjoyed being part of the award winning WOODSTOCK model development team. I also liked the FONAS community of German scientific peace researchers and was glad to get to know the followers of responsibility at conferences of VDW, Union of Concerned Scientists, and Pugwash.

Of course I thank my parents as well as my brothers and sister for early education, and I thank my friends and bike-mates for spending time with me.
Finally I want to express my deep gratitude to Jana for the well-being and for us.

A Emission inventory used for the background simulation

The data used for the global ^{85}Kr background simulation is documented in the following tables. All annual emission values are given in PBq ^{85}Kr activity release.

	West Valley	*Yongbyon*	*Trombay*	*Tomsk*	*Tokai*	*Tarapur*	*Subei*
	USA	DPRK	India	Russia	Japan	India	China
LAT	42.4	39	19.5	56.63	36.5	20.3	39.3
LON	-78.6	125.7	72.8	84.92	140.6	72.9	97
1971	6.04	0	1.15	28.84	0	0	1
1972	0	0	1.15	24.89	0	0	1
1973	0	0	1.15	27.08	0	0	1
1974	0	0	1.15	26.88	0	0	1
1975	0	0.1	0	61.85	0	0	1
1976	0	0	0	47.12	0	0	1
1977	0	0	0	29.27	0.2	0	1
1978	0	0	0	29.82	2.41	0	1
1979	0	0	0	35.84	0.67	0.23	1
1980	0	0	0	30.91	6.63	0.23	1
1981	0	0	0	48.08	6.09	0.23	1
1982	0	0	0	48.6	9.75	0.23	1
1983	0	0	0	41.54	0.51	0.23	1
1984	0	0	0.08	38.42	0.01	0.15	1
1985	0	0	0.08	49.77	11.73	0.15	1
1986	0	0	0.08	40.79	8.86	0.15	1
1987	0	0	0.15	35.64	10.95	0.15	1
1988	0	0	0.15	40.7	7.75	0.15	1
1989	0	0.1	0.15	39.45	4.21	0.15	1
1990	0	0.1	0.15	28.55	15.36	0.15	1
1991	0	0.1	0.15	44.54	14.45	0.23	1
1992	0	0.1	0.15	36.85	12.82	0.23	0
1993	0	0	0.15	42.64	5.23	0.23	0
1994	0	0	0.23	48.98	13.77	0.23	0
1995	0	0	0.23	30	12.64	0.23	0
1996	0	0	0.23	20	9.14	1.2	0
1997	0	0	0.23	13	2.87	1.2	0
1998	0	0	0.23	13	0	1.2	0
1999	0	0	0.23	13	0	1.2	0
2000	0	0	0.23	13	1.6	1.2	0
2001	0	0	0.23	13	4	1.2	0
2002	0	0	0.23	13	2.9	1.2	0
2003	0	0.1	0.23	13	2.3	1.2	0
2004	0	0.1	0.23	13	3.7	1.2	0
2005	0	0.1	0.23	13	3.1	1.2	0
2006	0	0.1	0.23	13	1.4	1.2	0

	Sellafield	*Savannah*	*Saluggia*	*Rotondella*	*Rokkasho*	*OakRidge*	*Nilore*
	UK	USA	Italy	Italy	Japan	USA	Pakistan
LAT	54.415	33.3	45.2	41.1	40.96	36	33.65
LON	-3.498	-81.7	8	16.3	141.33	-84.3	73.26
1971	39.53	20.56	0.09	0	0	0	0
1972	41.87	22.2	0.1	0	0	0	0
1973	34.09	28.49	0.17	0	0	0	0
1974	25.37	18.5	0.16	0	0	0	0
1975	38.69	19.24	0	0.1	0	0	0
1976	35.05	27.38	0	0.1	0	0	0
1977	28.46	16.59	0	0.1	0	0	0
1978	25.9	19.61	0	0.1	0	0	0
1979	35	17.76	0	0.1	0	0	0
1980	31	21.46	0.1	0.1	0	0.33	0
1981	52	31.08	0.1	0	0	0.25	0
1982	44	19.06	0	0	0	0	0
1983	41.8	25.83	0.1	0	0	0	0
1984	37.1	25.83	0	0	0	0	0
1985	23.8	25.9	0	0	0	0	0
1986	53.3	24	0	0	0	0	0
1987	34.1	12	0	0	0	0	0
1988	39.7	4	0	0	0	0	0
1989	51.7	0	0	0	0	0	0
1990	37.6	0	0	0	0	0	0
1991	44.6	0	0	0	0	0	0
1992	27.4	0	0	0	0	0	0
1993	57	0	0	0	0	0	0
1994	38	0	0	0	0	0	0
1995	97	0	0	0	0	0	0
1996	101	0	0	0	0	0	0
1997	95	0	0	0	0	0	0
1998	99	0	0	0	0	0	0
1999	90.7	0	0	0	0	0	0
2000	73.6	0	0	0	0	0	0.16
2001	104	0	0	0	0	0	0.16
2002	101	0	0	0	0	0	0.16
2003	120	0	0	0	0	0	0.16
2004	120	0	0	0	0	0	0.16
2005	49.8	0	0	0	0	0	0.16
2006	22.8	0	0	0	17	0	0.16

	Mol	*Marcoule*	*LaHague*	*Krasnoyarsk*	*Karlsruhe*	*Kalpakkam*	*Idaho*
	Belgium	France	France	Russia	Germany	India	USA
LAT	51.2	44.133	49.683	56.37	49	12.2	43.4
LON	5.2	4.717	-1.883	93.68	8.4	80	-112.1
1971	4.68	3.7	4.2	23.53	0.61	0	5.07
1972	7.39	1.74	6.1	20.31	2.52	0	1.7
1973	8.02	4.81	5.6	22.09	0.93	0	0.19
1974	3.71	4.07	16	21.93	0.03	0	9.62
1975	0	3.7	14	50.46	1.59	0	0.89
1976	0	3.4	8.9	38.44	3.17	0	1.22
1977	0	4.33	16	23.88	4.25	0	4.11
1978	0	11.4	22	24.33	1.24	0	3.74
1979	0	10.36	24	29.24	1.87	0	0
1980	0	19.8	28	25.22	1.2	0	3.4
1981	0	11.47	29	39.22	2.6	0	2.18
1982	0	11.47	34	39.65	0.61	0	0.33
1983	0	22.94	49	33.89	2.8	0	0.11
1984	0	23	52	31.35	1.2	0	0
1985	0	23	85	40.61	3.4	0	0
1986	0	23	63	33.28	3.09	0	0
1987	0	23	70	29.07	2.71	0	0
1988	0	23	62	33.2	1.66	0	0
1989	0	23	92	32.19	0.76	0	0
1990	0	23	98	22.45	0.94	0	0
1991	0	23	100	40.33	0	0	0
1992	0	23	95	18.84	0	0	0
1993	0	23	115	28.87	0	0	0
1994	0	23	189	30.26	0	0	0
1995	0	15	230	20	0	0	0
1996	0	16	260	15	0	5.99	0
1997	0	5.7	300	10	0	5.99	0
1998	0	0	320	10	0	5.99	0
1999	0	0	300	10	0	5.99	0
2000	0	0	234	10	0	5.99	0
2001	0	0	227	10	0	5.99	0
2002	0	0	245	10	0	5.99	0
2003	0	0	252	10	0	5.99	0
2004	0	0	263	10	0	5.99	0
2005	0	0	301	10	0	5.99	0
2006	0	0	242.39	10	0	5.99	0

	Hanford	*Guangyan*	*Dounray*	*Dimona*	*Chelyabinsk*	*Ezeiza*	*Pelindaba*
	USA	China	UK	Israel	Russia	ARG	RSA
LAT	46.6	32.4	58.578	30.6	55.7	-34.85	-25.75
LON	-114.7	105.8	-3.753	35.1	60.7	-58.53	28.00
1971	17.8	0	0	0.23	49.63	0	0
1972	0	0	0	0.23	45.8	0	0
1973	0	0	0	0.23	49.82	0	0
1974	0	0	0	0.23	49.45	0	0
1975	0	3	0	0.23	113.79	0	0
1976	0	3	0.07	0.41	86.68	0	0
1977	0	3	0.03	0.41	53.85	0	0
1978	0	3	0.05	0.41	54.86	0	0
1979	0	3	0.05	0.41	65.93	0	0
1980	0	3	0.11	0.41	56.87	0	0
1981	0	3	0	0.41	88.45	0	0
1982	0	3	0	0.41	89.42	0	0
1983	0	3	0	0.41	76.42	0	0
1984	12.14	3	0	0.41	70.69	0	0
1985	5.72	3	0	0.41	65	0	0
1986	12.31	3	0	0.41	53.27	0	0.01
1987	18.17	3	0	0.41	53.71	0	0.01
1988	6.07	3	0	0.41	64.78	0	0.01
1989	0	3	0.57	0.41	63.65	0.1	0.01
1990	0	3	0.57	0.41	40	0.1	0.01
1991	0	3	0.57	0.41	70.68	0	0.01
1992	0	0	0.57	0.41	66.03	0	0.01
1993	0	0	0	0.41	101.57	0	0
1994	0	0	0	0.41	106.49	0	0
1995	0	0	0.49	0.41	60	0	0
1996	0	0	0	0.41	25	0	0
1997	0	0	0	0.41	25	0	0
1998	0	0	0	0.41	25	0	0
1999	0	0	0	0.41	33.01	0	0
2000	0	0	0	0.41	27.23	0	0
2001	0	0	0	0.41	35.01	0	0
2002	0	0	0	0.41	38.9	0	0
2003	0	0	0	0.41	19.45	0	0
2004	0	0	0	0.41	29.18	0	0
2005	0	0	0	0.41	29.18	0	0
2006	0	0	0	0.41	23.34	0	0

B Figures of background evaluation at further stations

This Appendix shows the comparison of simulated concentrations with measurements for further observation sites.

- At Krakow (Figure B.1) a peak caused by the Chernobyl accident in 1986 can clearly be seen in three measured samples.
- Perl (Figure B.2) is influenced by plumes from La Hague.
- In Heidelberg (Figure B.3) the end of operation of the Karlsruhe reprocessing plant at 40 km distance is clearly distinguishable.
- In Vienna (Figure B.4) there is quite realistic weekly variability simulated.
- At Cape Grim (Figure B.5) there is good agreement from 1987 to 1989, but from 1991 as well higher concentrations as higher variability observed than simulated.
- At Cape Point (Figure B.5) there is a abrupt change of observed variability and an elevation of absolute measured concentrations in 1989.

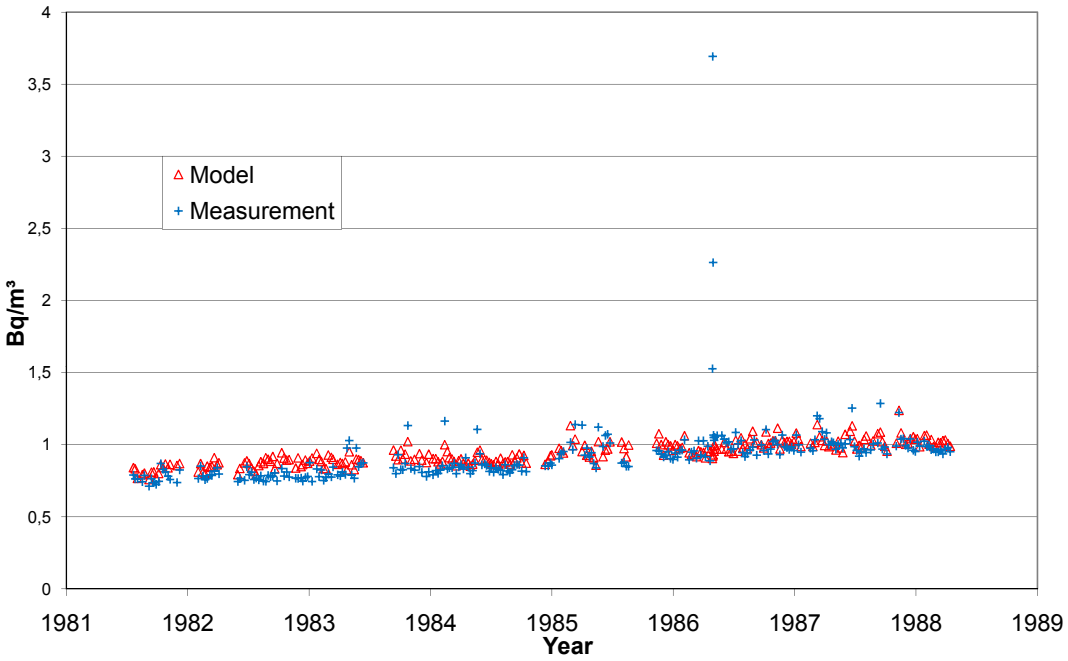

Figure B.1: Comparison between ^{85}Kr concentration in week samples from Krakow and simulated concentrations averaged over the corresponding week.

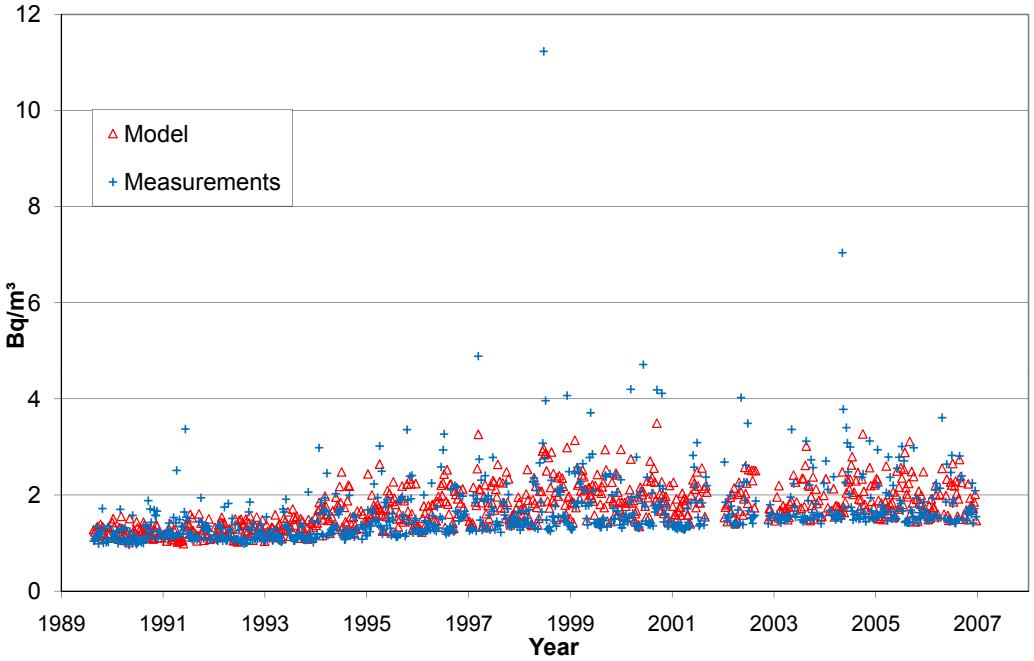

Figure B.2: Comparison between ^{85}Kr concentration in week samples from Perl and simulated concentrations averaged over the corresponding week.

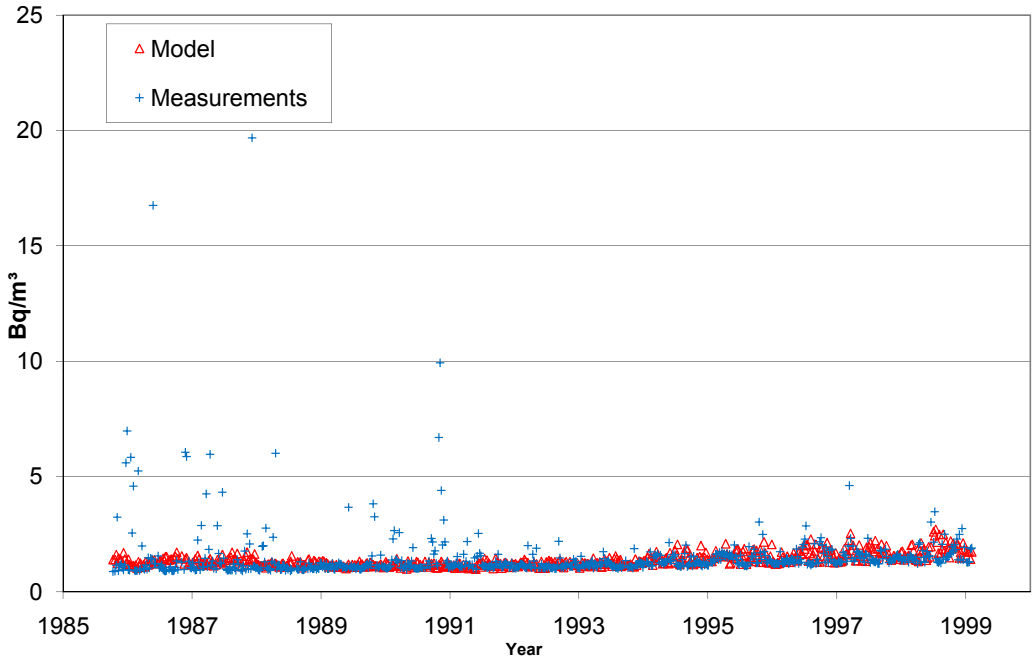

Figure B.3: Comparison between ^{85}Kr concentration in week samples from Heidelberg and simulated concentrations means over the corresponding week.

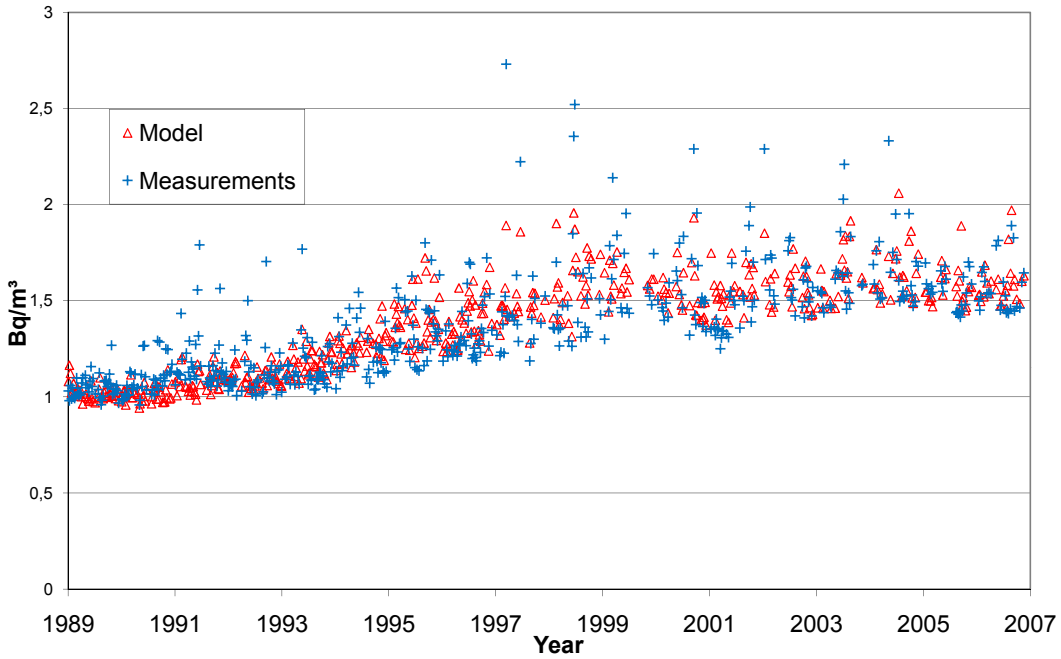

Figure B.4: Comparison between ^{85}Kr concentration in week samples from Vienna and simulated concentrations averaged over the corresponding week.

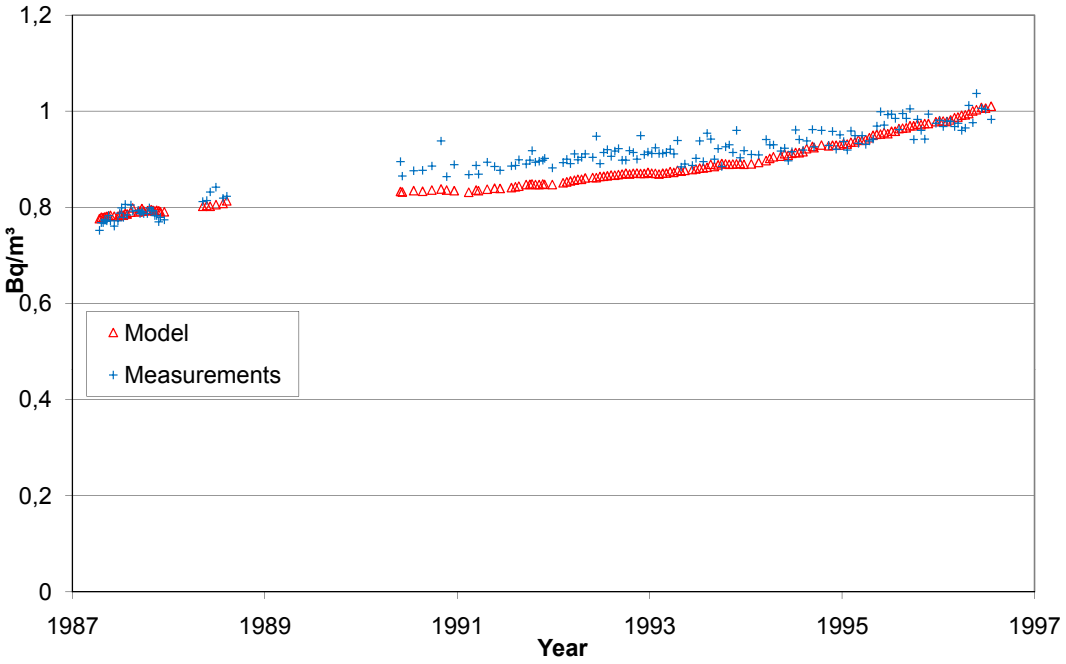

Figure B.5: Comparison between ^{85}Kr concentration in week samples from Cape Grim and simulated concentrations means over the corresponding week.

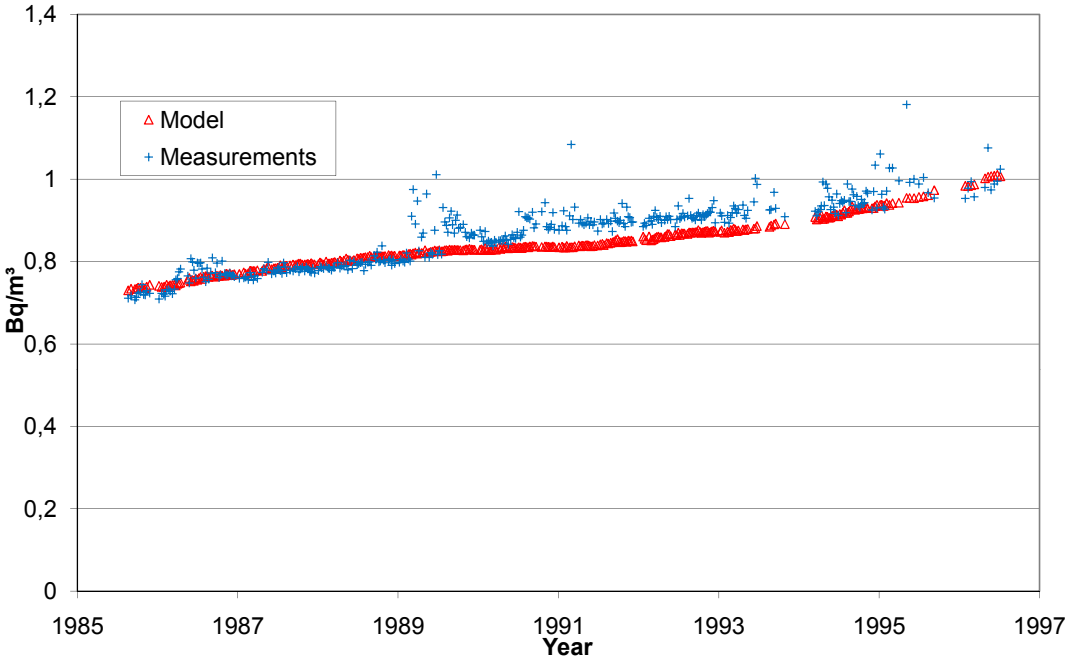

Figure B.6: Comparison between ^{85}Kr concentration in week samples from Cape Point and simulated concentrations means over the corresponding week.

C Two-Box-Model equations

A setup is considered with two equally sized boxes representing:

- Northern Hemisphere with index 1, tracer mass m_1, source S_1
- Southern Hemisphere: index 2, tracer mass m_2, source S_2

The tracer decays with the proportional factor λm_i. The tracer transport from hemisphere i to j is considered to be proportional to the tracer mass and determined by the exchange coefficient $\varphi_{ij} m_i$.

The system is described by the following equations with $\lambda, \varphi_{12}, \varphi_{21}, S_1, S_2 \geq 0$:

$$\dot{m_1} = -\lambda m_1 - \varphi_{12} m_1 + \varphi_{21} m_2 + S_1 \tag{C.1}$$
$$\dot{m_2} = -\lambda m_2 - \varphi_{21} m_2 + \varphi_{12} m_1 + S_2 \tag{C.2}$$

In the special case with $S_1 = S_2 = \lambda = 0$ and $m_1 = m_2 = m$:

$$\dot{m_1} = -\varphi_{12} m + \varphi_{21} m$$
$$\dot{m_2} = -\varphi_{21} m + \varphi_{12} m.$$

Assuming a uniform tracer distribution $\dot{m_1} = \dot{m_2} = 0$, thus because $m_i > 0$ it results:

$$\varphi \equiv \varphi_{12} = \varphi_{21}$$

The total air mass is conserved and the tracer mass distribution does not influence the air mass transport. So the system of differential equations for $m_1 \neq m_2$ can be written as

$$\dot{m_1} = -\lambda m_1 - \varphi m_1 + \varphi m_2 + S_1 \tag{C.3}$$
$$\dot{m_2} = -\lambda m_2 - \varphi m_2 + \varphi m_1 + S_2 \tag{C.4}$$

In order to decouple the equations we consider a variable transformation:

$$m_+ = m_1 + m_2$$
$$m_- = m_1 - m_2$$

With $S_+ = S_1 + S_2$ and $S_- = S_1 - S_2$ follows from (C.3)+(C.4) and (C.3)-(C.4):

$$\dot{m}_+ = -\lambda m_+ + S_+ \tag{C.5}$$
$$\dot{m}_- = -(\lambda + 2\varphi) m_- + S_- \tag{C.6}$$

with starting conditions $m_+(0) = m_{+0}$ and $m_-(0) = m_{-0}$.
The equation of the form $\dot{y} = -ay + b$ can be solved by substitution:

$$\begin{aligned} u &= y - \frac{b}{a} \\ \dot{u} &= \dot{y} \\ u(0) &= y_0 - \frac{b}{a} \\ u(t) &= u(0) e^{-at} \\ y(t) &= \left(y_0 - \frac{b}{a} \right) e^{-at} + \frac{b}{a} \end{aligned}$$

This gives the following solutions for (C.5) with $a = \lambda$ and $b = S_+$ and (C.6) with $a = \lambda + 2\varphi$ and $b = S_-$:

$$m_+(t) = \left(m_{+0} - \frac{S_+}{\lambda} \right) e^{-\lambda t} + \frac{S_+}{\lambda} \tag{C.7}$$
$$m_-(t) = \left(m_{-0} - \frac{S_-}{\lambda + 2\varphi} \right) e^{-(\lambda + 2\varphi)t} + \frac{S_-}{\lambda + 2\varphi} \tag{C.8}$$

Replacing $m_+(t)$ and $m_-(t)$ by definition and building (C.7)+(C.8) leads to the temporal evolution of $m_1(t)$:

$$\begin{aligned} m_1(t) = \frac{1}{2} \Bigg[& m_1^{(0)} e^{-\lambda t} (1 + e^{-2\varphi t}) + m_2^{(0)} e^{-\lambda t} (1 - e^{-2\varphi t}) - e^{-\lambda t} \left(\frac{S_1 + S_2}{\lambda} + \frac{S_1 - S_2}{\lambda + 2\varphi} e^{-2\varphi t} \right) \\ & + \frac{S_1 + S_2}{\lambda} + \frac{S_1 - S_2}{\lambda + 2\varphi} \Bigg] \end{aligned}$$

The equation for $m_2(t)$ can be obtained by subtraction (C.7)-(C.8) or by changing all indices.

Discussion of limits for large t and special cases

For a decaying tracer, the total mass will reach an equilibrium as soon as the source rate is equal to the decay:

$$\lim_{t\to\infty} m_+(t) = \frac{S_1 + S_2}{\lambda} \tag{C.9}$$

The mass difference m_- approaches a constant value for large times:

$$\lim_{t\to\infty} m_-(t) = \frac{S_1 - S_2}{\lambda + 2\varphi} \tag{C.10}$$

Without radioactive decay ($\lambda = 0$) and constant sources the limits are:

$$\lim_{\lambda\to 0} m_+(t) = m_{+0} + (S_1 + S_2)t \tag{C.11}$$

$$\lim_{t\to\infty}\lim_{\lambda\to 0} m_-(t) = \frac{S_1 - S_2}{2\varphi} \tag{C.12}$$

$$\lim_{\lambda\to 0} m_1(t) = \frac{S_1 + S_2}{2}t + \frac{S_1 - S_2}{4\varphi}(1 - e^{-2\varphi t}) \tag{C.13}$$

$$\lim_{\lambda\to 0} m_2(t) = \frac{S_1 + S_2}{2}t + \frac{S_2 - S_1}{4\varphi}(1 - e^{-2\varphi t}) \tag{C.14}$$

Thus, for large times t according to (C.13) m_1 and m_2 approach linear asymptotes with slope $\frac{S_1+S_2}{2}$.

Timeshift between $m_1(t)$ and $m_2(t)$ (without radioactive decay):
Assuming $S_1 > S_2$ there is a $\Delta t > 0$ with $m_1(t) = m_2(t + \Delta t)$ which is the time lag until a certain tracer mass is reached on the other hemisphere. The asymptotes for large times t with $e^{-2\varphi t} \longrightarrow 0$ give:

$$\begin{aligned}
\frac{S_1 + S_2}{2}\,t + \frac{S_1 - S_2}{4\varphi} &= \frac{S_1 + S_2}{2}\,(t + \Delta t) + \frac{S_2 - S_1}{4\varphi} \\
\frac{S_1 - S_2}{2\varphi} &= \frac{S_1 + S_2}{2}\,\Delta t \\
\Delta t &= \frac{S_1 - S_2}{S_1 + S_2}\,\frac{1}{\varphi}
\end{aligned}$$

For $S_1 = S_2$ follows trivially $\Delta t = 0$ and for $S_2 = 0$ it is

$$\Delta t = \frac{1}{\varphi} = \tau_{\text{ex}} \tag{C.15}$$

the characteristic exchange time of interhemispheric transport.

D Documentation of ECHAM5 modifications

D.1 Submodel mo-transport

1. The subroutine `INIT_TRANSPORT` calculates the grid indices for longitude and latitude of the emission locations and creates an emission mask which is written to the stream `{expname}_trans.nc`.
2. The emission mask is scaled with the emission strength for the current year of each source.
3. The subroutine `REQUEST_TRACER_TRANSPORT` introduces the tracer to the model. The tracer properties are set using the ECHAM5 routines `REQUEST_TRACER`/ `NEW_TRACER`. The different transport processes advection, diffusion, and convection can be individually switched on or off using the variables `NTRAN`, `NVDIFF`, and `NCONV` in the call of these routines. The decaytime is set by a module variable to that of ^{85}Kr The emissions are added to the tracer tendency `pxtte` using the tracer emission flux multiplied by the value of the emission mask. The emission mask is zero for all locations except the grid box of the source.

D.2 Program structure of the convection scheme

The steering procedure is `cumastr.f90` which collects all variables which are passed to the convection routine and which updates the tracer tendencies, i.e. the rate of mass mixing ratio change. It is called by `cucall.f90` which is called from `physc.f90` in the physics calculation part of ECHAM5. The computation of the convective mass flux is done in steps by the following subroutines (located in the echam directory `/src/`):

1. The interpolation of variables from full to half levels and initialisation of updraft and downdraft is done in `cuini.f90`.
2. In `cubase.f90` the cloud base is calculated and the mass flux at cloud base is defined.
3. The ascent in clouds without downdrafts is calculated in `cuasc.f90`.
4. The downdraft is calculated by
   a) Specifying values of the "level of free sinking" in `cudlfs.f90`.
   b) Determining the moist descent in `cuddraf.f90`.
   c) Recalculating the cloud base massflux according to downdrafts
5. Final cloud ascent calculation in `cuasc.f90` .
6. Call `cuflx.f90` for final adjustments of convective fluxes
7. Calculate increments of T and q in `cudtdq.f90` and of u and v in `cududv.f90`.

D.3 Implementation of the convection correction routine

The correction routine is part of the module `mo_transport` and called from `physc` after calculation of the convection processes. It consists of the following steps:

1. in `physc` values of tracer mass mixing ratio and tracer tendency before the call of the convection routine `CUCALL` are stored to variables prext and prexte.
2. After the convection scheme was fully processed the correction routine `convection_correction` is called.
3. The maximum effective height of the convection colum `npctop` is determined for each grid point block in order to shrink level loops.
4. `convflag` is a three dimensional field which indicates whether convection may affect the tracer tendency in the respective boxes.
5. By subtracting the stored tracer tendency `prexte` (ΔX_{t-}) before convection from the updated value after (`postxte` $= \Delta X_{t+}$) the effective change through convection is determined.
6. The routine `column_sum` calculates the tracer mass $M(X_{t-})$ in the column before convection.
7. the hypothetical concentration X'_{t+} after convection `prognoxt` is calculated.
8. new concentrations are corrected to be positive for each column by adding absolut value of smallest `prognoxt` smaller than zero ($/Rightarrow\tilde{X}t+$).
9. hypothetical new column tracer mass $M(\tilde{X_{x+}})$ is calculated by `column_sum` .
10. corrected tracer tendency `convxte` is calculated
11. new `pxtte` is assigned with `prexte+convxte`.

Steps 5 to 11 are repeated for each specified tracer.

D.4 Implementation of the mass fixer

Because the tracer transport scheme did not fulfill the requirement of global mass conservation a mass fixing routine was introduced. The absence of atmospheric sinks for ^{85}Kr except radioactive decay allows to calculate the theoretical ^{85}Kr budget due to emissions for every single time step. The following subroutines stored in the module `mo_tracermassfixg` are called in the ECHAM5 calculation control routine `scan1` after completion of the time filter `tf2` and before entering the process of advection:

- `inibudget` For the intialisation of global tracer mass
- `emissionbudget` For calculation of the theoretical tracer content of the atmosphere
- `burdencalc` for calculating a two dimensional field of column tracer masses in the model
- `tracer_massdiag` for diagnosis the global sum of tracer mass and calculation of the correction factor
- `tracermassfixer` for scaling the tracer field by the correction factor

For initialization either a file can be used or the mass of the initial tracer content of the model. The emission budget `mass_budget` B is determined in a loop over all individual trace species by equation (D.1) with B_- (`budgetm1`) being the budget of the previous time step and E the emissions of the current time step.

$$B = B_- e^{\frac{-\Delta t}{\tau_{\text{decay}}}} + E(1 - e^{\frac{-\Delta t}{\tau_{\text{decay}}}}) \tag{D.1}$$

After calculating the actual global tracer mass M in the model, the correction factor `corrfactor` c is calculated as

$$c = \frac{B}{M}$$

In the ^{85}Kr background simulation the correction $|1 - c|$ was usually in th order of 10^{-7} per time step. In agreement with the finding of erroneous mass increase in Chapter 3, the case with $c < 1$ occurred more often than $c > 1$.

List of Acronyms

BfS	*Bundesamt für Strahlenschutz* German federal radiation protection office
BMWi	*Bundesministerium f. Wirtschaft u. Technologie* German federal ministry for economy and technology
CTBT(O)	Comprehensive Test-Ban Treaty (Organization)
CTM	Chemical transport model
DPRK	Democratic People's Republic of Korea
ECMWF	European Center for Medium Range Weather Forecast
ENSO	El Niño Southern Oscillation
FMCT	Fissile Material Cut-off/Control Treaty
GCM	General Circulation Model
HYSPLIT	Hybrid Single-Particle Lagrangian Integrated Trajectory
IAEA	International Atomic Energy Agency
iGSE	independent Group of Scientific Experts on the detection of clandestine nuclear weapons usable material production
ITCZ	Intertropical Convergence Zone
MPI-OM	Ocean Model developed and used at MPI
NPT	(nuclear) Non Proliferation Treaty
IMS	International Monitoring System
IDC	International Data Center
PTS	Provisional Technical Secretariat
SOI	Southern Oscillation Index

List of Figures

List of Tables

Bibliography

Aghedo, A. M., Schultz, M. G., Rast, S., 2008. Sensitivity of tracer transport to model resolution, forcing data and tracer lifetime in the general circulation model ECHAM5. Atmospheric Chemistry and Physics Discussions 8, 137–160.

Ahlswede, J., Hebel, S., Kalinowski, M., Ross, O., 2009. Update of the global krypton-85 emission inventory. Occasional Paper 9, Centre for Science and Peace Research, University of Hamburg.

Andryushin, L., Voloshin, N., Ilkaev, R., Matushchenko, A., Ryabev, L., Strukov, V., Chernyshev, A., Yudin, Y., 1999. Catalog of worldwide nuclear testing. Begell Atom.

Aregbe, Y., Mayer, K., Valkiers, S., Debievre, P., 1997. Detection of reprocessing activities through stable isotope measurements of atmospheric noble gases. Fresenius Journal of Analytical Chemistry 358 (4), 533–535.

Becker, A., Wotawa, G., DeGeer, L.-E., Seibert, P., Draxler, R. R., Sloan, C., D'Amours, R., Hort, M., Glaab, H., Heinrich, P., Grillon, Y., Shershakov, V., Katayama, K., Zhang, Y., Stewart, P., Hirtl, M., Jean, M., Chen, P., 2007. Global backtracking of anthropogenic radionuclides by means of a receptor oriented ensemble dispersion modelling system in support of Nuclear-Test-Ban Treaty verification. Atmospheric Environment 41 (21), 4520–4534.

Bergman, C., Pettersson, B. G., 1994. Radiation applications and waste management: Taking the final steps. IAEA Bulletin 1, 36–40.

Blackadar, A. K., 1962. The vertical distribution of wind and turbulent exchange in a neutral atmosphere. Journal of Geophysical Research 67, 3095–3102.

Bowman, K. P., Cohen, P. J., 1997. Interhemispheric Exchange by Seasonal Modulation of the Hadley Circulation. Journal of the Atmospheric Sciences 54(16), 2045–2059.

Brinkop, S., Sausen, R., 1997a. A Finite Difference Approximation for Convective Transports Which Maintains Positive Tracer Concentrations.

Brinkop, S., Sausen, R., 1997b. A modified mass-flux scheme for convection which maintains positive tracer concentrations.

Bureau of Meteorology,Australian Government, 2009. SOI archive, 1876 to present. http://www.bom.gov.au/climate/current/soihtm1.shtml Oct. 2009.

Chen, C. Y., Li, Y. M., Bailey, K., O'Connor, T. P., Young, L., Lu, Z. T., 1999. Ultrasensitive isotope trace analyses with a magneto-optical trap. Science 286, 1139–1141.

Cleveland, W. S., Devlin, S. J., 1988. Locally-Weighted Fitting: An Approach to Fitting Analysis by Local Fitting. Journal of the American Statistical Association 83, 596–610.

Collon, P., Kutschera, W., Lu, Z.-T., 2004. Tracing noble gas radionuclides in the environment. Annual Review of Nuclear and Particle Science 54 (1), 39–67.

Czeplak, G., Junge, C., 1974. Studies of interhemispheric exchange in the troposphere by a diffusion model. In: Transactions of the AGU 55.

Denning, A., Holzer, M., Gurney, K., 1999. Three-dimensional transport and concentration of SF6–A model intercomparison study. Tellus B 51, 266–297.

Draxler, R. R., Rolph, G. D., 2003. HYSPLIT (HYbrid Single-Particle Lagrangian Integrated Trajectory) Model. Tech. rep., NOAA Air Resources Laboratory, Silver Spring, MD.

Eckermann, K., Ryman, J. J., 1993. Federal Guidance Report No. 12: External exposure to radionuclides in air, water, and soil. Tech. rep., Oak Ridge National Laboratory and US Environmental Protection Agency.
URL `http://www.epa.gov/rpdweb00/docs/federal/402-r-93-081.pdf`

Feichter, J., Crutzen, P. J., 1990. Parameterization of vertical tracer transport due to deep cumulus convection in a global transport model and its evaluation with ^{222}Radon measurements. Tellus B 42(1), 100–117.

Feichter, J., Schultz, M., Diehl, T., Sep/Oct 2002. Modeling chemical constituents of the atmosphere. Computing in Science & Engineering 4 (5), 56–63.

Firestone, R. B., Shirley, V. S., Baglin, C. M., Chu, S. Y. F., Zipkin, J., 1999. Table of Isotopes. 8th Edition, John Wiley & Sons, Inc., New York.

Garland, J., Wakeford, R., 2007. Atmospheric emissions from the Windscale accident of October 1957. Atmospheric Environment 41, 3904–3920.

Geller, L. S., Elkins, J. W., Lobert, J. M., Clarke, A. D., Hurst, D. F., Butler, J. H., Myers, R. C., 1997. Tropospheric SF6: Observed latitude distribution and trends, derived emissions and interhemispheric exchange time. Geophysical Research Letters 24, 675–678.

Gilliland, A. B., 1997. The potential influences of ENSO on interhemispheric transport, Thesis (Ph.D.). Ph.D. thesis, School of Earth and Atmospheric Sciences, Georgia Institute of Technology.

Gleckler, P. J., Taylor, K. E., Doutriaux, C., 2008. Performance metrics for climate models. Journal of Geophysocal Research 113, .

Goodman, M. S., 2007. Spying on the nuclear bear: Anglo-American Intelligence and the Sovjet bomb. Stanford University Press.

Grassl, H., 1989. Krypton-85: Literaturrecherche mit wissenschaftlicher Bewertung. Study for the Bavarian government.

Grosch, M., 2008. Complications of the medical radioisotope production for the non-proliferation regime. Master's thesis, University of Hamburg, IFSH.

Gupta, M. L., Douglass, A. R., Kawa, S. R., and, S. P., 2004. Use of radon for evaluation of atmospheric transport models: sensitivity to emissions. Tellus B 56 (5), 404–412.

Hebel, S., 2008. personal communication.

Hudson, G. B., 1993. Noble Gas isotope Measurements for Spent Nuclear Fuel Reprocessing. Tech. rep., IAEA Task 90/0A211 - Lawrence Livermore National Laboratory.

IAEA, 1970. Treaty on the non-proliferation of nuclear weapons. INFCIRC/140.

IAEA, 1986. Summary report on the post-accident review meeting on the Chernobyl accident. Safety Series No. 75-INSAG-1.

IAEA, 1997. Model Protocol additional to the agreements between State(s) and the IAEA for the application of safeguards. INFCIRC/540.

IAEA, 1999. Use of Wide Area Environmental Sampling in the Detection of Undeclared Nuclear Activities. Tech. Rep. STR-321, IAEA.

IAEA, September 2004. Strengthening the Effectiveness and Improving the Efficiency of the Safeguards System and Application of the Model Additional Protocol. Resolution GC(48)/RES/14.

IAEA, September 2005. Technical Meeting on Noble Gas Monitoring Sampling And Analysis for Safeguards Applications. Tech. Rep. STR-351, IAEA.

Izrael, Y. A., Nazarov, I. M., Riabosapko, 1982. Kr-85 anthropogenic emissions into the atmosphere. Soviet-Meteorology and Hydrology 6, 1–9.

Jacob, D. J., Orather, M. J., Wofsy, S. C., McElroy, B., 1987. Atmospheric Distribution of ^{85}Kr Simulated with a General Circulation Model. Journal of Geophysocal Research 92, NO D6, 6614–6626.

Jöckel, P., Kuhlmann, R., Lawrence, M. G., Steil, B., Brenninkmeijer, C. A. M., Crutzen, P. J., Rasch, P. J., Eaton, B., 2001. On a fundamental problem in implementing flux-form advection schemes for tracer transport in 3-dimensional general circulation and chemistry transport models. Quarterly Journal of the Royal Meteorological Society 127(573), 1035–1052.

Jeuken, A., Siegmund, P., Heijboer, L., Feichter, J., Bengtsson, L., 1996. On the potential of assimilation meteorological analysis in a global climate model for the purpose of model validation. Journal of Geophysical Research 101 (D12), 16939–16950.

Kajikawa, Y., Wang, B., 2009. Monsoon Index set 1948-2008 derived from NCEP reanalysis data. Tech. rep., International Pacific Research Center, Hawaii.
URL `http://apdrc.soest.hawaii.edu/projects/monsoon/`

Kajikawa, Y., Wang, B., Yang, J., 2009. A multi-time scale Australian monsoon index. International Journal of Climatology, accepted.

Kalinowski, M. B., Axelsson, A., Bean, M., Blanchard, X., Bowyer, T. W., Brachet, G., McIntyre, J. I., Peters, J., Pistner, C., Raith, M., Ringbom, A., R.J.Saey, P., Schlosser, C., Stocki, T. J., Taffary, T., Ungar, R. K., 2010. Discrimination of nuclear explosions against civilian sources based on atmospheric xenon isotopic activity ratios. Pure and Applied Geophysics Topical Volume Recent Advances in Nuclear Explosion Monitoring,accepted.

Kalinowski, M. B., Pistner, C., 2006. Isotopic signature of atmospheric xenon released from light water reactors. Journal of Environmental Radioactivity 88/3, 215–235.

Kalinowski, M. B., Ross, O., 2006. Data analysis and interpretation of the North Korean nuclear test explosion of 9 October 2006. INESAP Information Bulletin No. 27, 39–43.

Kalinowski, M. B., Sartorius, H., Uhl, S., Weiss, W., 2004. Conclusions on plutonium separation from atmospheric krypton-85 measured at various distances from the Karlsruhe reprocessing plant. Journal of Environmental Radioactivity 73 (2), 203–222.

Kalinowski, M. B., Tuma, M. P., 2009. Global radioxenon emission inventory based on nuclear power reactor reports. Journal of Environmental Radioactivity 100, 58–70.

Kemp, R. S., Schlosser, C., 2008. A performance estimate for the detection of undeclared nuclear-fuel reprocessing by atmospheric Kr-85. Journal of Environmental Radioactivity 99 (8), 1341–1348.

Kjellström, E., Feichter, J., Hoffmann, G., 1999. Transport of SF_6 and $^{14}CO_2$ in the atmospheric general circulation model ECHAM4. Tellus 52B, 1–18.

Kunz, C., Wahlen, M., Peterson, K. R., Rodriguez, D. J., 1985. Krypton-85 purge at Three Mile Island: a comparison of measured and calculated surface air concentrations. Health Physics 49:3, 522–526.

Lehmann, B. E., Love, A., Purtschert, R., Collon, P., Loosli, H. H., Kutschera, W., Beyerle, U., Aeschbach-Hertig, W., Kipfer, R., Frape, S. K., Herczeg, A., Moran, J., Tolstikhin, I. N., Gröning, M., 2003. A comparison of groundwater dating with 81Kr, 36Cl and 4He in four wells of the Great Artesian Basin, Australia. Earth and Planetary Science Letters 211 (3-4), 237–250.

Levin, I., Hesshaimer, V., 1996. Refining of atmospheric transport model entries by the globally observed passive tracer distributions of (85)krypton and sulfur hexafluoride (SF6). Journal of Geophysical Research-Atmosphere 101 (D11), 16745–16755.

Li, J., Zeng, Q., 2003. A new monsoon index and the geographical distribution of the global monsoons. Advances in Atmospheric Sciences 20, 299–302.

Lin, S. J., Rood, R. B., 1996. Multidimensional flux form semi-Lagrangian transport. Monthly Weather Review 124, 2046–2068.

Lintner, B. R., 2003. Mechanisms of Passive Tracer Interhemispheric Transport: An Analysis of Model-Derived and Observational Interhemispheric Transport Climatology and Interannual Variations. Ph.D. thesis, University of California, Berkeley.

Lintner, B. R., Gilliland, A. B., Fung, I. Y., 2004. Mechanisms of convection-induced modulation of passive tracer interhemispheric transport interannual variability. Journal of geophysical research 109, 13102.

Maiss, M., Levin, I., 1994. Global increase of SF6 in the atmosphere. Geophysical Research Letters 21, 569–572.

Mesinger, F., Arakawa, A., 1976. Numerical methods used in atmospheric models. Tech. rep., WMO.

Newell, R. E., Vincent, D. G., Kidson, J. W., 1969. Interhemispheric mass exchange from meteorological and trace substance observations. Tellus 21, 641–647.

Nichols, J. P., Binford, F. T., 1971. Status of Noble Gas Removal and Disposal. Intra Laboratory Correspondence ORNL-TM-3515, Oak Ridge National Laboratory.

NOAA, National weather service, 2009. Teleconnection Patterns. http://origin.cpc.ncep.noaa.gov/data/teledoc/ Oct. 2009.

Nordeng, T. E., 1994. Extended versions of the convective parametrization scheme at ECMWF and their impact on the mean and transient activity of the model in Tropics. Tech. rep., ECMWF.

Nydal, R., 1968. Further investigation on transfer of radiocarbon in nature. Journal of Geophysical Research 73, 3617–3625.

Office of the Director of National Intelligence, P. A. O., 16 October 2006. Statement by the Office of the Director of National Intelligence on the North Korea Nuclear Test. Press Release.
URL `www.dni.gov/announcements/20061016_release.pdf`

Palmer, B. D., 1969. Interhemispheric Transport of Atmospheric Fission Debris from French Nuclear Tests. Science 164 (3882), 951–952.
URL `http://www.sciencemag.org/cgi/content/abstract/164/3882/951`

R Development Core Team, 2009. R: A Language and Environment for Statistical Computing. R Foundation for Statistical Computing, Vienna, Austria, ISBN 3-900051-07-0.
URL `http://www.R-project.org`

Reistad, O., Hustveit, S., 2008. Heu Fuel Cycle Inventories and Progress on Global Minimization. The Nonproliferation Review 15, 265–287.

Ringbom, A., Elmgren, K., Lindh, K., 2007. Analysis of radioxenon in ground level air sampled in the Republic of South Korea on October 11-14, 2006. Tech. rep., FOI-R-2273-SE.

Roeckner, E., Bäuml, G., Bonaventura, L., Brokopf, R., Esch, M., Giorgetta, M., Hagemann, S., Kirchner, I., Kornblueh, L., Manzini, E., Rhodin, A., Schlese, U., Schulzweida, U., Tompkins, A., 2003. The atmospheric general circulation model ECHAM5 - Part I: Model Description. MPI Report Series 349.

Roeckner, E., Brokopf, R., Esch, M., Giorgetta, M., Hagemann, S., Kornblueh, L., Manzini, E., Schlese, U., Schulzweida, U., 2006. Sensitivity od Simulated Climate to Horizontal and Vertical Resolution in the ECHAM5 Atmosphere Model. Journal of Climate 19:16, 3771–3791.

Ross, O., Ahlswede, J., Annewandter, R., Feichter, J., Rast, S., Schlünzen, H., Schoetter, R., Stanoszek, P., Kalinowski, M., 2009. Simulation of atmospheric noble gas concentrations to assess sampling procedures for the detection of clandestine reprocessing. Project report, Joint programme of IAEA and BMWi, JOPAG/01.09-PRG-373.

Rózanski, 1979. Krypton-85 in the Atmosphere 1950-1977: a Data Review. Environment International 2, 139–143.

Saey, P. R. J., Bean, M., Becker, A., Coyne, J., d'Amours, R., DeGeer, L.-E., Hogue, R., Stocki, T. J., Ungar, R. K., G., W., 2007. A long distance measurement of radioxenon in Yellowknife, Canada, in late October 2006. Geophysical Research Letters 34, L20802.

Schlünzen, K. H., 2002. Simulation of transport and chemical transformations in the atmospheric boundary layer - review on the past 20 years developments in science and practice. Meteorologische Zeitschrift 11, 303–313.

Schlünzen, K. H., Sokhi, R., 2008. Overview of tools and methods for meteorological and air pollution mesoscale model evaluation and user training. In: GAW report 181. WMO.

Shimizu, M., 1981. Beta ray thickness gauge. Fuji Jiho 54:4, 295–302.

Sich, A. R., Borovoi, A. A., Rasmussen, N. C., 1994. The Chernobyl accident revisited: source term analysis and reconstruction of events during the active phase. MITNE 306.

Simmons, A. J., Burridge, D. M., Jarraud, M., Girard, C., Wergen, W., 1989. The ECMWF medium-range prediction model: Development of the numerical formulations and the impact of increased resolution. Meteorology and Atmospheric Physics 40, 28–60.

Solomon, S., Qin, D., Manning, M., Chen, Z., Marquis, M., Averyt, K. B., Tignor, M., Miller, H. L., 2007. Contribution of Working Group I to the Fourth Assessment Report of the Intergovernmental Panel on Climate Change. Cambridge University Press.

Stanoszek, P., 2008. Krypton-85 signatures for different plutonium production schemes. Master's thesis, University of Hamburg, Centre for Science and Peace Research.

Stanoszek, P., Kalinowski, M. B., 2009. Krypton-85 source term for various plutonium production schemes. In: ESARDA 31st annual Meeting, Vilnius, Lithuania, 26-28 May 2009, Proceedings.

Styra, B., Butkus, D., 1991. Geophysical Problems of Krypton-85 in the Atmosphere. Taylor & Francis.

Teichmann, C., 2009. Climate and air pollution modelling in South America with emphasis on megacities. Ph.D. thesis, International Max Planck Research School on Earth System Modelling.

Tiedtke, M., 1989. A comprehensive mass-flux scheme for cumulus parameterization in large-scale models. Monthly Weather Review 117, 1779–1800.

UNSCEAR, 1982. Exposures resulting from nuclear explosions, ANNEX E to Report to the UN General Assembly. Tech. rep., United Nations Scientific Committee on the Effects of Atomic Radiation.

Uppala, S., Kallberg, P., Simmons, A., Andrae, U., da Costa Bechtold, V., Fiorino, M., Gibson, J., Haseler, J., Hernandez, A., Kelly, G., Li, X., Onogi, K., Saarinen, S., Sokka, N., Allan, R., Andersson, E., Arpe, K., Balmaseda, M., Beljaars, A., van de Berg, L., Bidlot, J., Bormann, N., Caires, S., Chevallier, F., Dethof, A., Dragosavac, M., Fisher, M., Fuentes, M., Hagemann, S., Holm, E., Hoskins, B., Isaksen, L., Janssen, P., Jenne, R., McNally, A., Mahfouf, J. F., Morcrette, J. J., Rayner, N., Saunders, R., Simon, P., Sterl, A., Trenberth, K., Untch, A., Vasiljevic, D., Viterbo, P., Woollen, J., 2005. The ERA-40 re-analysis. Quarterly Journal of the Royal Meteorological Society 131, 2961–3012.

van Oldenborgh, G. J., Philip, S. Y., Collins, M., 2005. El Niño in a changing climate: a multi-model study. Ocean Science, 1, 81–95.

von Hippel, F., Albright, D. H., Levi, B. G., 1986. Quantities of Fissile Materials in US and Soviet Nuclear Weapons Arsenals. Tech. Rep. PU/CEES Report No. 168, Center for Energy and Environmental Studies, The Engineering Quadrangle, Princeton University.

Wang, B., Fan, Z., 1999. Choice of South Asian summer monsoon indices. Bulletin of the American Meteorological Society 80, 629–638.

Webster, P. J., Yang, S., 1992. Monsoon and ENSO: Selectively interactive systems. Quarterly Journal of the Royal Meteorological Society 118, 877–926.

Weiss, W., Sittkus, A., Stockburger, H., Sartorius, H., 1983. Large-scale atmospheric mixing derived from meridional profiles of krypton 85. Journal of Geophysical Research 88, 8574–8578.

Winger, K., 2002. Compilation and evaluation of Krypton-85 emission inventories from 1945 until 2000. Diploma thesis, Max-Planck-Institute for Meteorology, Hamburg.

Winger, K., Feichter, J., Kalinowski, M. B., Sartorius, H., Schlosser, C., 2005. A new compilation of the atmospheric krypton-85 inventories from 1945 to 2000 and its evaluation in a global transport model. Journal of Environmental Radioactivity 80 (2), 183–215.

Wotawa, G., DeGeer, L.-E., Denier, P., Kalinowski, M. B., Toivonen, H., D'Amours, R., Desiato, F., Issartel, J. P., Langer, M., Seibert, P., Frank, A., Sloan, C., Yamazawa, H., 2003. Atmospheric transport modelling in support of CTBT verification–overview and basic concepts. Atmospheric Environment 37, 2529–2537.

Zimmermann, P. H., Feichter, J., Rath, H.-K., Crutzen, P. J., Weiss, W., 1989. A global threedimensional source-receptor model investigation using 85Kr. Atmospheric Environment 23, 25–35.

Die gesamten Veröffentlichungen in der Publikationsreihe des MPI-M
„Berichte zur Erdsystemforschung“,
„Reports on Earth System Science“,
ISSN 1614-1199

sind über die Internetseiten des Max-Planck-Instituts für Meteorologie erhältlich:

http://www.mpimet.mpg.de/wissenschaft/publikationen.html



ISSN 1614-1199